Experimental studies of sorption and transport of moisture in cement based materials with supplementary cementitious materials

MAHSA SAEIDPOUR

LUND
UNIVERSITY

DOCTORAL DISSERTATION
by due permission of the Faculty of engineering, Lund University, Sweden.
To be defended at Lilla hörsalen, Designcentrum. Date 2015-10-1 and time 13:00.

Faculty opponent
Veronique Baroghel Bouny

Organization	Document name
LUND UNIVERSITY	DOCTORAL DISSERTATION
Faculty of engineering, Division of Building Materials	Date of issue 2015-08-07
Author(s) Mahsa Saeidpour	Sponsoring organization

Experimental studies of sorption and transport of moisture in cement based materials with supplementary cementitious materials

Most deterioration processes in cement based materials are closely related to moisture sorption and moisture transport properties. Therefore, it is important to study these properties, both theoretically and practically. This work is an experimental investigation in this field.

Nowadays, the cement industry produces cements with increasing amounts of supplementary cementitious materials (SCMs) to limit CO_2 emissions from concrete production. Knowledge about the moisture properties of concrete made from these blended cements is limited. This project has therefore been an attempt to further develop our understanding of the moisture properties of cement based materials, such as sorption isotherms and sorption transport properties in the presence of SCMs. This has been done by studying sorption isotherms mainly using the sorption balance method, and moisture transport coefficients using both the cup method and a sorption dynamic method. The experimental investigations were made on three types of hydrated cement pastes and mortars (OPC, OPC + 70% slag and OPC + 10% silica fume) with three different w/b –ratios (w/b) for cement paste (0.6, 0.5, 0.4) and two different w/b for cement mortar (0.5, 0.4).

Sorption isotherms were determined for cement pastes and mortars in both hygroscopic and the super-hygroscopic relative humidity ranges using the sorption balance method, and the pressure plate method. The conclusion from this part of the study was that the desorption isotherms at low RH (0-30%) for different binders and different w/b-ratios are similar. At higher RHs the samples with silica fume and slag have higher moisture content than OPC samples. This is explained by that they have a higher amount of gel pores and a lower amount of capillary pores than OPC samples. The sorption isotherm at high RHs is difficult to validate experimentally, due to the critical RH of pore solutions.

Steady-state and transient measurements of transport coefficients were also made. The dynamic sorption method was used to evaluate the diffusivity in small paste samples. The results show that Fick's law cannot completely describe the transport process in such small samples and sorption behavior is therefore anomalous with two processes with different timescales. One of these is macro-diffusion into the sample, which takes place on a shorter time scale in the small samples used. The second process takes place on longer timescales and it is possibly related to the sorption in nanometer-structure of materials.

To better understand the transport properties in sorption cycles, steady-state diffusion coefficients of mortar samples were measured with a newly developed cup method set-up. The measurements were done on both the absorption and desorption limbs of sorption isotherms. For OPC samples the results show a clear difference between the diffusion coefficients in absorption and desorption with vapor content as potential (D_v) and presented as a function of relative humidity (RH). The D_v in desorption is higher than absorption especially at high RHs. For samples with SCMs the dependence of D_v on RH is small. The D_v:s were also recalculated to diffusivity (D_ε) using the sorption isotherms to study the effect of different potentials on the effect of hysteresis on transport properties.

Key words: Cement, Concrete, Moisture transport, Hysteresis, Supplementary cementitious materials, Water vapor sorption, Sorption isotherms, Anomalous sorption

Classification system and/or index terms (if any)

Supplementary bibliographical information	Language
	English

ISSN and key title	ISBN
0348-7911	978-91-7623440-2

Recipient's notes	Number of pages 157	Price
	Security classification	

Experimental studies of sorption and transport of moisture in cement based materials with supplementary cementitious materials

MAHSA SAEIDPOUR

LUND
UNIVERSITY

DOCTORAL DISSERTATION

Division of Building Materials, Faculty of Engineering, Lund University
ISBN 978-91-7623440-2
ISSN 03487911
ISRN LUTVDG/TVBM-15/1033-SE (1-60)

Printed in Sweden by Media-Tryck, Lund University
Lund 2013

Contents

List of Publications

This thesis is based on the work contained in the following papers, which are referred to by Roman numerals in the text. The papers are appended at the end of the thesis.

I. Saeidpour, M. and L. Wadsö, Moisture equilibrium of cement based materials containing slag or silica fume and exposed to repeated sorption cycles. Cement and Concrete Research, 2015. 69(0) 88-95.

II. Saeidpour, M. and L. Wadsö, Evidence for anomalous water vapor sorption kinetics in cement based materials. Cement and Concrete Research, 2015. 70(0) 60-66.

III. Saeidpour, M. and L. Wadsö, The influence of sorption hysteresis on diffusion coefficients represented with different moisture potentials (submitted).

IV. Saeidpour, M. and L. Wadsö, , Effect of different potentials on moisture diffusion hysteresis in absorption and desorption (submitted).

V. Baquerizo, L.G., et al., Methods to determine hydration states of minerals and cement hydrates. Cement and Concrete Research, 2014. 65(0) 85-95.

VI. Baquerizo, L.G., et al., Hydration states of AFm cement phases. Cement and Concrete Research, 2015. 73(0) 143-157.

The contribution of Mahsa Saeidpour (MS) to the papers included in this thesis was as follows:

Paper I: MS produced the specimens, planned and carried out the experiments and analyzed the data. MS wrote the manuscript. LW contributed in planning the experiments and commented on the manuscript.

Paper II: MS produced the specimens, planned and carried out the experiments and analyzed the data. MS and LW wrote the manuscript.
Paper III: MS produced the specimens, planned and carried out the experiments and analyzed the data. MS wrote the manuscript. LW contributed in planning the experiments and commented on the manuscript.
Paper IV: MS produced the specimens, planned and carried out the experiments and analyzed the data. MS wrote the manuscript. LW contributed in planning the experiments and commented on the manuscript.
Paper V: MS contributed in sorption isotherms and sorption calorimetric experiments planning and data analyzing. MS commented on the manuscript.
Paper VI: MS contributed in sorption isotherms and sorption calorimetric experiments planning.

Nomenclature

Symbols

A	Cross sectional area	(m^2)
c	Concentration	(g m^3)
D_v	Moisture diffusion coefficients, with vapor content as driving potential	(m^2 s^{-1})
D_c	Moisture diffusivity, with moisture concentration as driving potential	(m^2 s^{-1})
E	Fractional of mass change	1
J	Mass flow	(g s^{-1})
k	Intrinsic permeability	(m^2)
n^0	Initial moles of gas	(mol)
n^a	Moles of absorbed gas	(mol)
p	Pressure	(Pa)
Q	Heat	(J)
q	Mass flux	(g m^2 s^{-1})
R	Gas constant	(J $mol^{-1}K^{-1}$)
r_m	Mean radius curvature	(m)
r_p	Pore radius	(m)

S	Entropy	(J K^{-1})
s	Degree of saturation	1
t	Absorbed layer thickness	(m)
u	Moisture content by mass	1
V	Volume	(m^3)
W	Work	(J)
γ	Surface tension	(N m^{-1})
μ	Viscosity (dynamic)	(Pa.s)
ρ	Density	(g m^{-3})
φ	Relative humidity	1

Abbreviations

AFm ($C_4A\,\bar{S}H_{12\text{-}14}$)	Mono-sulfate
AFt ($C_6A\,\bar{S}_3H_{32\text{-}36}$)	Ettringite
BJH	Barrett-Joyner-Halenda model for pore size distribution
C-S-H	Calcium silicate hydrate
C_3S	Tricalcium silicate
C_2S	Dicalcium silicate
C_3A	Tricalcium aluminate
C_4AF	Calcium ferro aluminate
CH	Calcium hydroxide (portlandite)

C_3AH_6	Hydrogarnet
$C_4AH_{13\text{-}19}$	Aluminate hydrate
$C_4A\,\bar{C}_{0.5}H_{12}$	Hemi-carbonate
$C_4A\,\bar{C}H_{11}$	Mono-carbonate
IGP	Intraglobular pores in C-S-H structure
LGP	Large gel pores in C-S-H structure
H-NMR	^{1}H nuclear magnetic resonance
OPC	Ordinary portland cement
RH	Relative humidity
SEM	Scanning electron microscopy
SCM	Supplementary cementitious material
SGP	Small gel pores in C-S-H structure
SSA	Specific surface area
TEM	Transmission electron microscopy
w/b	Water to binder ratio

Abstract

Most deterioration processes in cement based materials are closely related to moisture sorption and moisture transport properties. Therefore, it is important to study these properties, both theoretically and practically. This work is an experimental investigation in this field.

Nowadays, the cement industry produces cements with increasing amounts of supplementary cementitious materials (SCMs) to limit CO_2 emissions from concrete production. Knowledge about the moisture properties of concrete made from these blended cements is limited. This project has therefore been an attempt to further develop our understanding of the moisture properties of cement based materials, such as sorption isotherms and sorption transport properties in the presence of SCMs. This has been done by studying sorption isotherms mainly using the sorption balance method, and moisture transport coefficients using both the cup method and a sorption dynamic method. The experimental investigations were made on three types of hydrated cement pastes and mortars (OPC, OPC + 70% slag and OPC + 10% silica fume) with three different w/b –ratios (w/b) for cement paste (0.6, 0.5, 0.4) and two different w/b for cement mortar (0.5, 0.4).

Sorption isotherms were determined for cement pastes and mortars in both hygroscopic and the super-hygroscopic relative humidity ranges using the sorption balance method, and the pressure plate method. The conclusion from this part of the study was that the desorption isotherms at low RH (0-30%) for different binders and different w/b-ratios are similar. At higher RHs the samples with silica fume and slag have higher moisture content than OPC samples. This is explained by that they have a higher amount of gel pores and a lower amount of capillary pores than OPC samples. The sorption isotherm at high RHs is difficult to validate experimentally, due to the critical RH of pore solutions.

Steady-state and transient measurements of transport coefficients were also made. The dynamic sorption method was used to evaluate the diffusivity in small paste samples. The results show that Fick's law cannot completely describe the transport process in such small samples and sorption behavior is therefore anomalous with two processes with different time scales. One of these is macro-diffusion into the sample, which takes place on a shorter timescale in the small samples used. The second process takes place on longer timescales and it is possibly related to the sorption in nanometer-structure of materials.

To better understand the transport properties in sorption cycles, steady-state diffusion coefficients of mortar samples were measured with a newly developed cup method set-up. The measurements were done on both the absorption and desorption limbs of sorption isotherms. For OPC samples the results show a clear difference between the diffusion coefficients in absorption and desorption with vapor content as potential (D_v) and presented as a function of relative humidity (RH). The D_v in desorption is higher than absorption especially at high RHs. For samples with SCMs the dependence of D_v on RH is small. The D_v:s were also recalculated to diffusivity (D_c) using the sorption isotherms to study the effect of different potentials on the effect of hysteresis on transport properties.

Key words: Cement, Concrete, Moisture transport, Hysteresis, Supplementary cementitious materials, Water vapor sorption, Sorption isotherms, Anomalous sorption

1. Introduction

1.1. Background

Concrete is the most widely used construction material in the world. The worldwide concrete production is estimated to be approx. $7.5 \cdot 10^9$ cubic meters per year, which is about one cubic meter per person per year [1]. This huge amount of production makes it responsible for 5-8% of the global CO_2 emissions [2]. These emissions come from the clinker production processes. Around 60% of this CO_2 results from the reaction (calcination) of limestone in the kiln to produce calcium oxide and CO_2, and around 40% is generated from burning fuels [2].

The cement industry needs solutions to reduce this CO_2 production. There are three main ways for this to happen:

- Reduce energy consumption by optimizing the processes in cement producing factories.
- Reduce the use of fossil fuels by substituting them with other energy sources such as: biofuels, industrial waste and tires.
- Use more sustainable binders with high amounts of supplementary cementitious materials (SCMs), such as slag, fly ash, silica fume and pozzolans.

The first two approaches are already applied by the leading cement industries, and further minor improvements are possible. Modern cement plants, for example approach 70% of the theoretical efficiency and some plants only use about 20% primary fossil fuels [3]. The third approach is also used to some extent, but at present most cements have low levels of SCMs. Using supplementary cementitious materials thus seems the most promising solution to reduce the CO_2 of concrete, but this approach can have other side effects because it will change the nano and micro-structure of cement based materials, and there is currently little knowledge about these changes [4-6].

The demands for new environmentally friendly cement base materials increase. The SCMs' rich binders change the amount and kind of products formed during the hydration and these cause changes in pore structure. The pore-water interaction is a factor for most degradation processes. To be able to guarantee the durability of these materials in the long term and in different environments, there is a need for scientific

understanding and longterm prediction of water transport in these materials. The European Community (Framework 7) funded a Marie Curie Initial Training Network, called **TRANSCEND** (understanding **Trans**port for **C**oncrete which is **E**co friendly, i**N**novative and **D**urable). The aim of this program is to understand the transport process in cement based materials with a special emphasis on durability issues, for the introduction of lower CO_2 impact materials (SCMs) in cement based products. TRANSCEND consisted of 15 projects based at universities and industrial partners and can be divided into two themes: experimental and modeling (see Fig. 1.1). This thesis presents the results of one of these projects: number 6 in Fig. 1.1. Collaboration occurred mainly in projects 5, 13 and 10.

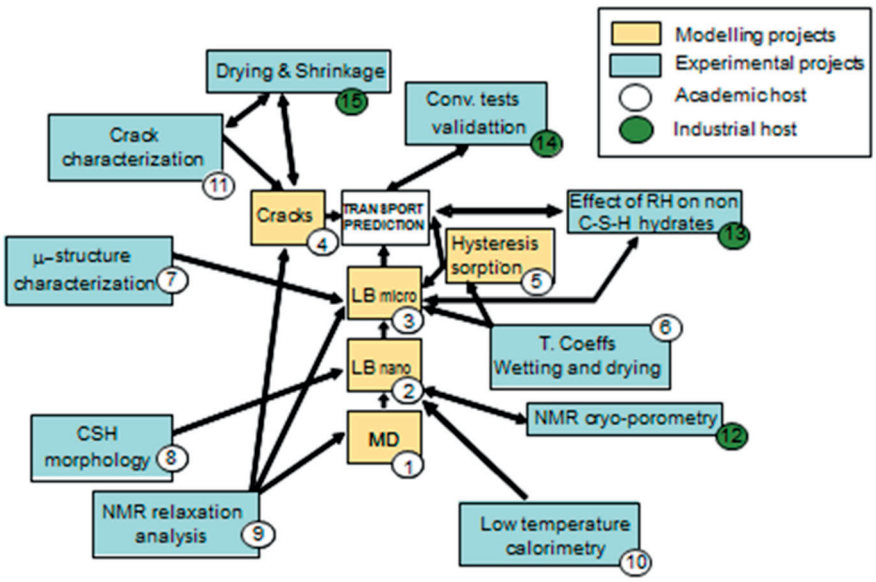

Figure 1.1. An overview of the TRANSCEND program showing the connections between different projects. The yellow boxes are modeling projects and the blue boxes are experimental projects (taken from the TRANSCEND application).

1.2. Aim and research questions

The aim of the present research project was to develop a better understanding of sorption and transport properties of cement based materials with a special focus on the presence of two SCMs, 70% slag and 10% silica fume. More specifically, the following research questions have been investigated:

1. How do the SCMs (slag and silica fume) change the sorption isotherms?
2. How do these SCMs influence the transport properties?
3. Are moisture transport coefficients different for samples in absorption and desorption?
4. How do different potentials change the diffusion coefficient's dependence on the potential?
5. Which methods should be used to characterize sorption and transport properties of cement based materials?

2. Cement based materials

In this chapter the hydration process and the reaction products of Portland cement are briefly explained. In part 2.2.1 the most important model proposed for the structure of the main product of hydration, calcium silicate hydrate (C-S-H), is described. As this study focuses on the effect of SCMs on transport properties of cement based materials, in the last part of this chapter the properties of two SCMs, slag and silica fume, are briefly described.

2.1. Cement hydration

Portland cement has been used for more than 150 years and it still is one of the most widely used construction materials. The raw materials for Portland cement should contain calcium and silica, usually materials such as limestone and quartz sand or clays are used. These materials are mixed, crushed and heated to 1450-1550°C in long rotary kilns to form cement clinkers. The main phases in cement clinkers are tricalcium silicate $3CaO{\cdot}SiO_2$ (C_3S), dicalcium silicate $2CaO{\cdot}SiO_2$ (C_2S), tricalcium aluminate $3CaO{\cdot}Al_2O_3$ (C_3A), and calcium ferro aluminate $4CaO{\cdot}Al_2O_3{\cdot}Fe_2O_3$ (C_4AF). Note that C, S, A, F, $\bar{S}$ and $\bar{C}$ are cement chemists notations for CaO, SiO_2, Al_2O_3, FeO, SO_3 and CO_2.

When cement is mixed with water a chemical reaction between the present phases is started. This reaction is called hydration. The most common type of Portland cement is ordinary Portland cement (OPC). Hydration of OPC is complex since all phases in clinker react with water simultaneously to form different products, and these reactions are not independent of each other. The most complete authoritative review of cement hydration is probably still Taylor's Cement Chemistry from 1990 [7]; later developments in the subject are discussed in reference [8].

The clinker phases, C_3S and C_2S, react with water to produce calcium hydroxide (CH), which is also called portlandite, and calcium silicate hydrate (C-S-H). Note that the reactions below are not stoichiometrically balanced since the main hydration product, calcium silicate hydrate, does not have a well-defined composition.

$$C_2S + (2\text{-}x+y)\ H \rightarrow C_xSH_y + (2\text{-}x)\ CH \qquad (1)$$

$$C_3S + (3\text{-}x+y)\ H \rightarrow C_xSH_y + C_xSH_y + (3\text{-}x)\ H \qquad (2)$$

Aluminate phases can react in several ways and produce different hydration products. The C_3A in pure water will hydrate to produce hydrogarnet phase C_3AH_6, while in cement paste in the presence of calcium sulfate and calcium hydroxide it forms aluminate hydrate ($C_4AH_{13\text{-}19}$) and mono-sulphate (AFm) ($C_4A\bar{S}H_{12\text{-}14}$) and ettringite (AFt) ($C_6A\bar{S}_3H_{32\text{-}36}$). Mono-sulphate can carbonate and produce ettringite and hemi-carbonate ($C_4A\bar{C}_{0.5}H_{12}$). Hemi-carbonate can be converted into mono-carbonate ($C_4A\bar{C}H_{11}$) in the presence of sufficient CO_2.

Changes in temperature, impurities and availability of water may induce significant modification in Ferrite phases. The final product of C_4AF is hydrogarnet phase ($C_6AFS_2H_8$). The hydration can be simplified as below.

$$C_4AF + xC_2S + (2x+y-2)\,H \rightarrow C_6AFS_xH_y + (2x-2)\,CH \quad (3)$$

$$C_4AF + xC_3S + (3x+y-2)\,H \rightarrow C_6AFS_xH_y + (3x-2)\,CH \quad (4)$$

2.2. C-S-H

The main product of Portland cement hydration is calcium silicate hydrate (C-S-H); C-S-H is approx. 48% of the total products. The C-S-H is formed in hydration of C_3S and C_2S when these clinker phases are dissolved and the ions precipitated as C-S-H. The C-S-H has received a significant interest [9-13], but the knowledge about the structure of C-S-H still remains imperfect. The most important reason for this lack of knowledge is that the C-S-H structure is very dependent on the reaction conditions and the reacting phase composition, and it is believed to change (densify) during the reaction [14]. On the other hand, most methods used in these studies, such as scanning electron microscopy (SEM) and transmission electron microscopy (TEM), require that the materials are dried before the study and it is believed that drying under 30% RH causes irreversible changes in the C-S-H structure [13, 15-18]. The possible changes in C-S-H structure due to drying at low RHs are discussed in this study in **paper I**. To overcome this problem, ^1H nuclear resonance (NMR) method has recently received a lot of attention for the study of the C-S-H structure [14, 19-21].

The current knowledge is that C-S-H is nanocrystalline in the short range, while there is no order in the long range. These nanocrystals consist of small local regions (5-30 nm). They have a layered structure, similar to defective tobermorite. The regions are arranged with different densities depending on hydration conditions. How these regions are connected, or if they are discrete, is still an active area of research [5]. The C-S-H structure is primarily defined by the Ca/Si-ratio and the amount of water, which can be changed due to drying. The Ca/Si-ratio can be in the range of 0.7-2 [22].

Two main groups of structural models have been suggested for the C-S-H structure. The first group consists of layered structures as suggested by Powers [23, 24] and

Feldman and Sereda [15]. The second group has a colloidal structure that has mainly been discussed by Jennings [10, 11]. The Jennings' model is used in **paper I** to describe the pore size distribution in different cement pastes. The structure proposed by Jennings is discussed in the following section.

2.2.1. Jennings' model

The colloidal model was proposed by Jennings to better understand the microstructure quantitatively and relate it to its properties. The model (CM-I) was published in 2000 [10], and then modified later to CM-II in 2008 [11] (Fig. 2.1). In CM-I the C-S-H consists of spherical units which cluster together to make globules. The size of the globules is about 5 nm. The globules are gathered to make building blocks of C-S-H. The CM-I model does not describe properties such as drying, shrinkage or creep under load.

The improved model CM-II was based on the analysis of sorption isotherms, especially water sorption isotherms [23, 25-27]. This model gives information about the structural changes taking place while water absorbs or desorbs in the pores. In CM-II, the internal structure of globules is discussed more than in CM-I. The globules have a layered structure. Clusters of globules pack together in two packing densities; low densities (LD) C-S-H and high densities (HD) C-S-H.

The pores within the globules are called intraglobular pores (IGP), the water between layers is referred as interlayer water and the space that interlayer water exists in is the interlayer space. IGP pores are less than 1 nm in size. Water in IGPs and interlayer spaces has different binding energy. The removal of water from interlayer spaces causes collapse in the layered structure, while the removal of water from IGP does not change the volume of globules.

The gel pores are pores between globules and can be classified in two groups of small gel pores (SGP) and large gel pores (LGP). The SGPs are the space between packed globules; their size is less than 3 nm. The LGPs are bigger pores between globules with a size of 3-12 nm.

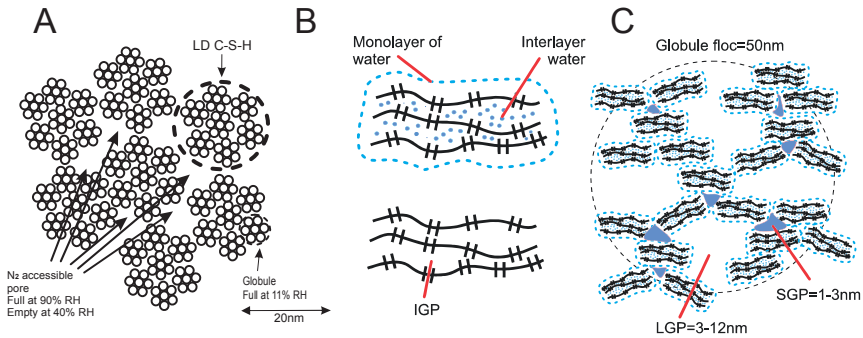

Figure 2.1. Jennings C-S-H models A:CM-I [10] , and B, C:CM-II [11].

2.3. Other hydration products

The AFm phases are hydrated tricalcium aluminate ferrite compounds such as monocarboaluminate, hemicarboaluminate, strätlingite, hydroxy AFm and monosulfate. These phases present different hydration states in different RHs and temperatures, which may cause shrinkage and damage in concrete structures. In **papers IV** and **V** different hydration states of these phases are discussed.

2.4. SCMs

Supplementary cementitious materials (SCMs) are added to cement clinkers to reduce the consumption of clinker. They are often used to make concrete mixtures more economical, and in they can enhance some properties such as reduced permeability, increased strength and improved workability [28]. These materials are generally by-products from other processes or natural materials; typical examples are fly ash, granulated blast furnace slag, silica fume and natural pozzolans.

The knowledge about the hydration process and the hydration products in systems with Portland cement and SCMs (blended cements) is insufficient [6]. The reaction of SCMs is usually slower than the reaction of the clinker phases. The SCMs act as ”fillers” in the beginning of hydration processes. This filler effect increases the reaction rate of clinker phases. Studies [5, 29, 30] show a significant difference in structure between

the C-S-H formed in Portland cement and blended cements containing SCMs. In Portland cement the C-S-H has a "fiber" structure, while with the addition of SCMs, it has a more "foil" like structure. In reality the hydration of SCMs influence the hydration of the clinker phases and the reactions happen simultaneously, therefore there is no point in studying them separately. The changes in structure lead to changes in the pore structure, which can improve some properties of blended cements such as long term strength and transport properties, but which can possibly also change some properties for the worse.

Cementitious materials are made of Ca-Si-Al-O. These four elements are the most common elements in the earth's crust: oxygen (49.4%), silicon (25.8%), aluminum (7.57%), calcium (3.39%). Figure 2.2.A shows the ternary diagram of CaO-SiO_2-Al_2O_3. OPC and commonly used SCMs are shown in this diagram; it can be seen that most SCMs fit into this diagram and that they are silica-aluminate materials with lower Ca in comparison with OPC. Figure 2.2.B shows hydration products in the same type of phase diagram.

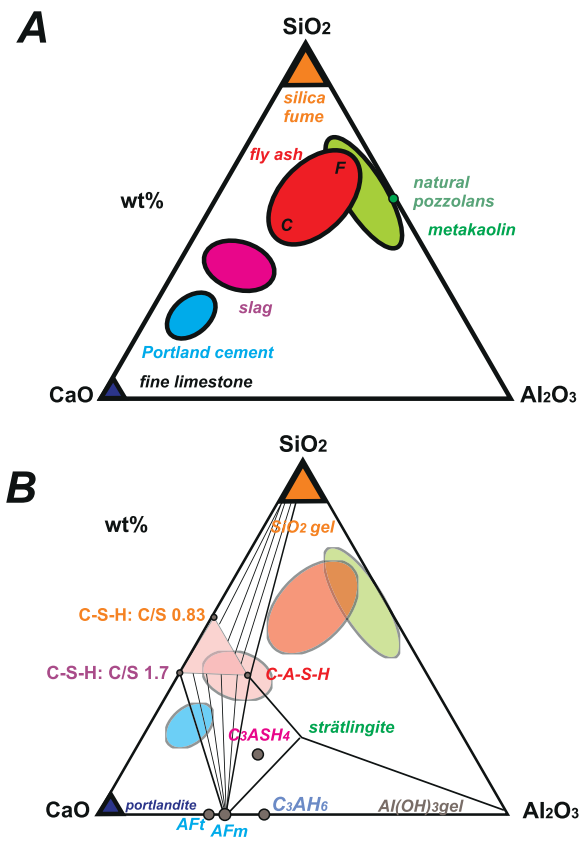

Figure 2.2. A:CaO-Al_2O_3-SiO_2 ternary diagram of cementitious materials , B:hydrated phases in the CaO-Al_2O_3-SiO_2 system [6].

2.4.1. Slag

Slag is a nonmetallic by-product from the blast furnace in the iron producing industry. The liquid slag to be used as an SCM is rapidly cooled and then ground into grains with a similar size as cement powder. The slag should satisfy the standard specification of EN-15167-1 [31]. The slag is usually used to 20-70 % by mass of cementitious materials [32].

The presence of slag causes the formation of C-S-H with a lower Ca/Si ratio, and Al uptake in the C-S-H structure. In addition, the monocarbonate disappears and more hydritalcite-like solids are formed due to the presence of MgO in slag. The amount of portlandite decreases in comparison with OPC and AFm phases formed including strätlingite [6, 29, 33, 34].

2.4.2. Silica fume

Silica fume is a fine particle material with the particle size 100 times smaller than the average size of cement grains. Silica fume is the by-product from the manufacture of silicon or ferro-silicon metal. It is collected from the fuel gases in electronic arc furnaces. The standard specified for silica fume in concrete is EN 13263-1 [35], and it is generally used to about 5-12% by mass of cement materials in concrete structures to increase strength and reduce the permeability to water [32].

Because of the small particle size of silica fume, its reactivity is higher than that of, for example, slag. The hydrate products in the presence of silica fume are mainly C-S-H with a low Ca/Si-ratio, ettringite, AFm phases and the amount of portlandite is reduced compared to that of pure OPC [6, 36, 37].

3. Sorption isotherms and hysteresis

Sorption isotherms are used to predict the moisture content in cementitious materials under changing moisture conditions. Concrete structures are constantly exposed to different relative humidities (RHs). It is known that these materials show hysteresis between absorption and desorption. In this section the general theories for the nature of hysteresis in low and high RH intervals are summarized. The chapter continues with moisture in cement based materials. In the final part the nitrogen isotherms are compared with water vapor isotherms.

In **paper I** there is a description of the water state in material related to microstructure. This discussion is made in terms of a few different populations of pore sizes, as proposed by Jennings. No pore size distributions were calculated. A previous study [38] shows that the commonly used Barrett, Joyner and Halenda method (BJH) [39] is difficult to use and the results are uncertain as they depend on which model is used for multilayer adsorption and if the absorption or desorption curve is used. We, therefore, avoid using the BJH model and it is not discussed further in this chapter.

State of the art:

Water vapor sorption isotherms are essential data for durability models of cement based materials. In addition, they contain information about pore structure, surface area and pore water interaction. It is well known that cement-based materials show sorption hysteresis and there are theories of why there is hysteresis.

Presently there is a lack of systematic studies of sorption isotherms and sorption hysteresis for cement based materials with SCMs.

Questions to be answered:

How does the presence of SCMs change the sorption isotherms and the sorption hysteresis compared to OPC?

How do the SCMs change the pore size distribution?

What does the sorption isotherm look like at high RHs (the super hygroscopic range)?

Answers (paper I):

The sorption isotherms for OPC samples and samples with SCMs (OPC+70% slag and OPC+10% silica fume) have a similar qualitative appearance. The samples with SCMs have a higher moisture content than OPC samples with the same w/b-ratio; they have a greater amount of gel pores and a lower amount of capillary pores. At low RHs all samples have similar desorption curves and the introduction of SCMs induce only slight increases in BET surface area.

It is difficult to experimentally validate sorption isotherms at high RHs because the critical RH of the pore solution is lower than 100%. This critical RH depends on the amount of alkali in the pore solution. A more detailed discussion about these problems is presented in **paper I**.

3.1. Moisture in cement based materials

Moisture in cement based materials can be provided from two different sources. Firstly, the water is added to dry cement for the hydration during casting. This amount of water is usually higher than the amount of water needed for full chemical reactions; typically w/c=0.25 is enough for all chemical reaction for OPC [40], but usually cement based materials cannot reach a fully hydrated state because of the slow kinetics of the reactions. The excess water will be left in the material and is usually dried out to some extent before the material is used. Secondly, when a material is in its use phase it can

take up water both from the vapor in the air (the ambient RH) and liquid water (rain, condensation, ground water etc.), and it can lose water (dry) to the ambient air if this is drier than the material.

The moisture state of cement based materials is usually discussed in terms of sorption isotherms, i.e., the relation between RH and moisture content at equilibrium. Water vapor sorption isotherms of cement paste and mortars studied in this project are presented in **paper I**.

3.2. Sorption

Generally, when a porous material such as a cement based material is exposed to a certain relative humidity the moisture content of the material is changed (it absorbs or desorbs water) to reach the equilibrium. If the surrounding RH is higher than the RH inside the material, the material start to absorb water; if it is lower it will desorb water.

The physical sorption in cement based material takes place in two different processes: adsorption and capillary condensation. At low RH (RH<40%) the vapor molecules only adsorb on the surface of the material. In this range the specific surface area (*SSA*) can be estimated using the BET equation:

$$SSA = \frac{AN_A}{M_w} V_m \quad (3.1).$$

Here *SSA* is a specific surface area, V_m is the volume of adsorbed gas when the surface of the material is completely covered with a mono layer molecule, N_A is Avogadro constant, M is molar mass of vapor, and A is the area occupied with one gas molecule.

At higher RHs (RH>40%) the capillary condensation takes place in the pores. The capillary condensation is a process in which the pores become filled with condensed liquid from the vapor phase. Capillary condensation is formulated with the Kelvin equation:

$$\ln \varphi = \frac{2\gamma V_m}{r_m RT} \quad , \quad (3.2)$$

where γ is surface tension (N m^{-1}), V_m is molar volume of the liquid (m^3) and r_m (m) is the mean radius of curvature of the meniscus (complete wetting is assumed).

The sorption isotherm can be measured in hydroscopic and super hygroscopic range. The hygroscopic range is up to approx. 98% RH, and higher than this range is called super-hygroscopic range [41]. Common methods to measure sorption isotherm are the

dynamic vapor sorption (DVS) method for the hygroscopic range and the pressure plate for the super-hygroscopic range. These methods were used in **paper I**.

3.3. Hysteresis

Generally, a system shows hysteresis when the amount of a dependent variable Y as a function of X is dependent on the direction of the changes of the variable X. A closed loop can be seen when the dependent value Y is plotted as a function of X. The loop corresponding [41] to the maximum range of values of X over hysteresis is called the boundary loop, main loop or the envelope. A scanning curve is the path the system follows when the direction is reversed before it reaches the limit of loops [42].

Hysteresis has been seen for many different phenomena in different fields of science. It has been seen in ferromagnetic and ferroelectric materials and also in the mechanical behavior of some materials like viscoelastic materials. For example, when a ferromagnetic material is exposed to an external magnetic field, the atomic dipoles align to the magnetic field. When the magnetic field is removed parts of the alignment still remain. This effect is used in hard disks, magnetic tapes and credit cards. Hysteresis can occur during sorption processes. In this case, the amount of vapor absorbed is different in absorption than desorption.

The hysteresis can be described with irreversible thermodynamic changes. The thermodynamic requirements for hysteresis in sorption were discussed by Everett [42]. He mentioned that the thermodynamic requirement for any mechanisms to be able to show hysteresis is that the mechanisms should increase the entropy of system. Everett considered a cylinder with a piston that contains a sample of absorbent and a very dilute gas (effectively at zero pressure). The piston could move reversibly until the saturation condition is reached and then move back to the starting condition under isothermal conditions. The work W (J) done by the surroundings on the system in any step in the cycle is calculated from Eq. 3.3. Here p (Pa) is the pressure and V (m^3) is the volume of the system.

$$dW = -pdV \quad (3.3).$$

If it assumed that the vapor behaves as a perfect gas and the cylinder contains n^0 moles of gas and at the given pressure n^a moles are adsorbed,

$$V = \frac{(n^0 - n^a)RT}{p} \qquad (3.4),$$

$$dV = [(n^0 - n^a)RT / p^2]dp - (RT / p)dn^a \qquad (3.5),$$

$$dW = (n^0 - n^a)RTd\ln p + RTdn^a \qquad (3.6).$$

In a complete cycle from $p=0$ to $p=p^0$ and back to p^0 the total work can be calculated as,

$$\Delta W = \oint dW = -RT\oint n^a d\ln p \qquad (3.7).$$

Thus, in the presence of hysteresis the area of the loop in curve of n^a vs. lnp, multiplied by RT, shows an increase in the potential energy of system in one cycle. If it is assumed the components in the system return to their initial states, the system must be accompanied the energy by an irreversible entropy production:

$$\Delta S = R\oint n^0 d\ln p \qquad (3.8).$$

This can be described with the difference between the heat given out by the adsorption process (ΔQ_{ads}) and that taken in during the desorption process (ΔQ_{des}):

$$\left|\Delta Q_{ads}\right| - \left|\Delta Q_{des}\right| = T\Delta S \geq 0 \qquad (3.9).$$

The isotherm is smooth on a macroscopic scale. The irreversible entropy changes are too small to be detected individually and they show as a series of microscopically irreversible processes.

For cement based materials hysteresis can be found at all RH ranges. Different mechanisms have been suggested by different authors to explain the origin of hysteresis. As sorption takes place by partly different mechanisms at different RH-ranges the discussion is divided into low and high RHs.

3.4. Hysteresis at high RHs

At high RH intervals (RH>50%) the capillary condensation in pores in the material are described as the main reason for hysteresis. The mechanisms that describe the hysteresis at high RHs are mentioned below.

3.4.1. Different curvature of interface liquid-vapor

During capillary condensation and capillary desorption the hysteresis can be explained with the Kelvin equation (Eq. 3.2).In a single cylindrical pore Eq. 3.10 is valid.

$$\frac{2}{r_m} = \frac{1}{r_1} + \frac{1}{r_2} \qquad (3.10)$$

Here r_1 and r_2 are the principle radii of the curvature of the liquid vapor interface. In cylindrical pores with two sides open (Fig. 3.1) the mean curvature is different during absorption and desorption. In absorption $r_1=\infty$ and $r_2 = r^p - t$. Here, t is the thickness of the adsorbed layer and r^p is the pore radius (note that t is not a constant as it is a function of RH).

Thus, the kelvin equation in absorption is:

$$\frac{2}{r_m} = \frac{1}{(r^p - t)}\ , \qquad (3.11)$$

$$\varphi_{cap,abs} = \exp\left(\frac{-\gamma V_m}{RT(r^p - t)}\right)\ . \qquad (3.12)$$

However, in desorption $r_1 = r^p - t$, and $r_2 = r^p - t$; so the $\varphi_{cap,des}$ that the same pore is emptied at is:

$$\frac{2}{r_m} = \frac{1}{(r^p - t)} + \frac{1}{(r^p - t)}\ , \qquad (3.13)$$

$$\varphi_{cap,des} = \exp\left(\frac{-2\gamma V_m}{RT(r^p - t)}\right). \qquad (3.14)$$

From above it can be concluded that for a pore with radius of r^p, $\varphi_{cap,des}=\varphi^2_{cap,ads}$. These mechanisms depend on the pore geometry. For example, for cylindrical pores with one open end, hysteresis does not exist [43, 44].

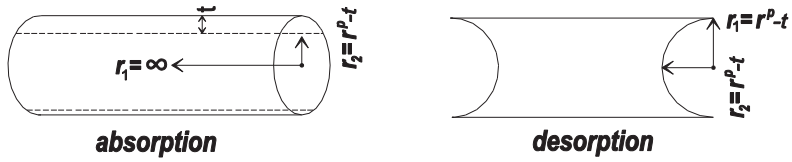

Figure 3.1. Schematic picture of cylindrical pore with open sides in A: absorption and B: desorption. The curvature of liquid vapor interface are shown with r_1 and r_2.

3.4.2. Inkbottle model

Inkbottle is used as a mathematical model to describe hysteresis in real pore systems. In this model (Fig. 3.2), the bottle and neck of pores are cylindrical with a radius of r and R. The pores with radius R are connected to one or more pore necks with radius r. Espinosa et al. [45] mentioned that the drying and chemical aging in cement-based materials leads to the formation of inkbottle pores.

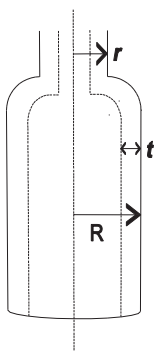

Figure 3.2. Ink bottle pore

According to the Kelvin equation in absorption, the neck and bottles of pores are filled in different water activities. The necks are cylindrical pores with open ends on two sides and the bottle is a cylinder pore with one open end.

$$\varphi_{cap,cond,r} = \exp\left(\frac{-\gamma V_m}{RT(r-t)}\right) \qquad (3.15)$$

$$\varphi_{cap,cond,R} = \exp\left(\frac{-2\gamma V_m}{RT(R-t)}\right) \qquad (3.16)$$

In this case if $R-t$ is larger than $2.(r-t)$, then $\varphi_{cap,cond,r} > \varphi_{cap,cond,R}$, which means the capillary condensation takes place first in the neck and then at the bottle. On the other hand if $R-t$ is smaller than $2.(r-t)$, capillary condensation starts at the bottle of the pores and then fills up the necks at a higher RH.

In desorption at a water activity of $\varphi_{cap,des}$ the meniscus formed in the neck and the whole inkbottle is emptied at

$$\varphi_{cap,des} = \exp\left(\frac{-2\gamma V_m}{RT(r-t)}\right). \qquad (3.17)$$

For the reasons mentioned above, the pores with larger radius (*R*) are emptied at smaller φ corresponding to neck pores and this leads to hysteresis in sorption. An attempt to take into account the inkbottle effect in modeling the hysteresis has been done by Espinosa at al. [45].

3.4.3. Chemical reaction and aging

Cement-based materials are not inert to water and in the presence of enough water the hydration process can proceed. This effect is more noticeable at lower ages and at high RHs [44, 46]. Carbonation is another chemical reaction that can cause changes in cement-based materials. However, none of these mechanisms leads to hysteresis.

3.5. Hysteresis at low RHs

Theoretically there should not be any hysteresis at low RHs, and it has not been seen in the case of non-polar vapors at low temperature, such as nitrogen and helium for cement based materials [47-49]. In this range the hysteresis can be explained as being due to the irreversible uptake of interlayer water in C-S.H structure. In this theory the remove of water between C-S-H layer causes pore collapse and microstructure changes. [12, 15, 16, 50].

Bazant and Bazant [51, 52] argue that the pore collapse has never been documented experimentally and it cannot fulfill the mechanical models. They describe two mechanisms that may be responsible for hysteresis at low RHs. In the small pores, for which the pore radius is smaller than free absorption thickness (according to the BET equation) the pore does not have any surface in contact with the vapor, the absorption

is hindered and transverse disjoining pressure is formed in the wall. In cement based materials the free absorption thickness can be up to 5 molecules, therefore disjoining pressure exists in pores with a diameter of less than 2.6 nm. The absorption hindered due to the disjoining pressure cannot cause hysteresis by itself, but two mechanisms suggested by Bazant and Bazant try to describe the hysteresis in this range by taking into account hindered sorption.

3.5.1. Snap through instabilities

If a wedge-shaped nanopore between two diverging planer walls is considered (Fig. 3.3), for any individual molecule, the chemical potential can be altered by transverse tension, which is formed at the filling front, or compression, which acts across the monomolecular layer, until the pore is completely filled. This leads to many metastable points in the chemical potential of adsorbed molecules.

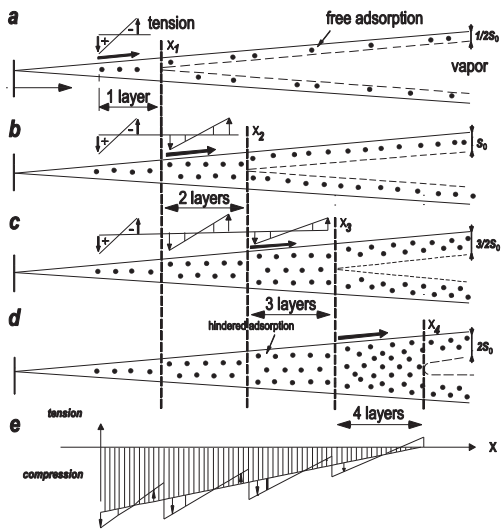

Figure 3.3. Filling of a diverging nano pore and disjoining pressure [51].

This means that when the filling front reaches the critical points of X1, X2 or X3, which represent different numbers of monomolecular layers, the absorbed amount jumps at a constant vapor pressure. The snap through instabilities for absorption and desorption follow different paths, and this can explain hysteresis. This mechanism is weak for pores wider than 3 nm [51].

3.5.2. Molecular condensation

The second mechanism is a molecular coalescence or capillary condensation, within the partially filled surface in nanopores or the nanopores network. Bazant and Bazant [52] present a model in which the adsorbed layer can coalesce into non-uniform patches or droplets (low and high density phases) at low RHs due to short range intermolecular attractions. A simple example is molecular condensation in a straight monolayer thick pore in absorption and desorption (Fig. 3.4). By increasing the humidity the situation (Fig. 3.4a) become thermodynamically unstable and separate into locally stable low density and high density phase (Fig. 3.4b), which quickly absorb molecules and become stable, homogenous absorbate at high density (Fig3.4c). When the humidity decreases, the homogenous phase (Fig. 3.4d) destabilizes and coalesces to form the stable high and low density phases (Fig. 3.4e), which quickly change to homogenous low density absorbate (Fig. 3.4f). In this model the system passes through metastable states in absorption and desorption (Fig. 3.4b and c). These two states are not the same, which means the metastable state is irreversible and this causes hysteresis.

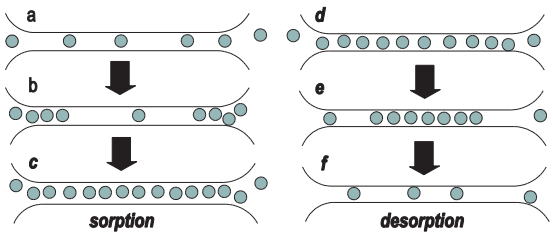

Figure 3.4. Molecular condensation in monolayer thick pore during absorption and desorption[52].

3.6. Nitrogen sorption isotherms

In the present project nitrogen isotherms were also measured at a low temperature to calculate the specific surface area [26, 53-55] (these results are only presented here and not in the papers).

Nitrogen sorption isotherms were measured at 77 K for cement paste samples (OPC paste, OPC+70% slag, OPC+10% SF with w/b=0.5). The hydration in the samples was stopped before analysis using isopropanol [56]. The samples were dried at 105 °C for 24 h before the experiment. These measurements were made at Holcim,

Holderbank, Switzerland. Figure 3.5 shows N_2 sorption isotherm measurement and water vapor sorption isotherms for the same samples.

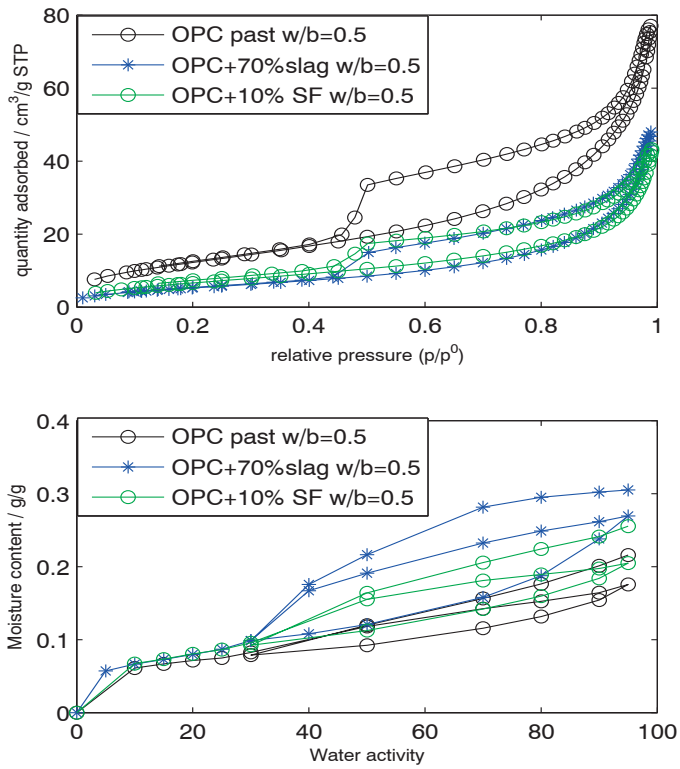

Figure 3.5. N_2 sorption isotherm and water vapor sorption isotherms for OPC, OPC+70% slag and OPC+10% silica fume (SF) paste samples with w/b=0.5. The data for water vapor is from paper I.

Table 3.1 shows the specific surface area (*SSA*) calculated for N_2 and water sorption isotherms using the BET equation. There is a different trend in N_2 and water vapor sorption isotherms. For water vapor sorption isotherms the moisture content is higher for samples with SCMs, while for N_2 isotherms the OPC samples absorbed a higher amount of vapor.

Tabe 3.1. Specific surface area (SSA) calculated from the BET model for N_2 and water vapor sorption isotherms

Sample	SSA (m^2g^{-1}) for N_2 isotherms	SSA (m^2g^{-1}) for water isotherms
OPC	45	203
OPC+70% slag	19.5	246
OPC+10% silica fume	24.7	242

The *SSA* calculated from water vapor sorption isotherms is around 5 times greater than that of N_2 isotherms. The SSA of OPC is twice that of the sample with slag and silica fume for N_2 isotherms, while it is higher for samples with slag and silica fume in water vapor sorption isotherms.

The higher *SSA* of water vapor isotherms as compared to that of N_2 isotherms was observed by other researchers and there have been different explanations for this [11, 15, 24, 57]. For example, N_2 molecules cannot penetrate into the neck of ink-bottle pores, while water vapor can enter all small pores. Also, water can enter the interlayer spaces, while this is not possible for N_2. Jennings explains that the N_2 penetrates only into low density (LD) C-S-H structure, while the high density (HD) parts are inaccessible for N_2.

These results for N_2 isotherms are in agreement with our discussion in which we concluded that the samples with SCMs have a greater amount of pores, but with a greater amount of gel pores and a lower amount of capillary pores than OPC. In N_2 isotherms the nitrogen cannot penetrate into gel pores, so the isotherms of the samples with SCMs absorb less N_2 than OPC.

3.7. Hydration state change of AFm phases

Water absorbs or desorbs in hydrated OPC mainly in tC-S-H structure. In addition of C-S-H, AFm phases are one of the main products formed during the hydration of cement based materials. Examples of these phases are monocarboaluminate, hemicarboaluminate, monosulfate, etc. Changes in RH and temperature can change the hydration state of AFm phases. Varying the state of hydration of these phases can have an effect on the density of these phases that can cause volume changes in structure. The impact of these hydration changes are rather small in OPC, but in systems containing SCMs with high amount of Al the amounts of AFm phases that can be formed is more than in OPC and the impact of hydration state changes can be more significant.

Currently there is a lack of systematic method of study and information about the critical RH where the transformation of phases of different hydration takes place and also the thermodynamic properties of the changes. X-ray diffraction method (XRD) and thermo gravimetric analysis (TGA) can provide information about the structure of different hydration states. In **Paper V** sorption balance and sorption calorimetry were used in addition to TGA and XRD. In this paper these techniques were discussed and the results from each are used to complement each other. Sorption balance and sorption calorimetry measurements were done in Lund University and XRD and TGA measurements were done at the laboratory of Holcim in Holderbank, Switzerland. Sorption calorimetry can measure moisture sorption isotherms and enthalpy of sorption process simultaneously [3]. This unique method was used for the first time in this project for the study of hydrated cement phases.

In **paper VI** an attempt was made to provide a database of hydration state and thermodynamic properties for absorption and desorption of water in the crystal structure of AFm phases.

State of art:

Significant advances have been made in the thermodynamic modeling of the hydration of cement based systems, and there are now several databases with thermodynamic data on hydrated substances. This makes it possible to predict, e.g., the resulting phase composition of a cement based material made with new binders and new additive materials. A limitation of the present data is that it only valid at water saturated conditions, something that may limit the usefulness of the data in predicting deterioration processes in cement based materials.

Questions to be answered:

Develop a methodology to determine thermodynamic properties of hydrated cement phases as a function of water activity.

Determine thermodynamic properties of selected hydrated cement phases.

Answers (papers V and VI):

Multi-method approach to study thermodynamic properties of hydrated cement phases has been developed. The phase diagrams and thermodynamic properties of monocarboaluminate-water, hemicarboaluminate-water, strätlingite-water, hydroxyl-AFm-water and monosulfoaluminate-water have been determined.

4. Moisture transport

An interaction of gases and liquids with concrete structure, steel bars and pore water leads to the deterioration in structures. Examples of these phenomena are alkali silica reaction (ASR), alkali aggregate reaction, chloride ingress, carbonation and frost damage. For all of these mechanisms the diffusion and transport of ions, liquid and gases are central [58-60].

Depending on the driving force for the water transport process and the nature of the transport phenomena different transport mechanisms can be distinguished. These mechanisms can be divided into two main groups, permeation and diffusion. Diffusion is formulated with Fick's first and second laws. In diffusion, matter is transported from one part of the system to another part due to differences in concentration (because of the random motion of molecules). Permeability is formulated with Darcy's law and describes fluid or gas movement through a sample under a (total) pressure difference.

In this part of the study we quantified the moisture transport coefficients with steady-state and dynamic methods. The cup method was used in the steady-state study and the sorption balance was used in the dynamic studies. The results of the dynamic method are presented in **paper II** with discussions about the limitations of Fick's law to evaluate the results. The steady-state results are presented in **paper III** and **paper IV**. **Paper III** is mainly focused on the new experiment set-up for cup measurements, and the effect of SCMs on moisture diffusion coefficients measured with the samples on absorption and desorption limbs, respectively. In **paper IV** different potentials were used to present the results from paper III in order to investigate if it was possible to decrease the hysteresis in transport coefficients.

State of art:

The durability of concrete structures is dependent on the transport properties of concrete (ion transport and moisture transport). Moisture transport is a function of the moisture state in the material. Most transport studies and models in the literature only focus on drying processes but structures in use are exposed to repeated drying and wetting cycles. Sorption hysteresis is a well-known phenomenon in sorption for cement based materials, but it is also necessary to understand hysteresis in the moisture transport coefficients for samples in absorption and desorption cycles.

Questions to be answered:

How do SCMs change the transport properties?

What is the RH-dependence of diffusion coefficients for cement based materials with SCMs?

Are moisture transport coefficients different for samples in absorption and desorption?

If there is such a difference, what is the best way to consider the hysteresis effect in evaluating moisture transport coefficients, and what is the best driving force in evaluating moisture diffusion coefficient?

Answers (papers III and IV):

The diffusion coefficient for OPC materials shows a strong dependence on RH at RH>60%. For materials with SCMs the dependence of D_v on RH is small. For OPC samples there are differences between D_v (diffusion coefficient with vapor content as potential) in absorption and desorption when presented as a function of RH. Samples in desorption have higher D_v than samples in absorption especially at RH>60%. This can be explained by using sorption isotherms and sorption hysteresis. For samples with SCMs, there is no clear difference. The hysteresis in the transport coefficient becomes smaller when D_v is drawn as a function of moisture content.

4.1. Fick's law

Mass diffusion can be described with Fick's laws. In this case the particles move as a results of random molecular motion from higher to lower concentrations, to decrease the concentration differences (see Fig. 4.1). This is formulated with Fick's first law (Eq. 4.1) [61],

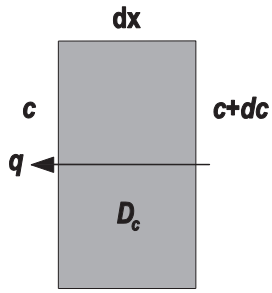

Figure 4.1. An illustration of Fick's law for mass diffusion.

$$q = -D_c \frac{dc}{dx} \qquad (4.1)\ .$$

Here q (g m^2 s^{-1}) is the mass flux, D_c (m^2 s^{-1}) is diffusivity, c (g m^{-3}) is the concentration of the diffusing particles, and x (m) is the distance.

The change in the concentration of diffusing particles over time can be described with Fick's second law, which is a combination of Eq. 4.1 and mass conservation:

$$\frac{\partial c}{\partial t} = \frac{\partial q}{\partial x} = \frac{\partial}{\partial x} D_c \frac{\partial c}{\partial x} \qquad (4.2).$$

In most cases it is assumed that the D_c is constant and Eq 4.2 can then be written as [61]:

$$\frac{\partial c}{\partial t} = D_c \frac{\partial^2 c}{\partial x^2} \qquad (4.3).$$

Solutions to Eq. 4.3 are discussed for different boundary and initial conditions by Crank [62]. If D_c is not constant the mathematics for solving Eq. 4.2 becomes complex.

4.2. Darcy's law

The flow of liquid through porous materials is described with Darcy's law. The law was formulated based on the results of experiments on the flow of water through beds of sand. A schematic illustration of Darcy's law is given in Fig. 4.2 and related formulation is shown in Eq. 4.4 [63].

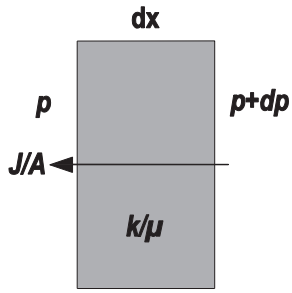

Figure 4.2. An illustration of Darcy's law

$$J = \frac{kA}{\mu}\frac{dp}{dx} \qquad (4.4)$$

Here J ($m^3 s^{-1}$) is the total flow, k (m^2) is intrinsic permeability of material, A (m^2) cross section area to flow, μ (Pa·s) is dynamic viscosity, and p (Pa) is the pressure. Note that the structure of Darcy's law is similar to the structure of Fick's law, but Darcy's law is written in terms of volumetric flow and that for convenience the cross sectional area and the viscosity are given as separate terms.

Darcy's law for liquid flow through porous material is related to Hagen-Poiseuille's equation for liquid flow through a cylindrical pipe [64],

$$J = \frac{\pi r^4}{8\mu}\frac{dp}{dx} \qquad (4.5).$$

Here, ρ ($g\ m^{-3}$) is the water density, μ (Pa·s) is the dynamic viscosity, and p (Pa) is the pressure of the pore water. In Hagen-Poiseuille's and Darcy's equation the pore water pressure can be written in terms of the vapor content using the Kelvin equation. In some studies [50, 65, 66] related to cement based materials the Eq. 4.4 was written as:

$$q = \frac{kA}{\mu v_s}\frac{\partial s}{\partial x}\frac{\partial \varphi}{\partial s}. \qquad (4.6)$$

Here, s is water saturation φ is water activity, ∂s/∂x can be calculated from the equilibrium moisture profile and ∂φ/ ∂s is the reverse of slope of sorption isotherms.

4.3. Total moisture transport

Total moisture flux can be calculated as a sum of water vapor diffusion and water liquid diffusion.

$$q_{total} = q_v + q_l = -D_v \frac{\partial v}{\partial x} - \frac{k^{\alpha}}{\mu} \frac{\partial p}{\partial x} \qquad (4.7)$$

However, in most experimental methods it is only possible to measure total flux and it cannot be separated into vapor and liquid flux. However, some models assume that in low RHs the transport is controlled with vapor transport and at high RHs the vapor transport is negligible in comparison to liquid transport [66, 67]. In the mixed region the situation is complex, as we have mixed vapor and liquid transport at all points, as seen from a macroscopic perspective.

4.4. Transport in a single pore

In one single pore, the basic phenomena that are active during water vapor transport are adsorption-desorption, diffusion and condensation-evaporation. Figure 4.3 shows the active mechanisms in a single pore in different RHs or moisture content. At low RHs (Fig. 4.3A) the water molecules start to form an adsorbed layer on the pore wall and vapor molecules move by diffusion. In this RH range the vapor diffusion is the main mechanism. Two different mechanisms of vapor flow can be distinguished depending on the pore radius. In small pores (<2.5 nm) the main diffusion resistance is the collisions between molecules and wall. In this case the diffusion mechanism is Knudsen diffusion. Knudsen diffusivity for straight cylindrical pore is formulated as:

$$D = \frac{d}{3} \sqrt{\frac{8RT}{\pi M_A}} \qquad (4.8).$$

Where R ($Jmol^{-1}K^{-1}$) is the gas constant, M_A (g) is the molecular weight of a diffusive particle, T (K) is temperature and d (m) is pore diameter. This diffusivity can be used in Fick's law. In the larger pores the molecular diffusion is the main mechanisms and modeled with Fick's law.

At higher RHs (Fig. 4.3B) the thickness of the adsorbed layer is increased. Another active transport mechanisms that is active in Fig. 4.3A and b is surface diffusion. Surface diffusion is usually described with two mechanisms. At low water contents (lower than that of the monolayer region) the molecules jump randomly from site to site. At higher

moisture content (Fig. 4.1B), when a thicker adsorbed layer is formed, the surface transport is modeled with a hydrodynamic model. In this model the molecules on the solid surface are considered to be a thin flowing film of viscous liquid. According to most studies, surface diffusion can be ignored in comparison to molecular diffusion [68, 69].

At high enough RHs the adsorbed water starts to form a meniscus in pores and the pore starts to become completely filled according to Kelvin's equation. At this point water molecules condense at one end of the pore while at the other end they evaporate (Fig. 4.1C). In Fig. 4.1D the pore is filled with condensed liquid and the liquid phase flow is the main mechanisms, and Darcy's law and Hagen-Poiseuille equations can be used.

As mentioned above, in real cement based materials it is hard to separate each of these mechanisms as they do not combine in a simple way, and it is only possible to measure the combination of all mechanisms. In addition, in a cement based material structure the pores are connected and aggregates and cracks also affect the transport properties [70] .

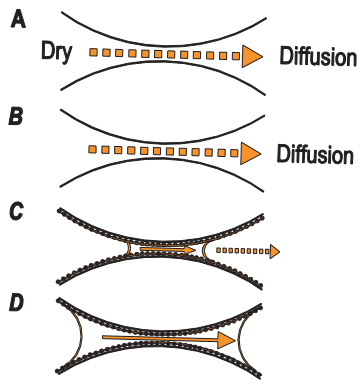

Figure 4.3. Different active transport mechanisms in a single pore by increasing moisture content in the pore from A to D: A) vapor diffusion; B) an absorbed layer is formed on the wall of pore- vapor diffusion and surface diffusion and are active; C) capillary condensation starts and conensation-evaporation is the main mechanisms; D) The pore is filled with liquid- liquid phase flow is the transport mechanism.

4.5. Moisture transport with different potentials

Different methods can be used to measure moisture transport properties. Some of these methods are described in reference [71]. The moisture transport coefficient can be described with different potentials (driving forces) based on different potential that were used. All these coefficients are possible to convert into each other with mathematical equations (Eq. 4.9-4.11). The common potentials that can be used are vapor content v (g m^3), pore water pressure P_w (Pa), moisture content c (g m^3), moisture content by mass u (g g^{-1}), degree of saturation s, and pore humidity φ.

$$q = -k_{RH}\frac{\partial \varphi}{\partial x} = -D_c\frac{\partial c}{\partial x} = -D_v\frac{\partial v}{\partial x} = -\frac{k}{\mu}\frac{\partial p_w}{\partial x} \qquad (4.9)$$

$$D_v = k_{RH}\frac{\partial \varphi}{\partial v} = \frac{k_{RH}}{v_s} \qquad (4.10)$$

$$D_c = D_v\frac{v_s}{\frac{\partial c}{\partial \varphi}} = \frac{k}{\mu}\frac{\partial p_w}{\partial c} \qquad (4.11).$$

In Eq. 4.11, $\partial c/\partial \varphi$ is the slope of sorption isotherms (the moisture capacity) and $\partial c/\partial P_w$ is the slope of suction curve [72].

It is essential to understand the differences between these transport coefficients. In **paper II** we used sorption balance measurements to evaluate transport coefficients for cement paste samples. The results are naturally D_c (diffusivity) and moisture content is the potential, as the measurement was dynamic. To be able to compare these results with results from the steady-state cup method which gives D_v (vapor content as potential) we need to use Eq. 4.11. In **paper IV** the D_v results from the cup method are recalculated to D_c using the slope of sorption isotherms.

4.6. Steady-state and unsteady-state diffusion

If a sample has been placed between different constant RHs for a long time, the flow through it will be in steady-state. If the boundary conditions are changed to new constant values there is a transient (unsteady-state) period during which flows and moisture conditions are changing; after this a new steady-state is reached.

Steady-state diffusion is formulated with Fick's first law (Eq. 4.1), while under unsteady-state circumstances, where concentrations and fluxes are varying with time, Fick's second law needs to be used (Eq. 4.2).

The main principle for measuring steady-state diffusion coefficient is to apply a potential difference over a sample with a certain thickness and weight until steady flow is reached, and evaluate the diffusion coefficient with Fick's first law. The most common method for this is the cup method. In the cup method the steady-state flow is calculated from the mass change rate of the cup as the cup contains a saturated salt with constant RH that either absorbs water vapor diffusing into the cup or desorbs water vapor that will leave the cup. The steady-state flow is reached when the mass change rate of the cup is constant. This is described further in **paper III** and **paper IV**.

The principle of unsteady-state method is to measure profile or mass gain/loss in a sample at a certain time or as a function of time. An example of unsteady-state method is the dynamic sorption method. In this case a sample equilibrated to a certain RH with a thickness of 2L is exposed to an external constant RH on both sides, for example in a sorption balance [73]. With this method the flow is one-dimensional and it is possible to measure mass of the sample by time. The analytical solution for this situation is given by Crank [62]:

$$E = \frac{\Delta M_t}{\Delta M_\infty} = 1 - \sum_{n=0}^{\infty} \frac{8}{(2n+1)^2 \pi^2} \exp\left[\frac{-D_c (2n+1)^2 \pi^2 t}{4l^2}\right] \qquad (4.12).$$

Here E is a fraction mass change, ΔM_t and ΔM_∞ (g) are mass changes at time t and after infinitive time.

For the above type of process, the plot of E as a function of the square root of time is linear up to at least E=0.5, and the diffusivity can be calculated from the slope of the linear part of this curve:

$$D_c = \frac{\pi l^2}{4} \left(\frac{dE}{d\sqrt{t}}\right)^2 \quad . \qquad (4.13)$$

We have used small cement paste samples (diameter 5.5 mm, L=2mm) to measure diffusion coefficients with concentration as potential (D_c) using the dynamic sorption method. The results are discussed in **paper II**. Our results show that the sorption in these thin samples is taking place at two different timescales and they cannot be evaluated only with Fick's law; we have described this sorption as being anomalous. The initial part of the sorption curve which takes place on a shorter timescale is the transport of water vapor into the sample. There is also sorption taking place on a much longer timescale - not related to the one dimensional Fickian transport into the material - that temporarily takes place in the nanostructure of the materials (see the next section). With this method it may be possible to get more information related to the transport and sorption of water in the nanostructure of cement based materials, like in the C-S-H-structure.

The cup method was used to measure steady-state diffusion coefficients with vapor content as potential (D_v). In this method the samples are larger than in the dynamic

sorption method (diameter 65mm, L=15mm), and the steady-state diffusion is measured as results. The cup method is more practical than the dynamic sorption method since most transport processes in concrete structures are slow and macro diffusion is close to steady-state conditions is the main transport mechanisms. The anomalous diffusion can be seen in very small samples.

4.7. Anomalous diffusion

In many studies it has been found that the measured transport cannot be described with Fick's law, especially in polymers [74-78] and wood [79]. The basic equation for mass uptake as a function of time after an external step change of RH can be written as Eq. 4.14. Here n and k are constants, and n shows the type of diffusion mechanism.

$$\frac{M_t}{M_\infty} = kt^n. \qquad (4.14)$$

Neogi [80] generalized different diffusion mechanism as below.

n=1/2 Fickian diffusion (case I)

n>1 super case II

n=1 case II

1<n<1/2 anomalous

n<1/2 psedu-Fickian

Case II diffusion and anomalous diffusion have received a lot of attention in glassy polymers. Crank [62] described anomalous sorption as being related to the influence of the changing polymer structure on solubility and penetrant mobility, or as being caused by internal stresses from one part of the medium on another as diffusion proceeds. The latter explanation is called relaxation in polymers, and is not a likely explanation for the anomalous sorption discussed in **paper II**.

State of art:

It is known that Fick's law cannot fully describe diffusion of solvents in polymers. For cement based materials no convincing evidence has been presented to the effect that vapor transport does not obey Fick's law.

Question to be answered:

Does moisture transport in cement based materials follow Fick's law?

Answer (papers II):

We have shown that non-Fickian transport mechanisms operate in cement based materials, but their timescales are quite short so they will not influence the calculation on real structures. However, it is not optimal to measure transport coefficients on small samples with short time constants if one wants to assess transport coefficients for use in real structures.

5. Summary of results

- Sorption isotherms both in absorption and desorption were measured (**paper I**).
- Dynamic sorption measurements made on thin paste samples showed that there is a slow (anomalous) sorption component in cement based materials (**paper II**).
- A new set-up for carbon dioxide free cup measurements was developed and tested (**paper III**).
- Measurements of steady-state transport coefficients were made (**paper III**).
- It was shown that sorption hysteresis influences the transport coefficients (**paper III**).
- Different ways of representing the transport coefficients were tested, but none of these could remove the influence of hysteresis (**paper IV**).
- A systematic methodology to determine hydration states of cement hydrates and related thermodynamic properties were investigated (**paper V**).
- Different hydration states of AFm phases and thermodynamic properties associated with changes during absorption and desorption were studied (**paper VI**).
- From the present studies it seems that the best methods to characterize sorption and transport properties of uncarbonated cement based materials is by sorption measurements on paste or mortar in sorption balances and by cup measurements in CO_2-free atmosphere.

6. Future research

- To be able to predict the shape of the sorption isotherms at high RHs, the critical RHs should be assessed. This is possible with computer modeling of pore solutions and also by extracting pore solution from saturated samples.
- A systematic method to separate the anomalous and Fickian part of the sorption curve for dynamic sorption measurements needs to be developed.
- More investigations are needed to describe the effect of SCMs on diffusion coefficients hysteresis. The reason for the minimum in absorption and maximum in desorption in D_v for such samples is not clear.
- There should be further investigations of the relations between transport coefficients of pastes, mortars and the corresponding concretes.
- The possibility of using the critical RH of the saturated pore solution as the maximum RH inside the cups in the cup method instead of reverse cups and 100% RH inside the cups should be investigated.
- Use the present set of methods on materials made from other types of blended cements, for example the newly developed LC^3-cements.

Acknowledgments

The research leading to these results has received funding from the European Union Seventh Framework Program (FP7/2007-2013) under grant agreement 264448.
I would like to use this opportunity to thank my supervisor Lars Wadsö and my co supervisor Peter Johansson for their support during my PhD project and also my cultural shocks in Sweden. I also want to thank Lars-Olof Nilsson for time to time useful discussions and advices.
I would like to thank all PhD students in Transcend project for all nice time we had together during courses, meetings and after courses drinks. Special thank to Arnoud Muller and Luis Baquerizo for helping me to find my way during my stay in sunny Switzerland.
Thanks go to the people in construction materials in EPFL and Holcim for all their help with my project.
I would like to thank technical staff in our department for their help. Thank you Bosse Johansson not only for helping me with casting samples and my cup measurements but also for nice time during wine testing and discussion about art and movies. Thank you Stefan Backe because of your magic hand to solve all technical problems. Thank you Bengt Nilsson for helping with all DVS problems and angry discussions about politics.
I would like to thank all my colleagues at BM, especially Nilla Olsson for sharing the moments of "hard to understand the results" and Magnus Åhs for lighting a candle in our darkness of lack of knowledge while he passes our office. Thank you, Katja Fridh for always make me believe that my work make sense. Thank you Heidi Francke and Marita Persson for helping me to find my way in all complicated administration systems.
I would not have made it without the support of my old friends in Iran and new friends in Sweden. I would like to thank my family especially my parents and my sisters for their support. At the end, I would like to thank my Love (I would not write any name here in the case of change the person).

References

1. Gartner, E., *Industrially interesting approaches to "low-CO2" cements.* Cement and Concrete Research, 2004. **34**(9): p. 1489-1498.
2. Hendriks, C.A., et al., *Emission Reduction of Greenhouse Gases from the Cement Industry* Proceeding of the 4th International Conference on Greenhouse Gas Control Technologies, 1998.
3. Wray, P., *Straight talk with Karen Scrivener on cements, CO2 and sustainable development*. 2012, American Ceramic Society. p. 47-50.
4. *MC ITN TRANSCEND Website*. [cited 2014; Available from: http://www.nanocem.org/index.php?id=282.
5. Scrivener, K.L. and A. Nonat, *Hydration of cementitious materials, present and future.* Cement and Concrete Research, 2011. **41**(7): p. 651-665.
6. Lothenbach, B., K. Scrivener, and R.D. Hooton, *Supplementary cementitious materials.* Cement and Concrete Research, 2011. **41**(12): p. 1244-1256.
7. Taylor, H.F.W., *Cement Chemistry*. 1990: Academic Press.
8. Bullard, J.W., et al., *Mechanisms of cement hydration.* Cement and Concrete Research, 2011. **41**(12): p. 1208-1223.
9. Richardson, I.G., *The calcium silicate hydrates.* Cement and Concrete Research, 2008. **38**(2): p. 137-158.
10. Jennings, H.M., *A model for the microstructure of calcium silicate hydrate in cement paste.* Cement and Concrete Research, 2000. **30**(1): p. 101-116.
11. Jennings, H.M., *Refinements to colloid model of C-S-H in cement: CM-II.* Cement and Concrete Research, 2008. **38**(3): p. 275-289.
12. Thomas, J.J., A.J. Allen, and H.M. Jennings, *Structural Changes to the Calcium–Silicate–Hydrate Gel Phase of Hydrated Cement with Age, Drying, and Resaturation.* Journal of the American Ceramic Society, 2008. **91**(10): p. 3362-3369.
13. Thomas, J.J. and H.M. Jennings, *A colloidal interpretation of chemical aging of the C-S-H gel and its effects on the properties of cement paste.* Cement and Concrete Research, 2006. **36**(1): p. 30-38.
14. Muller, A.C.A., et al., *Densification of C–S–H Measured by 1H NMR Relaxometry.* The Journal of Physical Chemistry C, 2012. **117**(1): p. 403-412.

15. Feldman, R.F. and P.J. Sereda, *A model for hydrated Portland cement paste as deduced from sorption-length change and mechanical properties.* Matériaux et Construction, 1968. **1**(6): p. 509-520.
16. Baroghel-Bouny, V., *Water vapour sorption experiments on hardened cementitious materials: Part I: Essential tool for analysis of hygral behaviour and its relation to pore structure.* Cement and Concrete Research, 2007. **37**(3): p. 414-437.
17. Feldman, R.F., *Sorption and Length-change Scanning Isotherms of Methanol and Water on Hydrated Portland Cement*. 1970: Division of Building Research, National Research Council.
18. M, J.H., *A model for the microstructure of calcium silicate hydrate in cement paste.* Cement and Concrete Research, 2000. **30**(1): p. 101-116.
19. Muller, A.C.A., et al., *Use of bench-top NMR to measure the density, composition and desorption isotherm of C–S–H in cement paste.* Microporous and Mesoporous Materials, 2013. **178**(0): p. 99-103.
20. McDonald, P.J., V. Rodin, and A. Valori, *Characterisation of intra- and inter-C–S–H gel pore water in white cement based on an analysis of NMR signal amplitudes as a function of water content.* Cement and Concrete Research, 2010. **40**(12): p. 1656-1663.
21. Valori, A., P.J. McDonald, and K.L. Scrivener, *The morphology of C–S–H: Lessons from 1H nuclear magnetic resonance relaxometry.* Cement and Concrete Research, 2013. **49**(0): p. 65-81.
22. Taylor, H.F.W., *Nanostructure of C-S-H: Current status.* Advanced Cement Based Materials, 1993. **1**(1): p. 38-46.
23. Powers, T.C., *Studies of the physical properties of hardened Portland cement paste*. 1948, Chicago: [Portland Cement Association, Research Laboratories].
24. Powers, T.C., *Structure and Physical Properties of Hardened Portland Cement Paste.* Journal of the American Ceramic Society, 1958. **41**(1): p. 1-6.
25. Brunauer, S., *A discussion of the helium flow results of R. F. Feldman.* Cement and Concrete Research, 1972. **2**(4): p. 489-492.
26. Feldman, R.F., *A discussion of "studies of water and nitrogen adsorption on hardened cement pastes, 1.": by R. SH. Mikhail and S. A. Abo-El-Enein.* Cement and Concrete Research, 1973. **3**(1): p. 107-108.
27. Feldman, R.F., *Helium flow characteristics of rewetted specimens of dried hydrated portland cement paste.* Cement and Concrete Research, 1973. **3**(6): p. 777-790.
28. Cyr, M., *8 - Influence of supplementary cementitious materials (SCMs) on concrete durability*, in *Eco-Efficient Concrete*, F. Pacheco-Torgal, et al., Editors. 2013, Woodhead Publishing. p. 153-197.
29. Taylor, R., I.G. Richardson, and R.M.D. Brydson, *Composition and microstructure of 20-year-old ordinary Portland cement–ground granulated blast-furnace slag blends containing 0 to 100% slag.* Cement and Concrete Research, 2010. **40**(7): p. 971-983.

30. *Nature of C–S–H in 20 year old neat ordinary Portland cement and 10% Portland cement–90% ground granulated blast furnace slag pastes.* Advances in Applied Ceramics, 2007. **106**(6): p. 294-301.
31. 15167-1:2006, E., *Ground granulated blast furnace slag for use in concrete, mortar and grout. Definitions, specifications and conformity criteria*. 2006, ISBN.
32. *NATIONAL READY MIXED CONCRETE ASSOCIATION (NRMCA) Webpage*. Available from: http://nrmca.org/.
33. Escalante-Garcia, J.I. and J.H. Sharp, *The chemical composition and microstructure of hydration products in blended cements.* Cement and Concrete Composites, 2004. **26**(8): p. 967-976.
34. Pane, I. and W. Hansen, *Investigation of blended cement hydration by isothermal calorimetry and thermal analysis.* Cement and Concrete Research, 2005. **35**(6): p. 1155-1164.
35. *EN 13263-1:2005+A1:2009*. 2005, BSI.
36. Cheng-yi, H. and R.F. Feldman, *Hydration reactions in portland cement-silica fume blends.* Cement and Concrete Research, 1985. **15**(4): p. 585-592.
37. Cheng-yi, H. and R.F. Feldman, *Influence of silica fume on the microstructural development in cement mortars.* Cement and Concrete Research, 1985. **15**(2): p. 285-294.
38. Wu, M., B. Johannesson, and M. Geiker, *Application of water vapor sorption measurements for porosity characterization of hardened cement pastes.* Construction and Building Materials, 2014. **66**(0): p. 621-633.
39. Barrett, E., L. Joyner, and P. Halenda, *The Determination of Pore Volume and Area Distributions in Porous Substances. I. Computations from Nitrogen Isotherms.* J. Am. Chem. Soc., 1951. **73**(1): p. 373-380.
40. Scrivener, K.L., et al., *Quantitative study of Portland cement hydration by X-ray diffraction/Rietveld analysis and independent methods.* Cement and Concrete Research, 2004. **34**(9): p. 1541-1547.
41. Johannesson, B. and M. Janz, *A two-phase moisture transport model accounting for sorption hysteresis in layered porous building constructions.* Building and Environment, 2009. **44**(6): p. 1285-1294.
42. Everett D.H, *Adsorption Hysteresis, The Solid-Gas Interface*, E.A.F. (Ed.), Editor. 1967, Marcel Dekker, Inc.,: New York. p. 1055-1113.
43. Gregg, S.J. and K.S.W. Sing, *Adsorption Surface Area and Porosity*. Second ed. 1982: ACADEMIC PRESS INC.
44. Espinosa, R.M. and L. Franke, *Influence of the age and drying process on pore structure and sorption isotherms of hardened cement paste.* Cement and Concrete Research, 2006. **36**(10): p. 1969-1984.

45. Espinosa, R.M. and L. Franke, *Inkbottle Pore-Method: Prediction of hygroscopic water content in hardened cement paste at variable climatic conditions.* Cement and Concrete Research, 2006. **36**(10): p. 1954-1968.

46. Powers, T.C., *A Discussion of Cement Hydration in Relation to the Curing of Concrete*. 1947: Portland Cement Association.

47. Seaton, N.A., *Determination of the connectivity of porous solids from nitrogen sorption measurements.* Chemical Engineering Science, 1991. **46**(8): p. 1895-1909.

48. Beaudoin, J.J. and J. Marchand, *14 - Pore Structure*, in *Handbook of Analytical Techniques in Concrete Science and Technology*, V.S. Ramachandran and J.B. James, Editors. 2001, William Andrew Publishing: Norwich, NY. p. 528-628.

49. Feldman, R.F. and V.S. Ramachandran, *Microstructure of calcium hydroxide depleted portland cement paste I: Density and helium flow measurements.* Cement and Concrete Research, 1982. **12**(2): p. 179-189.

50. Baroghel-Bouny, V., *Water vapour sorption experiments on hardened cementitious materials. Part II: Essential tool for assessment of transport properties and for durability prediction.* Cement and Concrete Research, 2007. **37**(3): p. 438-454.

51. Bažant, Z.P. and M.Z. Bazant, *Theory of sorption hysteresis in nanoporous solids: Part I: Snap-through instabilities.* Journal of the Mechanics and Physics of Solids, 2012. **60**(9): p. 1644-1659.

52. Bazant, M.Z. and Z.P. Bažant, *Theory of sorption hysteresis in nanoporous solids: Part II Molecular condensation.* Journal of the Mechanics and Physics of Solids, 2012. **60**(9): p. 1660-1675.

53. Bodor, E.E., et al., *Pore structures of hydrated calcium silicates and portland cements by nitrogen adsorption.* Journal of Colloid and Interface Science, 1970. **34**(4): p. 560-570.

54. Brunauer, S., P.H. Emmett, and E. Teller, *Adsorption of Gases in Multimolecular Layers.* Journal of the American Chemical Society, 1938. **60**(2): p. 309-319.

55. Garci Juenger, M.C. and H.M. Jennings, *The use of nitrogen adsorption to assess the microstructure of cement paste.* Cement and Concrete Research, 2001. **31**(6): p. 883-892.

56. Thomas, M.D.A. *The suitability of solvent exchange techniques for studying the pore structure of hardened cement paste*. Advances in Cement Research, 1989. **2**, 29-34.

57. Ramachandran, V.S., *Concrete science : treatise on current research / V.S. Ramachandran, R.F. Feldman, J.J. Beaudoin*, ed. R.F. Feldman and J.J. Beaudoin. 1981, London: Heyden.

58. Basheer, L., J. Kropp, and D.J. Cleland, *Assessment of the durability of concrete from its permeation properties: a review.* Construction and Building Materials, 2001. **15**(2–3): p. 93-103.

59. Gagg, C.R., *Cement and concrete as an engineering material: An historic appraisal and case study analysis.* Engineering Failure Analysis, 2014. **40**(0): p. 114-140.

60. Nilsson, L.O., *On the role of moisture in degradation of concrete structures*, in *2005 International Congress - Global Construction: Ultimate Concrete Opportunities*. 2005, Thomas Telford: Dundee, Scotland, United Kingdom. p. 15 - 24.

61. Fick, A., *Ueber Diffusion.* Annalen der Physik, 1855. **170**(1): p. 59-86.

62. Crank, J., *The mathematics of diffusion / by J. Crank*. Oxford science publications. 1979: Oxford : Clarendon Press, 1979, 2. ed., pbk ed.

63. Whitaker, S., *Flow in porous media I: A theoretical derivation of Darcy's law.* Transport in Porous Media, 1986. **1**(1): p. 3-25.

64. White, F.M., *Fluid Mechanics, 5th Edition*. 2003: McGraw-Hill, Boston, MA.

65. Zamani, S., R.M. Kowalczyk, and P.J. McDonald, *The relative humidity dependence of the permeability of cement paste measured using GARField NMR profiling.* Cement and Concrete Research, 2014. **57**(0): p. 88-94.

66. Baroghel-Bouny, V., M. Thiéry, and X. Wang, *Modelling of isothermal coupled moisture–ion transport in cementitious materials.* Cement and Concrete Research, 2011. **41**(8): p. 828-841.

67. Zhang, Z., M. Thiery, and V. Baroghel-Bouny, *Numerical modelling of moisture transfers with hysteresis within cementitious materials: Verification and investigation of the effects of repeated wetting-drying boundary conditions.* Cement and Concrete Research, 2014. **68**: p. 10-23.

68. Quenard, D. and H. Sallee, *Water vapour adsorption and transfer in cement-based materials: a network simulation.* Materials and Structures, 1992. **25**(9): p. 515-522.

69. Quenard, D., et al., *Microstructure and transport properties of porous building materials.* Materials and structures, 1998. **31**(5): p. 317-324.

70. Xi, Y., et al., *Moisture diffusion in cementitious materials Moisture capacity and diffusivity.* Advanced Cement Based Materials, 1994. **1**(6): p. 258-266.

71. Basheer, P.A.M., *16 - Permeation Analysis*, in *Handbook of Analytical Techniques in Concrete Science and Technology*, V.S. Ramachandran and J.B. James, Editors. 2001, William Andrew Publishing: Norwich, NY. p. 658-737.

72. Nilsson, L.O., *Long-term moisture transport in high performance concrete.* Materials and Structures, 2002. **35**(10): p. 641-649.

73. Anderberg, A. and L. Wadsö, *Method for simultaneous determination of sorption isotherms and diffusivity of cement-based materials.* Cement Concrete Res., 2008. **38**(1): p. 89-94.

74. Fan, X.J., S.W.R. Lee, and Q. Han, *Experimental investigations and model study of moisture behaviors in polymeric materials.* Microelectronics Reliability, 2009. **49**(8): p. 861-871.

75. Berens, A.R. and H.B. Hopfenberg, *Diffusion and relaxation in glassy polymer powders: 2. Separation of diffusion and relaxation parameters.* Polymer, 1978. **19**(5): p. 489-496.

76. Berens, A.R. and H.B. Hopfenberg, *Diffusion of organic vapors at low concentrations in glassy PVC, polystyrene, and PMMA.* Journal of Membrane Science, 1982. **10**(2–3): p. 283-303.

77. Petropoulos, J.H., M. Sanopoulou, and K.G. Papadokostaki, *Physically insightful modeling of non-Fickian kinetic regimes encountered in fundamental studies of isothermal sorption of swelling agents in polymeric media.* European Polymer Journal, 2011. **47**(11): p. 2053-2062.

78. Hansen, C.M., *Diffusion in polymers.* Polymer Engineering & Science, 1980. **20**(4): p. 252-258.

79. Wadsö, L., *Describing non-Fickian water-vapour sorption in wood.* Journal of Materials Science, 1994. **29**(9): p. 2367-2372.

80. Neogi, P., *Anomalous diffusion of vapors through solid polymers. Part II: Anomalous sorption.* AIChE Journal, 1983. **29**(5): p. 833-839.

Paper I

Cement and Concrete Research 69 (2015) 88–95

Contents lists available at ScienceDirect

Cement and Concrete Research

journal homepage: http://ees.elsevier.com/CEMCON/default.asp

Moisture equilibrium of cement based materials containing slag or silica fume and exposed to repeated sorption cycles

M. Saeidpour *, L. Wadsö

Building Materials, Lund University, Lund, Sweden

ARTICLE INFO

Article history:
Received 23 April 2014
Accepted 10 December 2014
Available online 8 January 2015

Keywords:
Adsorption (C)
Cycles (C)
Supplementary cementitious materials (SCMs) (D)

ABSTRACT

Water vapor sorption isotherms are essential data in models to predict the service life of cement based structures. This study investigates the influence of water to binder ratio (0.4, 0.5 and 0.6), and the presence of two SCMs (70% slag and 10% silica fume) on sorption isotherms, both in the hygroscopic and in the super-hygroscopic relative humidity (RH) ranges.

In the present paper desorption isotherms are divided into different parts based on the Jennings CM-II model of the C–S–H structure. The samples with silica fume and slag have higher moisture content than OPC samples, but with a higher amount of gel pores and lower amount of capillary pores. At low RHs all samples have similar desorption curves and the introduction of SCMs induces only a slight increase in the BET surface area.

1. Introduction

All physiochemical processes that are responsible for durability issues in concrete, such as carbonation, chloride initiated corrosion, sulfate attack, freeze and thaw cycles, and alkali silica reaction (ASR), are moisture dependent [1,2], so the durability of cement and concrete structures depends on transport and sorption of moisture. To be able to predict the rates at which these processes occur or to prevent their occurrence, transport and sorption data are needed. Water vapor absorption and desorption isotherms are the equilibrium water contents of the material as a function of relative humidity (RH) at a constant temperature. These data are used in computer models to predict the service life of structures [3] and are essential to understand moisture distribution in cement based structures [4]. Sorption isotherms can also be used for the calculation of for example specific surface areas, and thus contribute to a better understanding of the microstructure.

The equilibrium moisture content at a certain RH is higher for materials subjected to drying than for the same material that is absorbing moisture (at the same RH). This phenomenon is referred to as sorption hysteresis and is important to take into account when modeling transport properties in materials exposed to wetting and drying cycles, such as many outdoor and indoor concrete structures [5,6]. One example of such a structure is the surface of indoor concrete floors that are often exposed to an initial drying, followed by a wetting by the water in applied adhesives or screeds, and finally a drying to the room climate [4]. Such a process cannot be understood without knowledge of hysteresis and scanning curves.

The first sorption isotherms on cement pastes were measured by Powers and Brownyard in 1948 (see references [7,8]) and there are many reports on sorption isotherms of pastes, mortars and concretes made with ordinary Portland cement (OPC), see for example references [9–13]. However, these results are often difficult to compare due to a number of factors being different between studies or not well described; for example hydration conditions, aging of samples during experiments (continued hydration and/or carbonation), absorption–desorption history and method of sorption studies. For example, Hagymassy et al. [12] reported low hysteresis for hardened OPC pastes in the high RH region and almost no hysteresis at low RHs, which is in contrast with isotherms reported by Feldman and Sereda [11] and Baroghel-Bouny [13].

The hysteresis at high RHs is commonly explained by the inkbottle effect in capillary pores [14,15], while the hysteresis at low RHs is still not fully understood. Pore collapse is described as responsible for low RH hysteresis by many authors (cf. [10,13,16]). However, Bazant and Bazant [17,18] debate this and describe two mechanisms as possibly responsible for low RH hysteresis: snap-through instabilities during the filling and emptying of non-uniform nano-pores and molecular coalescence within the partially filled surface in nano-pores.

In contrast to OPC, the knowledge about sorption isotherms for materials made with blended cements is limited; such knowledge is crucial today as there is a general trend of using more blended cements with supplementary cementitous materials (SCMs) as a way to limit the CO_2 emissions associated with concrete. The presence of SCMs changes the amount and kind of hydrates formed during the hydration, especially the calcium silicate hydrate (C–S–H) that is the main product of cement hydration [19]. This changes the internal surface and pore structure, and thus the sorption and transport properties.

* Corresponding author. Tel.: +46 2227786.
E-mail address: mahsa.saeidpour@byggtek.lth.se (M. Saeidpour).

http://dx.doi.org/10.1016/j.cemconres.2014.12.005
0008-8846/

Few studies of sorption isotherms of cement based materials with SCMs have been published and there is still a need for systematic studies in this field. Baroghel-Bouny et al. [13] investigated sorption isotherms and hysteretic behavior of high performance (HP) cement pastes and concretes made with OPC and 10% silica fume. They performed several scanning curves from different RHs and analyzed pore size distributions with the Barrett, Joyner, Halenda (BJH) model [20]. Their results showed that HP materials had lower moisture contents at high RHs compared to normal materials, and large RH changes at high RHs induced only slight changes in moisture content [13]. De Belie et al. [21] studied the microstructure and surface area change of cement pastes in which OPC had been replaced by SCMs in different mass fractions (10% silica fume, 50% fly ash, and 50 and 85% slag). They did static and dynamic (sorption balance) water vapor and nitrogen sorption isotherms on samples with water/binder ratios (w/b) 0.35–0.5 without any specific control on carbonation. They conclude that the result of the sorption isotherm measurement is dependent on the method used. Their results showed hysteresis over the whole range of RHs for all binders.

The evaluation of moisture properties of cement based materials require at least the main absorption and desorption curves of the sorption isotherm [22]. These can be measured with different techniques. The most common method is the desiccator method (see for example references [5,10,21]). In this method relatively large samples are equilibrated for several weeks at different vapor pressures above saturated salt solutions, and are weighed on a balance until they have reached equilibrium. This method is time consuming and needs many parallel specimens that are exposed to different RHs. In addition, the structure of the material may change during the long measurement time due to hydration and carbonation. In the present study we used the sorption balance method, in which small samples (10–100 mg) are continuously weighed on an analytical balance while exposed to an RH program. The main advantages with this technique are that the whole isotherm can be measured on a single sample in a CO_2-free environment. A measurement is comparatively quick as the external mass transfer resistance is low as the sample is exposed in a gas stream. However, each of our measurements still takes about three weeks.

In this study, the influence of w/b-ratio (0.4, 0.5 and 0.6) and the presence of two SCMs (70% slag and 10% silica fume) on the microstructure and water vapor isotherms of paste and mortar samples were studied in a systematic way. Care was taken so that the samples were exposed to the same treatment before the measurements, and the sorption balance method was used to avoid carbonation.

2. Materials

Nine pastes and six mortars with different binders have been used in this study. The binders were ordinary Portland cement OPC (CEM I), OPC with 10% silica fume, and OPC with 70% slag (CEM III). The chemical compositions of the cements and the silica fume are given in Table 1. The CEM III was premixed and the silica fume was added to the OPC as slurry. Three water/binder-ratios (w/b), 0.4, 0.5 and 0.6, for paste samples and two w/b ratios, 0.4 and 0.5, for mortar samples were used.

The mortar materials were mixed with water according to EN 196-1 and cast in a $40 \times 10 \times 10$ cm^3 steel mold. The mold was placed in a 20 °C climate room and cooled with fans during the first 24 h of hydration to limit the temperature increase. Temperature was measured with thermocouples on the surface of the steel mold and in the center of the samples during 24 h of hydration. The maximum temperature measured in the center was 24 °C (for samples with 10% silica fume). The samples were seal cured for 90 days at 20 °C and then crushed to pieces of approx. 5 mm. The crushed pieces were kept in sealed containers to avoid carbonation and in contact with wet cloth to become capillary saturated.

The preparation of the paste materials followed EN 196-1. The pastes were cast in cylindrical plastic bottles with 70 mm diameter and 200 mm height. After mixing, the bottles were rotated for 12 h to avoid segregation. All materials were then stored in the bottles at 20 °C. After 3–6 months of curing, the cylindrical samples were crushed to pieces of about 100 g, and these pieces were vacuum saturated. Saturated materials were stored in 100% RH in exsiccators until the measurements started.

Table 1
Chemical composition of the used materials.

Chemical analysis XRF (%)	CEM I 32.5R	CEM III/B 42.5 N	Silica fume
SiO_2	20.3	29.2	98.7
Al_2O_3	5.6	8.9	0.31
Fe_2O_3	2.4	1.2	0.02
CaO	63.4	48	0.15
MgO	1.6	4.8	0.04
SO_3	2.9	2.6	–
LOI	2.1	1.4	0.47
Slag content	–	69.9	–

Both mortar and paste samples were crushed to 1–2 mm pieces before being placed in a sorption balance. The measurements were done more than one year after casting. As the mortar samples were so small (20 mg), their paste content was not the same as that of the large sample from which they were taken. To be able to compare sorption isotherm measurements on pastes and mortars, the cement content of the latter were calculated from the calcium contents of the small samples as measured by inductivity coupled plasma mass spectroscopy (ICP-MS) after the sorption measurements.

The samples for pressure plate testing were small slab shaped cement paste samples of approx. $20 \times 15 \times 3$ mm^3 that were cut from the paste cylinders. All pressure plate samples were vacuum saturated before the tests.

3. Experimental techniques

3.1. Water vapor sorption balance

For the sorption balance measurements approx. 20 mg of water saturated samples were placed in a DVS Advantage (Surface Measurement Systems, UK) sorption balance. In these instruments the mass of the small sample is continuously measured with an analytical balance while exposed to an RH-program. The desired RH is reached by mixing different proportions of dry and water vapor saturated nitrogen gas streams. The relative humidity of the sorption balance was validated by measurements on saturated salt solutions and found to be within 1.5% of the set values. Most measurements were made with an RH-program consisting of desorption (95–90–80–…–40–30), absorption (30–40–…–80–90–95), and desorption (95–90–80–70–…50–40–30–25–20–15–10–5–0). One measurement was made with one more absorption–desorption cycle. An example of a typical RH-program and the corresponding mass change is shown in Fig. 1. Each RH step was ended when the mass change rate was lower than 0.0001% of the initial mass per minute, or if a maximum time of 2000 min had been exceeded; except for final drying that was continued for up to 6000 min. A complete measurement for one sample – including one desorption curve, one absorption curve, and one final desorption curve to 0% RH – took approx. 20 days.

The moisture content of the sample at equilibrium at each relative humidity was expressed as mass of water per mass of dry material. The mass for each step was curve fitted using an exponential function (Eq. (1)) and then extrapolated to infinite time to evaluate the final (equilibrium) mass m_f [23].

$$m(t) = m_0 + (m_f - m_0)\exp(-k(t-t_0)). \quad (1)$$

Here, $m(t)$ is mass of the sample (g), t is time (s), and m_0, m_f, k and t_0 are fitting parameters. Fig. 2A shows an example of measured data and

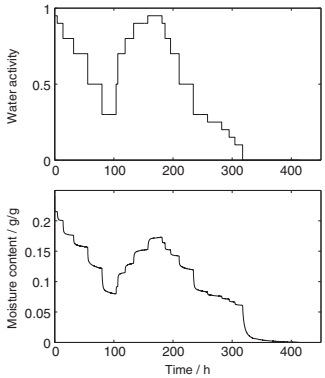

Fig. 1. Typical relative humidity program and the sample response for a sample of OPC paste with an w/b-ratio of 0.5.

the corresponding extrapolated curve using Eq. (1). Note that only the final part of the mass curve was used in the curve fitting (cf. Fig. 2A) and that m_0 and t_0 are free fitting parameters (not the initial mass and time). The extrapolation never changes the mass change during a single step more than 10%.

The measured mass responses after changes in the RH in many cases do not agree with what should be expected if external and internal mass transfer resistances (Fick's law) governed the gain or loss of moisture. The main deviation is that mass equilibrium is reached more slowly than would be expected from a "Fickian" behavior. This is clearly seen when the results are drawn as a function of the square root of time (Fig. 2B), as is normally done when evaluating diffusivities of slab shaped samples. The results in Fig. 2 show that although the exponential curve fit on a linear time scale looks reasonable, the mechanisms of water sorption are more complex than usually thought and true equilibrium can possibly only be reached on much longer time scales than our experiments. A detailed analysis of the kinetics of the sorption curves will be published separately.

In this study the dry mass was defined as the extrapolated mass at infinite time for the final drying at RH = 0%. To avoid microstructural damage due to drying, the samples did not dry to more than 30% RH during first desorption cycle [11].

The sorption balance measurements take about three weeks each, and it has not been possible to repeat these measurements. However, our experience from this type of measurements is that the difference between repeated measurements is very much smaller than the differences between the results presented in this paper.

3.2. Pressure plate

The sorption isotherm above the hygroscopic range was measured with a pressure plate instrument from Soilmoisture Equipment Corp., Santa Barbara, CA, USA [24]. Samples were vacuum saturated and placed in two different pressure cells with 3 and 1 MPa pressure, corresponding to 97.81 and 99.26% RH, respectively. In the pressure plate, a positive gas pressure ΔP (Pa) is applied to a wet specimen and water from the sample leaves through the out-flow tubes in the instrument until equilibrium is reached in the water menisci in the material. The pore radius and RH can be calculated from the pressure at equilibrium using Young–Laplace and Kelvin equations [25]. The samples were then dried at 105 °C. The moisture contents for the pressure plate and vacuum saturated samples were reported as mass of water per mass of dry sample at 105 °C. The method is described in references [24,26].

4. Results

The sorption isotherms measured for different w/b-ratios and different binders for both cement paste and mortars are shown in Figs. 3 and 4. Fig. 3 shows all measurements made in desorption–absorption–desorption and the pressure plate and vacuum saturation data. In Fig. 4 the results of a measurement that was continued for one more absorption–desorption cycle is shown. In this figure, it is also indicated in which order the sorption curves were measured. The order is the same for all results shown in Fig. 3 (for the first three sorption limbs).

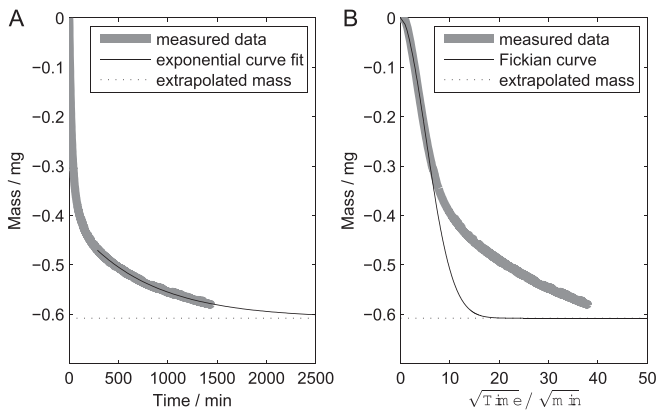

Fig. 2. An example of the mass change after an RH-step (A): as a function of time and (B): as a function of the square root of time. The gray line is the measured data, the black line is an exponential fitted curve in (A) and a simulated Fickian curve in (B), and the dashed line is the final (equilibrium) value found from the exponential curve fit.

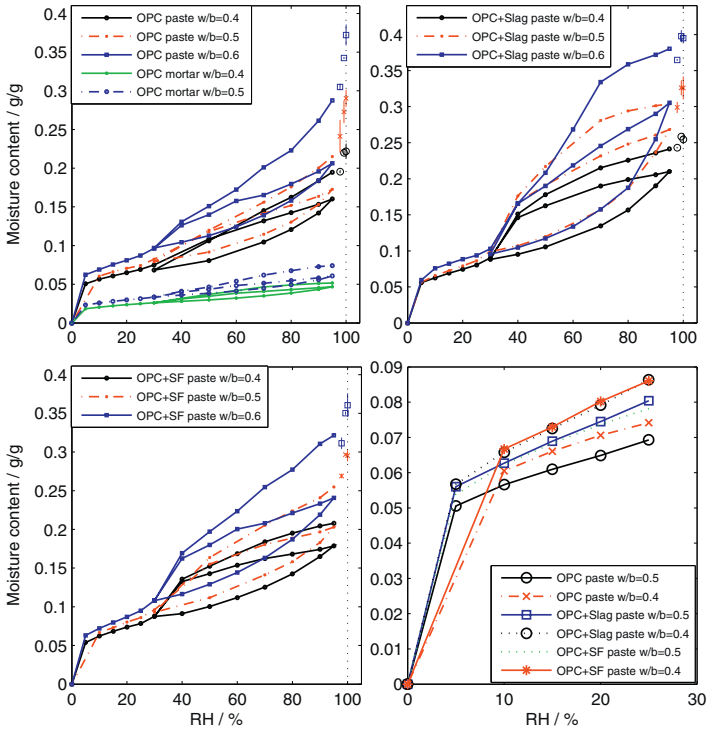

Fig. 3. The sorption isotherms of cement paste and mortars with different w/b-ratios and different binders. The data connected by lines are from the sorption balance measurements. The three data points shown at high RHs are the pressure plate results for 97.81 and 99.26% RHs, and the vacuum saturation moisture content (drawn at 100% RH). These are drawn with the same color as the corresponding sorption balance measurement. The error bars for these points are the standard deviation of the three measurements made for each case (the sorption balance measurements were not repeated). The lower right diagram shows the paste results for w/b-ratios 0.4 and 0.5 in the low RH range.

5. Discussion

The discussion part contains analyses of the shape of the isotherms, the influence of SCMs on the main desorption curve, the surface area, the influence of aggregates, and the shape of the sorption isotherms at high RHs.

5.1. Shape of isotherms

Figs. 3 and 4 show that all desorption–absorption–desorption curves have similar qualitative appearances; however, the OPC samples absorb less moisture than the samples with silica fume and slag. Further, the curve shapes follow a complex pattern that can be summarized in the following points:

- The initial desorption above 30–40% RH is higher than the following desorption, and the level decreases for every consecutive cycle.
- All desorption curves merge at about 30–40% RH. Below this, they follow same path for the same binder.
- Desorption isotherms show a significant change in slope between 40 and 30% RH.
- Absorption isotherms show a smooth increase over the whole RH range.
- There is a significant hysteresis over the whole RH range.

We use the Jennings CM-II model [27] and results from recent studies with ^{1}H nuclear magnetic resonance (NMR) relaxometry techniques [28,29] to describe the shape of the desorption isotherms. The CM-II model describes the C–S–H structure based on a combination of nitrogen and water vapor sorption isotherms [27]. In this model, the basic units of C–S–H are globules that have a layered sheet-like structure. The size of the globules is about 4.2 nm. A number of globules make up a floc. In this structure, the water can be found between the sheets (interlayer water) and in pores of three different sizes. Pores within the globules are referred to as interglobular pores (IGP) (pore size less than 1 nm), small gel pores (SGP) (pore size 1–3 nm) are formed between the globules, and large gel pores (LGP) (pore size 3–12 nm) are formed between flocs of globules. Much larger pores are called capillary pores. With the NMR technique two well-defined pore sizes have been found (0.85 nm and 2.5 nm [28]). These correspond to interlayer pores (IGP and interlayer water) and small gel pores (SGP). Interhydrate spaces

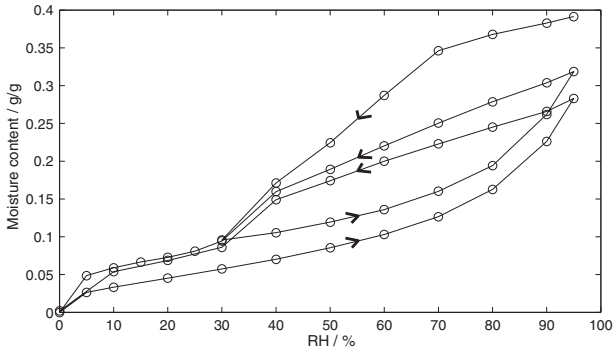

Fig. 4. Sorption isotherm for OPC with 70% slag and a 0.6 w/b-ratio paste. Note that there is no 5% RH measurement for the final desorption.

around 10 nm corresponding to large gel pores (LGP) were also found, but decreased in volume as C–S–H grows during continued hydration [28,29]. Based on these studies we divided the desorption isotherms into four parts (the RHs are our interpretation of Fig. 1 in reference [29]):

1. From saturated conditions to 90% RH, where capillary pores are emptied.
2. From 90 to 80% RH, where interhydrate spaces dry out.
3. From 80 to 30% RH, where gel pores are emptied.
4. From 30 to 0% RH where interlayer pores in the C–S–H structure are emptied.

Note that this is a simplified qualitative analysis to avoid the complicated and uncertain BJH calculations (cf. Wu et al. [30]), and that Jennings' model was developed for OPC and the nano-structure can be different when SCMs are used. Our analysis was made on desorption curves made by combining the initial desorption, 95 to 30% RH, with the final desorption 30 to 0% RH. This was made to avoid using the first part of the second desorption, that is made under scanning (change from absorption to desorption). Fig. 5 shows the amount of water in each of these classifications for the different materials.

At low RH intervals (0–30%), desorption takes place in the interlayer C–S–H pore structure [29]. It can be seen in Fig. 5 that cement based materials with different binders and different w/b have similar moisture

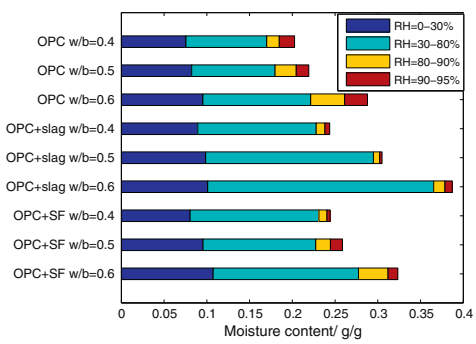

Fig. 5. Amount of water desorbed in each RH interval for different cement paste samples. Data is from sorption balance measurements only.

contents. The amount of water in this RH-range is a function of the C–S–H globule's surface area, while changes in w/b-ratio and the presence of SCMs only induce almost negligible increases in moisture content. Many studies have argued that drying below 30% RH can change the structure of C–S–H [13,31–33]; however there is only a minor difference between the first and the second desorption curves at RHs of 30% and lower in the measurement with an extra absorption–desorption cycle (Fig. 4). This indicates that if there are microstructural changes taking place during drying, these do not influence the sorption at low RH (cf. the specific surface discussed below) or the dry mass, or that they are reversible. It should be noted that there is hysteresis between absorption and desorption also in this range, but this cannot be related to the change in the microstructure of C–S–H.

Microstructural changes were investigated by Wu et al. [34] using a desorption test with resaturated samples. They observed no major difference between the first absorption isotherm and the absorption isotherm after resaturation. They found small differences in the corresponding desorption curves, but such differences can be due to the fact that the samples were not fully saturated during the resaturation process. These results support the idea that drying at low RHs does not change the C–S–H structure or that any change in the C–S–H structure is reversible when exposed to moisture again.

In the presence of slag and silica fume the amount of gel pores (30–80% RH) is higher than for OPC samples with the same w/b-ratio. In desorption from 80 to 40% RH, the gel pores are emptied and the amount of water lost represents the size and amount of gel pores. We thus find – using Jennings' model – that the pastes made from blended cements have higher gel porosity.

For each sample, consecutive desorption curves are different above 40% RH; the first desorption is always significantly higher and qualitatively different. This difference is probably due to the fact that the second desorption is in scanning from 95% RH, while the first desorption is the main desorption curve. This is also seen in Fig. 4 where the second and third desorption curves are similar, but with the third curve below the second.

We do not show calculated pore size distributions from our data as we find that calculations of such distributions are very uncertain. If the analysis is made on the absorption curve the result is very dependent on what function is assumed for the thickness of the adsorbed layer, and if the analysis is made in desorption the pore sizes will be underestimated because of the ink-bottle effect [15]. Except for the significant decrease in moisture content during desorption between 40 and 30% RH – which could indicate the effect of necks in ink-bottle pores – the sorption

isotherms are smooth and do not give support to models based on pores with only a few discrete sizes.

From 80% to 90% RH the interhydrate spaces are emptied, and above 90% the capillary pores are emptied. In both these RH ranges there is comparatively little water desorbed, and the samples with a lower w/b-ratio generally loose less water than the one with a higher w/b-ratio.

There is a hysteresis between absorption and desorption over the whole RH-range for all samples. The hysteresis is more significant above 40% RH and it is larger between the first desorption (main desorption) and the following absorption than in the subsequent desorption–absorption cycle. The presence of the two SCMs tested increased the hysteresis, especially the presence of 70% slag.

Fig. 6 shows the hysteresis as the moisture content difference between desorption and absorption for the first and the second cycles. The hysteresis has a maximum at 70% RH for both cycles, but it is lower for RH > 50% and higher for RH < 50% for the second cycle compared with the first. However, the first absorption is in scanning from 30% RH, while the second absorption starts from 0% RH. At RHs close to 30%, the amount of hysteresis for the first cycle is affected by scanning and can therefore be underestimated. In addition, the second absorption is a scanning curve from 0% RH and at low RHs, the amount of hysteresis is probably also underestimated. It would be interesting to compare the hysteresis between the second and the third cycles, but due to the long measurement time needed for this, it has not been made in this study.

Fig. 7 shows microstructures of the pastes of OPC and OPC with 70% slag, both with the same w/b-ratio of 0.4. It can be seen in Fig. 7a that there is a dense C–S–H structure around the unreacted alite, while the C–S–H structure around the slag particles is more open. Fig. 7 shows three areas with dense C–S–H; in two of these areas the C_3S phase has been completely consumed.

5.2. Surface area

The water vapor sorption data was used to calculate the specific surface area S ($m^2\ g^{-1}$) using the BET model [35]:

$$\frac{v}{v_m} = \frac{c\varphi}{(1-\varphi)(1+c\varphi-\varphi)}. \quad (2)$$

Here v_m is the monolayer moisture content ($g\ g^{-1}$), v is adsorbed moisture content ($g\ g^{-1}$), c is a constant related to interaction forces between adsorbent and adsorbate, and φ is relative humidity ($Pa\ Pa^{-1}$).

In the BET model, it is assumed that in all layers except the first, the enthalpy of adsorption is equal to the enthalpy of condensation. The enthalpy of adsorption of the first layer is higher. The monolayer moisture content can be used to calculate the specific surface area using Eq. (3).

$$S = \frac{AN_A}{M_w} v_m. \quad (3)$$

Here v_m is monolayer moisture content ($g\ g^{-1}$), N_A is Avogadro's constant (mol^{-1}), M_w is molar mass of water ($g\ mol^{-1}$) and A is the area (m^2) occupied by one water molecule ($1.06\ 10^{-19}\ m^2$). The BET analysis was made on desorption data in the range 40–0% RH. Above this RH-range, capillary condensation may take place and the BET model will then not be valid.

The monolayer moisture content and the calculated specific surface area are presented in Table 2. It can be seen that the specific surface area increases with a decreasing w/b-ratio. The presence of the two used SCMs cause an increase in specific surface area.

According to the CM-II model, the globules are fully saturated with a monolayer on the surface at 11% RH. We report moisture contents at 10% RH, which is our closest measured point to 11% RH, to compare with the monolayer moisture content calculated using the BET model. There is a good agreement between these values.

5.3. Sorption isotherms for mortar samples

The measured mortar isotherms were recalculated to gram water per gram paste. An example of our recalculation for OPC paste and mortar w/b = 0.5 is shown in Fig. 8.

Baroghel-Bouny [13] found that the sorption isotherms of cement pastes, mortars and concrete made with the same cement paste are the same when the moisture content is given as mass of water per mass of cement. This is natural as the aggregates of mortars and concrete normally have very low sorption of water.

Our results show that the cement paste and the cement mortar isotherms look similar, but the mortars are about 2% moisture content higher than pastes for all materials at all RHs. The reason for this is that the cement paste in the mortars loses more water in the final drying to 0% RH than do the pure cement pastes. Baroghel-Bouny only dried her samples to 3% RH, so the 2% moisture content loss of water seems to take place between 3 and 0% RH. This water loss indicates that the sand actually contributes to the sorption isotherm. We therefore measured sorption isotherms of standard sand, but found that its sorption was too low to account for the significant effect that we observed.

The only major microstructural difference between cement pastes in pastes and mortars is the interfacial transition zone (ITZ), i.e., the 30–50 μm interface between sand and mortar that has different properties from the paste [36]. One possibility is that the hydrated cement phases in the ITZ are different from those in bulk paste, for example containing phases that lose large amounts of water between 3 and 0% RH. Another possibility is that nano-sized cracks take up and lose a significant amount of water in the RH-range 0–3%. However, we have not found support in the literature for this.

5.4. Sorption isotherms at high RHs

For materials that are exposed to high (superhygroscopic) moisture conditions it is of interest to measure the sorption isotherms at high and very high RHs. As concretes frequently are exposed to rain, condensation etc. we have complemented our sorption balance results with pressure plate measurements. However, such results are probably of limited value for cement pastes, as is being discussed below.

In Fig. 3 we have drawn the pressure plate and vacuum saturation results at 97.81%, 99.26% and 100% RHs. However, both 100% and 99.26% are actually higher than the possible RH range [37]; isotherms of cement based materials cannot go all the way to 100% RH because of high concentrations of ions in the pore solutions. Depending on the alkalinity of the cement, the maximum RH of the pore solution is

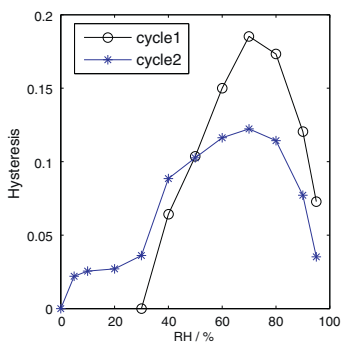

Fig. 6. The hysteresis calculated for the first and second cycles of the sorption measurement shown in Fig. 4.

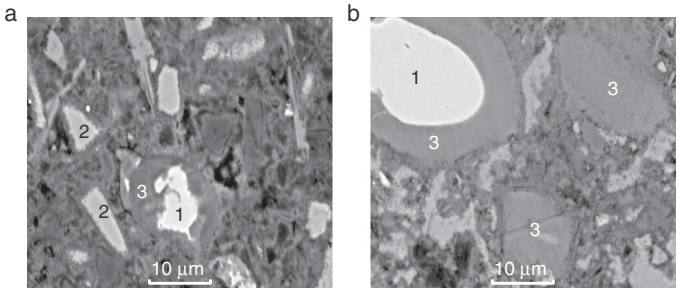

Fig. 7. SEM-BSE images of two of the pastes used in the present study. A. OPC with slag. B. OPC. Three phases are shown: unreacted alite (C_3S) (1), unreacted slag (2), and C–S–H (3).

about 98–99% [37]. Exposing samples to higher RHs than the RH of the pore solution will result in condensation of water on the outside of the material and bleeding of ions from the material to the condensation droplets.

When the whole pore system is filled, the material is saturated and cannot take up more water, i.e., this state corresponds to the highest possible moisture content. A complication is that it is difficult to fully saturate cement based materials; not even vacuum saturation will fill the whole pore system. The saturation moisture content at the sorption isotherm end point is thus uncertain and depends on the saturation method used.

Fig. 9 shows a schematic isotherm at high RHs. Taking the above limitations on RH and moisture content into account, the sorption isotherm ends at point 4. Below this point, the sorption isotherms can be measured with different techniques. Points 1–2 show the results of measurements in the hygroscopic region over saturated salt solutions or in a sorption balance. At higher RHs accurate equilibration through the gas phase is difficult and the highest part of the sorption isotherm is therefore measured with the pressure plate method (point 3).

The vertical dashed line in Fig. 9 shows how the moisture content can seem to increase at constant RH if external water on a specimen is included in a measurement. This can for example happen if a pressure plate measurement is made at a pressure corresponding to an RH higher than the saturation RH, resulting in accumulation of water on the outside of the saturated sample. If all such water is removed, point 4 is reached; if it is included in the weighing, a point on the dashed line will be reached.

Table 2
Monolayer moisture content (v_m) and specific surface area (S) calculated from the BET model, and the measured moisture content at 10% RH (desorption).

Sample	v_m (%)	S (m^2 g^{-1})	Moisture content at RH = 10% (%)
OPC paste w/b = 0.4	5.3	187	5.7
OPC paste w/b = 0.5	5.8	203	6.1
OPC paste w/b = 0.6	6.7	236	6.9
OPC mortar w/b = 0.4	1.9	65	2.5
OPC mortar w/b = 0.5	2.4	83	2.6
OPC + slag paste w/b = 0.4	6.3	222	6.3
OPC + slag paste w/b = 0.5	7	246	6.6
OPC + slag paste w/b = 0.6	7.3	255	7.7
OPC + slag mortar w/b = 0.4	2.2	77	2.3
OPC + slag mortar w/b = 0.5	2	70	2.1
OPC + SF paste w/b = 0.4	6.3	219	6.2
OPC + SF paste w/b = 0.5	6.9	242	6.7
OPC + SF paste w/b = 0.6	7.7	268	7.3
OPC + SF mortar w/b = 0.4	2.7	94	2.7
OPC + SF mortar w/b = 0.5	2.7	95	2.8

6. Conclusions

- Desorption isotherms at low RH (0–30%) for different binders and different w/b ratios are similar. An increase in the w/b-ratio and/or the presence of SCMs gives small increases in the calculated BET surface area.
- The moisture content above 30% RH in samples with the same w/b-ratio is higher in the presence of slag and silica fume than in OPC samples. The samples with silica fume and slag have a higher amount of gel pores and a lower amount of capillary pores than OPC samples.
- According to this study, drying at 0% RH at room temperature in a sorption balance for several days does not change the specific surface.
- Mortars showed a higher mass loss than pastes when dried at 0% RH.
- The sorption isotherm at high RHs is difficult to validate experimentally, both concerning RH and moisture content.

Acknowledgment

The research leading to these results has received funding from the European Union Seventh Framework Program (FP7/2007–2013) under grant agreement 264448. We thank Zhang Zhidong who prepared the

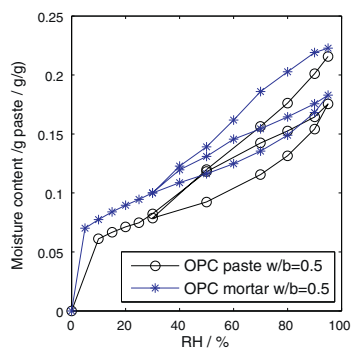

Fig. 8. The recalculated sorption isotherm for cement mortar to gram water per gram paste and the paste isotherm for OPC with a w/b-ratio of 0.5.

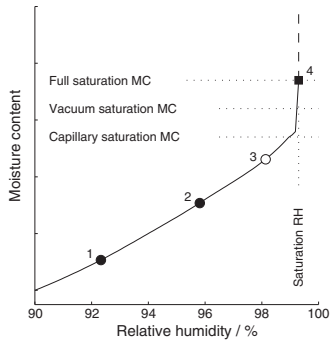

Fig. 9. Schematic sorption isotherm for cement based materials. Points 1 and 2 can be measured with a sorption balance or with the saturated salt solution method; point 3 can be measured with the pressure plate method; point 4 corresponds to a filled pore system.

paste material, Arnaud Muller who helped with the SEM-samples, and Lars-Olof Nilsson and members of the Nanocem Consortium with whom we discussed our results.

References

[1] C.R. Gagg, Cement and concrete as an engineering material: an historic appraisal and case study analysis, Eng. Fail. Anal. 40 (2014) 114–140.
[2] L.O. Nilsson, On the role of moisture in degradation of concrete structures, 2005 International Congress — Global Construction: Ultimate Concrete Opportunities, Thomas Telford, Dundee, Scotland, United Kingdom, 2005, pp. 15–24.
[3] A. Aït-Mokhtar, R. Belarbi, F. Benboudjema, N. Burlion, B. Capra, M. Carcassès, J.B. Colliat, F. Cussigh, F. Deby, F. Jacquemot, T. de Larrard, J.F. Lataste, P. Le Bescop, M. Pierre, S. Poyet, P. Rougeau, T. Rougelot, A. Sellier, J. Séménadisse, J.M. Torrenti, A. Trabelsi, P. Turcry, H. Yanez-Godoy, Experimental investigation of the variability of concrete durability properties, Cem. Concr. Res. 45 (2013) 21–36.
[4] M.S. Åhs, Sorption scanning curves for hardened cementitious materials, Constr. Build. Mater. 22 (2008) 2228–2234.
[5] V. Baroghel-Bouny, Water vapour sorption experiments on hardened cementitious materials. Part II: Essential tool for assessment of transport properties and for durability prediction, Cem. Concr. Res. 37 (2007) 438–454.
[6] T.M. Chrisp, W.J. McCarter, G. Starrs, P.A.M. Basheer, J. Blewett, Depth-related variation in conductivity to study cover-zone concrete during wetting and drying, Cem. Concr. Compos. 24 (2002) 415–426.
[7] H.J.H. Brouwers, The work of Powers and Brownyard revisited: Part 1, Cem. Concr. Res. 34 (2004) 1697–1716.
[8] H.J.H. Brouwers, The work of Powers and Brownyard revisited: Part 2, Cem. Concr. Res. 35 (2005) 1922–1936.
[9] R. Badmann, N. Stockhausen, M.J. Setzer, The statistical thickness and the chemical potential of adsorbed water films, J. Colloid Interface Sci. 82 (1981) 534–542.
[10] R.M. Espinosa, L. Franke, Influence of the age and drying process on pore structure and sorption isotherms of hardened cement paste, Cem. Concr. Res. 36 (2006) 1969–1984.
[11] R.F. Feldman, P.J. Sereda, A model for hydrated Portland cement paste as deduced from sorption-length change and mechanical properties, Matér. Constr. 1 (1968) 509–520.
[12] J. Hagymassy Jr., I. Odler, M. Yudenfreund, J. Skalny, S. Brunauer, Pore structure analysis by water vapor adsorption. III. Analysis of hydrated calcium silicates and portland cements, J. Colloid Interface Sci. 38 (1972) 20–34.
[13] V. Baroghel-Bouny, Water vapour sorption experiments on hardened cementitious materials: Part I: Essential tool for analysis of hygral behaviour and its relation to pore structure, Cem. Concr. Res. 37 (2007) 414–437.
[14] S.J. Gregg, K.S.W. Sing, Adsorption Surface Area and Porosity, Second ed.Academic Press Inc., 1982
[15] R.M. Espinosa, L. Franke, Inkbottle pore-method: prediction of hygroscopic water content in hardened cement paste at variable climatic conditions, Cem. Concr. Res. 36 (2006) 1954–1968.
[16] J.J. Thomas, A.J. Allen, H.M. Jennings, Structural changes to the calcium–silicate–hydrate gel phase of hydrated cement with age, drying, and resaturation, J. Am. Ceram. Soc. 91 (2008) 3362–3369.
[17] Z.P. Bažant, M.Z. Bazant, Theory of sorption hysteresis in nanoporous solids: Part I: Snap-through instabilities, J. Mech. Phys. Solid 60 (2012) 1644–1659.
[18] M.Z. Bazant, Z.P. Bažant, Theory of sorption hysteresis in nanoporous solids: Part II Molecular condensation, J. Mech. Phys. Solid 60 (2012) 1660–1675.
[19] B. Lothenbach, K. Scrivener, R.D. Hooton, Supplementary cementitious materials, Cem. Concr. Res. 41 (2011) 1244–1256.
[20] E. Barrett, L. Joyner, P. Halenda, The determination of pore volume and area distributions in porous substances. I. Computations from nitrogen isotherms, J. Am. Chem. Soc. 73 (1951) 373–380.
[21] N. De Belie, J. Kratky, S. Van Vlierberghe, Influence of pozzolans and slag on the microstructure of partially carbonated cement paste by means of water vapour and nitrogen sorption experiments and BET calculations, Cem. Concr. Res. 40 (2010) 1723–1733.
[22] Z. Zhang, M. Thiéry, V. Baroghel-Bouny, A review and statistical study of existing hysteresis models for cementitious materials, Cem. Concr. Res. 57 (2014) 44–60.
[23] H.H. Willems, K.B. Van Der Velden, A gravimetric study of water vapour sorption on hydrated cement pastes, Thermochim. Acta 82 (1984) 211–220.
[24] A. Cloutier, Y. Fortin, Moisture content—water potential relationship of wood from saturated to dry conditions, Wood Sci. Technol. 25 (1991) 263–280.
[25] W. Thomson, LX, On the equilibrium of vapour at a curved surface of liquid, Philosophical Magazine Series ~ 4421871. 448–452.
[26] M. Fredriksson, L. Wadsö, P. Johansson, Small resistive wood moisture sensors: a method for moisture content determination in wood structures, Eur. J. Wood Prod. 71 (2013) 515–524.
[27] H.M. Jennings, Refinements to colloid model of C–S–H in cement: CM-II, Cem. Concr. Res. 38 (2008) 275–289.
[28] A.C.A. Muller, K.L. Scrivener, A.M. Gajewicz, P.J. McDonald, Densification of C–S–H measured by ^{1}H NMR relaxometry, J. Phys. Chem. C 117 (2012) 403–412.
[29] A.C.A. Muller, K.L. Scrivener, A.M. Gajewicz, P.J. McDonald, Use of bench-top NMR to measure the density, composition and desorption isotherm of C–S–H in cement paste, Microporous Mesoporous Mater. 178 (2013) 99–103.
[30] M. Wu, B. Johannesson, M. Geiker, Application of water vapor sorption measurements for porosity characterization of hardened cement pastes, Constr. Build. Mater. 66 (2014) 621–633.
[31] R.F. Feldman, Sorption and Length-change Scanning Isotherms of Methanol and Water on Hydrated Portland Cement, Division of Building Research, National Research Council, 1970.
[32] H.M. Jennings, A model for the microstructure of calcium silicate hydrate in cement paste, Cem. Concr. Res. 30 (2000) 101–116.
[33] J.J. Thomas, H.M. Jennings, A colloidal interpretation of chemical aging of the C–S–H gel and its effects on the properties of cement paste, Cem. Concr. Res. 36 (2006) 30–38.
[34] M. Wu, B. Johannesson, M. Geiker, A study of the water vapor sorption isotherms of hardened cement pastes: possible pore structure changes at low relative humidity and the impact of temperature on isotherms, Cem. Concr. Res. 56 (2014) 97–105.
[35] S. Brunauer, P.H. Emmett, E. Teller, Adsorption of gases in multimolecular layers, J. Am. Chem. Soc. 60 (1938) 309–319.
[36] P.R. Rangaraju, J. Olek, S. Diamond, An investigation into the influence of interaggregate spacing and the extent of the ITZ on properties of Portland cement concretes, Cem. Concr. Res. 40 (2010) 1601–1608.
[37] P.L.J. Castro, F. Rajabipour, R. Henkensiefken, J. Weiss, Internal curing: discussion of the role of pore solution on relative humidity measurements and desorption of lightweight aggregate (LWA), ACI 270 (2010) 89–100.

Paper II

Cement and Concrete Research 70 (2015) 60–66

Contents lists available at ScienceDirect

Cement and Concrete Research

journal homepage: http://ees.elsevier.com/CEMCON/default.asp

Evidence for anomalous water vapor sorption kinetics in cement based materials

Mahsa Saeidpour *, Lars Wadsö

Building Materials, Lund University, Sweden

ARTICLE INFO

Article history:
Received 7 July 2014
Accepted 24 October 2014
Available online 22 January 2015

Keywords:
Cement pastes (D)
Transport properties (C)
Diffusion (C)
Anomalous sorption

ABSTRACT

We used dynamic sorption balance measurements to evaluate the diffusivity for cement pastes with three different binders (OPC, OPC + 70% slag, OPC + 10% silica fume). The diffusion of water vapor in cement based materials is normally assumed to follow Fick's law of diffusion, but our results clearly show that Fick's law cannot completely describe the sorption process in our materials. In this paper we report the evidence for this anomalous sorption behavior and discuss a possible method to evaluate diffusivities from such measurements.

1. Introduction

Diffusion is normally assumed to follow Fick's law. Although Fick's original experiments were made with ion diffusion in liquid water [1], Fick's law is also used for gas and vapor diffusion in solids. The most commonly discussed diffusing species is water vapor, and there is a general interest in understanding the relations between solids and water vapor for materials such as construction materials [2,3], food stuffs [4,5], and pharmaceutics [6–9].

It is commonly found that Fick's law describes different types of diffusion phenomena well, but there are also cases – mainly in the polymer [10–15] and wood [16,17] literature – where more or less strong deviations from Fick's law have been found. Such cases are termed non-Fickian behavior or anomalous sorption. A unique type of such behavior is sometimes found for solvent absorption in synthetic polymers in which the ingress of the solvent progresses with a front that moves at a linear velocity. This gives a linear mass uptake as a function of time that cannot be explained by Fick's law alone, as Fick's law will result in a mass change rate that decreases with time. The linear ingress has been termed case II [18] and is found when it is the rate of swelling (relaxation) at the front between dry and swollen material that determines the sorption kinetics [10].

A second type of anomalous behavior, the retarded sorption, can be seen in synthetic and natural polymers. It is then found that water vapor absorption is much slower than what can be expected from Fickian diffusion [10,19]. The slow sorption is then not related to the thickness of the sample, but governed by other processes; cf. the rate of sorption in wood cell walls that is independent of their thickness [20]. In general, anomalous sorption in polymers is thought to be controlled by diffusion coupled to mechanical relaxation phenomena [21,22].

Anomalous behavior has been seen for capillary (liquid) absorption (sorptivity) of porous building materials (bricks, aerated concrete, mortar, concrete etc.) by different authors. An overview of such behavior is given by Hall [23]. Capillary absorption is expected to be proportional to $\sqrt{t}$ but such results often show bilinear behavior when plotted as function of $\sqrt{t}$. Possible explanations given in different studies are inhomogeneity in sample structure or initial moisture content, gravitation effect on test method, air-trapping in large pores and microstructural changes due to delayed hydration. Only few of these phenomena are applicable on the vapor sorption discussed in this paper.

In this paper, based on sorption measurements on cement pastes, we present the first evidence that anomalous sorption behavior can also be found in cement based materials.

2. Theory

Fick's law is used for all types of mass transport that follow the following constitutive relation (here written for one diffusing species in one dimension)

$$q = -D_c \frac{dc}{dx}. \tag{1}$$

Here q (g m^{-2} s^{-1}) is the mass flux, D_c (m^2 s^{-1}) is the diffusivity, c (g m^{-3}) is the concentration of the diffusing species and x (m) is the distance. The concentration is the mass of the diffusing species per volume of material and the diffusivity can be a function of the

* Corresponding author. Tel.: +46 2227786.
E-mail address: mahsa.saeidpour@byggtek.lth.se (M. Saeidpour).

http://dx.doi.org/10.1016/j.cemconres.2014.10.014
0008-8846/

concentration. Other potentials (e.g. vapor pressure) can be used in Eq. (1), but concentration is the most common.

When measuring the diffusivity of water vapor in materials of different kinds, the boundary conditions have to be set by exposure of the sample to water vapor, even if it is the rate of change of moisture concentration in the material that is to be measured. The vapor state can be expressed in various ways; for example as the concentration in the gas phase (the vapor content) v (g m^{-3}) or as the water activity a_w, which has the value 0.0 in the absence of any water and 1.0 in liquid water (saturated conditions). In practice the water activity has the same numerical value as the relative humidity at equilibrium at 20 °C and 1 atm [24].

Eq. (1) is a constitutive transport equation. If this is combined with the mass balance equation

$$\frac{dc}{dt} = -\frac{dq}{dx}, \tag{2}$$

we will get the general Fick's law for non-steady state conditions (here written for a constant diffusivity)

$$\frac{dc}{dt} = D_c \frac{d^2c}{dx^2}. \tag{3}$$

Note that Eq. (2) is pure book-keeping and does not involve any new physics.

For hygroscopic materials, there is a relation between the water activity and the concentration at equilibrium. This non-linear relation is called the sorption isotherm

$$c = c(a_w). \tag{4}$$

The sorption isotherms for materials such as hardened cement paste, wood and meso-porous materials are complex as they generally have strong hysteresis.

A common way to measure diffusivities is by taking a sample in equilibrium with a certain relative humidity (water activity) and exposing it to another relative humidity. The sample will then change its mass and from the rate at which it does so the diffusivity can be calculated. The initial and boundary conditions to Eq. (3) are as follows for this type of measurement with one-dimensional flow

$$c(x, t<0) = c_0, \tag{5}$$

$$c(x = \pm L, t \geq 0) = c_1. \tag{6}$$

Here, L (m) is the half thickness of the sample, and $x = 0$ is at the center of the sample. We call this a sorption measurement. The analytical solution for the mass change during this type of measurement is given by, for example, Crank [25] (not given here). In the one-dimensional case, the mass change is normally expressed as the fractional mass change E

$$E = \frac{\Delta m(t)}{\Delta m(\infty)}. \tag{7}$$

The result of a step-change of water activity will give an E that is proportional to the square root of time up to at least $E = 0.5$, as is seen in the solid line in Fig. 1. The diffusivity can be calculated by approximations to the analytical solution. For the initial linear part, the following equation is useful [25]:

$$D_c = \frac{\pi L^2}{4}\left(\frac{dE}{d\sqrt{t}}\right)^2. \tag{8}$$

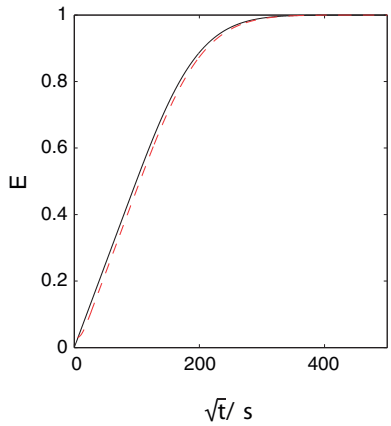

Fig. 1. Simulated results of sorption measurements for 2 mm thickness slab and $D_c = 2 \cdot 10^{-11}$ m^2 s^{-1}. The solid line shows the ideal Fickian case (Eqs. (1), (5), (6)) and the dashed line shows the Fickian case with an external mass flow resistance or a non-perfect step in water activity.

The dashed curve in Fig. 1 shows a case that is commonly seen in sorption curves: the initial part is delayed, resulting in a sigmoidal sorption curve. This can be caused by external mass transfer limitations or a non-perfect step in external conditions [12]. It has been shown that approximate diffusivities can be calculated from sigmoidal sorption curves and that the best agreement is found when Eq. (8) is used with the maximum $dE/d\sqrt{t}$ [26].

While Fick's law may be applicable in many diffusion cases, there are many cases that show deviation from Fickian sorption kinetics, especially in polymers [10,12–14]. As discussed above, such anomalous or non-Fickian cases cannot be fully explained by the above equations.

3. Materials and methods

The samples tested were cement pastes of ordinary Portland cement OPC (CEM I), OPC with 70% slag and OPC with 10% silica fume, with two different water/binder ratios (w/b), 0.5 and 0.4. The specimens were cast in small stainless steel tubes (rings) (inner diameter 5.5 mm, outer diameter 5.9 mm, sample thickness 2.0 mm) to make geometrically well-defined samples with one-dimensional transport. Samples were mixed and cast into tubes that were standing on a glass surface (microscope glass) covered with polyethylene film to avoid any reaction between cement and glass. The samples were slightly vibrated after casting and then a glass with polyethylene film was placed on top. The specimens were hydrated in sealed glass containers with a surplus of the same cement pastes. As the samples are small there is a significant risk that they will dry or be affected by carbonation during the long-term hydration even if they are kept in supposedly tight containers. They were therefore kept together with about 200 g of the same cement paste that would act as a buffer and decrease both moisture losses and carbonation. The hydration was continued for 90 days. After 90 days the samples were taken out and placed in sealed containers in contact with wet cloth to become capillary saturated. The 2 mm samples had start masses of approx. 135 mg and contained about 25 mg evaporable water. We also report some measurements on crushed cement paste (<1 mm particles) made with the same materials according to EN 196-1 [27].

Sorption measurements were made at 25 °C with a DVS 1000 (Surface Measurement Systems Ltd, London, UK). Measurements were

made by first capillary saturating the samples and then exposing them to the following RH-program: 95–90–80–70–60–50–40–30–40–50–60–70–80–90–95–90–80–70–60–40–20–10–0% RH. Each RH step was ended when the mass change rate was lower than 0.0001% of the initial mass per minute, or if a maximum time of 2000 min had been exceeded; except for some measurements that are presented in Sub-section 5.6. The samples in tubes were exposed hanging freely in the gas stream of the DVS; the crushed samples were exposed in a glass pan. The original aim of the measurements was to calculate diffusivities in absorption and desorption, but this was not trivial because of the anomalous behavior.

We also report results from measurements of steady-state diffusion coefficients (cup measurements). These were made on small disks of cement paste (thickness 3 mm, diameter 14.5 mm) that were fastened on glass vials with different relative RHs generated by saturated salt solutions (cf. reference [28]). The cups were exposed to an external RH in a closed environment with a fan to reduce external mass transfer limitations.

Analytical solutions and simulated sorption curves were calculated with ad hoc programs made in MATLAB R2013a.

4. Results

Selected results from measurements on a sample of OPC paste (w/b-ratio 0.5) are shown in Fig. 2, and some results from a crushed sample are shown in Fig. 3 (the bulk of our measurements will be reported elsewhere). It is seen that although some curves are Fickian (cf. Fig. 2A), many show deviations from Fickian behavior. Many curves show initial rapid sorption followed by slower further uptake (cf. Fig. 2C). Some have two almost linear parts in the sorption curves (bi-linear) (cf. Fig. 2B). Similar anomalous behavior was also seen in samples containing slag or silica fume.

5. Discussion

The sorption behavior expected from Fickian diffusion is discussed above. Here we discuss our measurements in terms of deviations from the Fickian behavior. As it is seen in Figs. 2 and 3, our sorption curves for cement based materials have different shapes, and many of these are distinctly anomalous in the sense that they do not look like the result expected from a process governed by a single Fickian process (cf. Fig. 1).

All sorption curves have an initial linear part – excluding a small initial delay – that can be used to calculate the diffusivity if the final mass is known. We have evaluated $dE/d\sqrt{t}$ as the mean slope in the interval $0.2 < E < 0.4$. For the curve in Fig. 2A, the slope $dE/d\sqrt{t}$ is 0.0083, which gives a diffusivity of $5.4 \cdot 10^{-11}$ m^2 s^{-1} (Eq. (8)). For the curves in Fig. 2B–C this type of analysis is more difficult as they do not come to equilibrium, but a method for this is discussed in Section 6.

If Figs. 2B and 3B – which both are for the same RH-step — are compared, it is seen that the initial part finishes at about 45 $\sqrt{s}$ for the crushed material (<1 mm), but lasts until about 90 $\sqrt{s}$ for the 2 mm slab. As the vapor quickly diffuses in between the particles, this is essentially a comparison between two different sample sizes. The diffusion of vapor into the samples thus follows Fick's law (cf. Eq. (8)). However, at longer times when the Fickian diffusion into the samples is completed, they still show the same anomalous mass change.

Anomalous sorption should be caused by the sorption behavior of a material and not by external factors, such as experimental limitations. Here we discuss if experimental limitations can explain the results.

5.1. External mass transfer limitation

When boundary layer resistance becomes significant, the half time of sorption becomes higher yielding a lower apparent diffusion coefficient than the true one. This has led some researchers to describe anomalous behavior as a boundary layer effect ([11,12]).

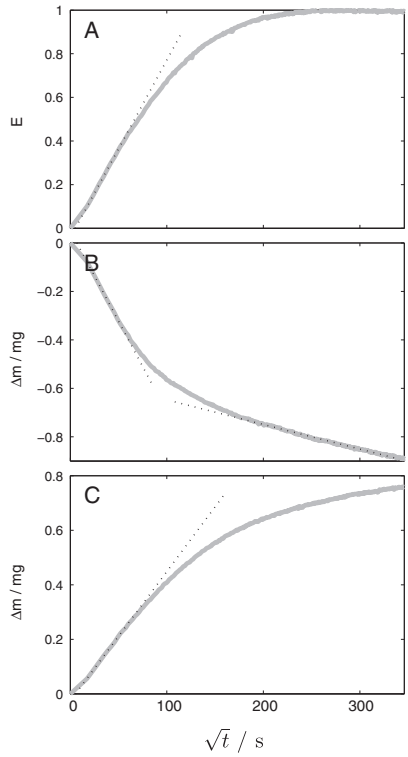

Fig. 2. Results from sorption measurements on a 2 mm thick sample of cement paste. A: example of a measured sorption curve with a similar shape as the Fickian curves in Fig. 1 (50–60% RH). B: example of a measured sorption curve that is bi-linear and distinctly non-Fickian (90–80% RH). C: example of a measured sorption curve that has an initial Fickian part, but that does not come to equilibrium as quickly as expected for a Fickian curve (60–70% RH). The dashed lines mark linear parts of the sorption curves.

To evaluate the mass transfer coefficient between the sample and the air in sorption balance, a water saturated sponge was fitted into the same type of steel tubes as used in the other experiments and the same method was used as described in reference [29]. This mass transfer coefficient k_v (m s^{-1}) is used in the following equation

$$q = k_v(v_a - v_s), \tag{9}$$

where v_a and v_s are the vapor contents (g m^{-3}) of the gas stream and the surface of the sample, respectively.

Our set-up has an external mass transfer coefficient of 0.172 m s^{-1}. Based on the value of the diffusion coefficient of water vapor in still air ($2.42 \cdot 10^{-5}$ m^2 s^{-1} at 20 °C) [30], the calculated mass transfer coefficient corresponds to 0.14 mm of still air. The importance of an external mass transfer limitation should be judged in relation to the internal diffusive mass transfer limitations. However, as k_v has vapor content as potential (as it is caused by the limited transfer through the boundary layer) it is not directly comparable to D_c (that has moisture

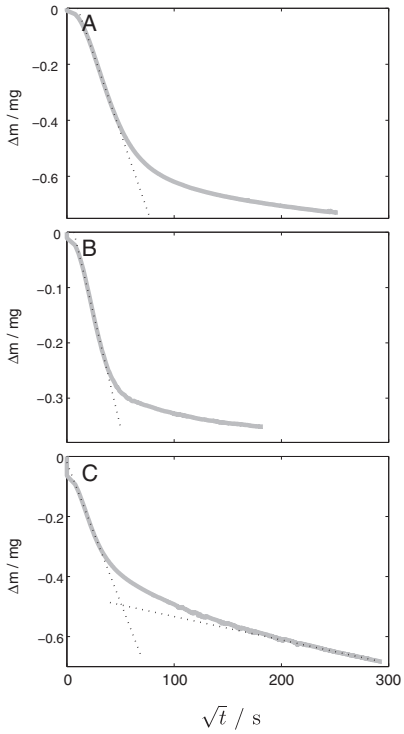

Fig. 3. Three examples of sorption curves that are non-Fickian for cement paste particles (approx. 1 mm). A: (90–80% RH). B: (90–80% RH) second desorption. C: example of a measured sorption curve that is bi-linear (70–50% RH).

concentration as potential). A conversion of k_v to k_c can be made using the following equation

$$k_c = k_v v_{sat} \frac{da_w}{dc}. \quad (10)$$

Here, v_{sat} (g m^{-3}) is the saturation vapor content, and da_w/dc is the inverse of the slope of the sorption isotherm. From our measurements, dc/da_w is about $6.5 \cdot 10^5$ g m^{-3} in the RH-range 95 to 70% and v_{sat} is 23.0 g m^{-3} [31]. The external mass transfer coefficient k_c is thus about $6.1 \cdot 10^{-6}$ m s^{-1}. Using this coefficient together with a diffusivity of $2 \cdot 10^{-12}$ m^2 s^{-1}, gives the slightly sigmoidal curve shape shown in Fig. 1. The external mass transfer limitation thus does not give the anomalous sorption behavior seen in Fig. 2.

5.2. Drift in balance

The stability of the microbalance was checked with placing empty sample holders in the sorption balance and exposing them to a step change RH program. The sample holders were equilibrated at five different RHs in absorption and desorption (0–50–95–70–30–0%), in each of these steps they were kept for 26 h while the mass was recorded. The maximum drift in the mass during the last 24 h of each measurement was 2 μg for 95% RH while at the five other lower RHs the noise level of the balance was ±1 μg (no drift). The drift in the balance is thus much lower than the measured anomalous mass changes (cf. Fig. 2B–C).

5.3. Continued hydration

Anomalously slow approach to equilibrium is seen in both absorption (mass increase) and desorption (mass decrease) and at both low and high RHs. If there was a significant continued hydration, this could have given a mass increase at the end of both absorption and desorption and only at high RHs [32]. The results of our measurements therefore do not support that continued hydration is the cause of the anomalous sorption. We would also expect that the rate of hydration was negligible as the samples were well hydrated. We therefore conclude that the anomalous sorption is not caused by continued hydration.

5.4. Concentration dependent diffusivity

The concentration dependence of the diffusivity influences the shape of the sorption curves, but not much, and not in the way shown in our results. Fig. 4 shows the sorption curves for constant and linearly decreasing and increasing diffusivities with a factor two change in the range of the sorption step (it is not probable that the diffusivity will change more than a factor two in the small RH-intervals of our measurements). Note that the increasing diffusivity in an absorption step has the same effect as a decreasing effect in a desorption step (and vice versa). It is seen that the sorption curves for the three cases are similar, and even if the diffusivity is decreasing and giving a slower approach to equilibrium, the approach is still not anything like the results seen in Fig. 2B–C.

5.5. Non-linear sorption isotherm

Sorption isotherms – the relations between concentration and RH – are non-linear, but this does not influence the result of a sorption measurement at all. The RH is only used as a way to produce new external moisture states; the measured mass and the calculated diffusivity are both concentration related parameters.

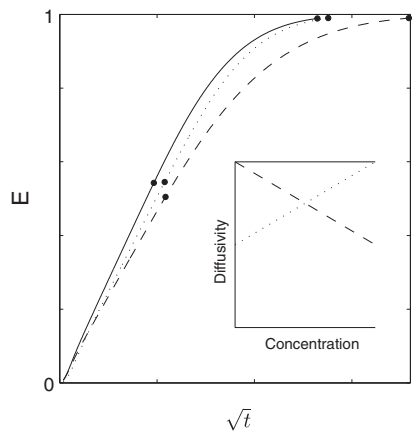

Fig. 4. The effect of a concentration dependent diffusivity. The sorption curves for constant, increasing and decreasing diffusivities (the two latter change by a factor 2 in the range of the simulation) are shown together with markers for when the slope of each curve has decreased 5% from its initial value, and when each curve has reached $E = 0.99$.

5.6. Non-complete previous step

It is clearly a complication in these measurements that few of the steps reach equilibrium. The measurements were meant to be a rapid way of generating diffusivities by not waiting for equilibrium at each level, but instead continuing to the next RH level when the major part – say 90–95% – of a step was made [29]. Because of the anomalous sorption behavior we instead end up with sorption curves that start with an unknown state and end up at another unknown state. However, this should not give longer time-scales if the process was Fickian. An example is given in Fig. 5 in which each sorption step continues until 80% of the equilibrium mass is reached. The sorption curves tend to become linear much longer than for the ideal Fickian sorption curves (Fig. 5), but they do not give the type of anomalous behavior seen in our results.

Fig. 6 shows the results for long measurement (the total time of this step is 10,000 min), for 80–70% RH. The sample was equilibrated in the step before this (90–80% RH) for 6000 min. We still see anomalous behavior.

5.7. Hysteresis and scanning

The anomalous behavior seen has a relation to hysteresis as it is not seen right after a change of sorption direction (scanning). Both cast samples and powder samples showed a complex behavior in scanning. This behavior was most clear after changing from desorption to absorption, when the first one or two steps showed a peak (Fig. 7). After this one or two steps were Fickian, but then the results again become non-Fickian. So anomalous behavior does not seem to be caused by hysteresis and scanning and it was also seen when we were on the envelope of the hysteresis loop, for example in the seventh consecutive desorption step 40–30% RH.

5.8. Inhomogeneous samples

As the samples are cast lying down (horizontally), there could be a separation so that the top and the bottom of the samples have different properties. The samples could also contain micro-cracks. Such inhomogeneity that could give rise to anomalous behavior, but as such behavior is also seen for the crushed material made from same binders with the same w/b-ratios (cf. Figs. 2–3), we conclude that inhomogeneity is not the cause of such behavior.

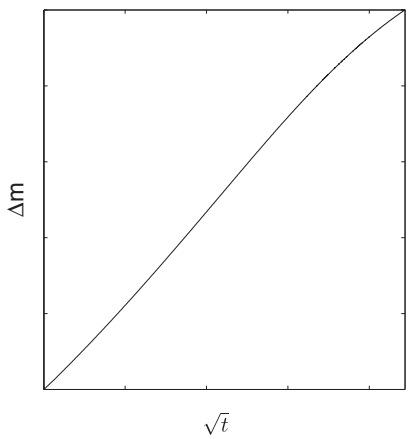

Fig. 5. The result from one RH step in a simulation in which nine previous steps were made and each step was not continued beyond 80% of the equilibrium step response.

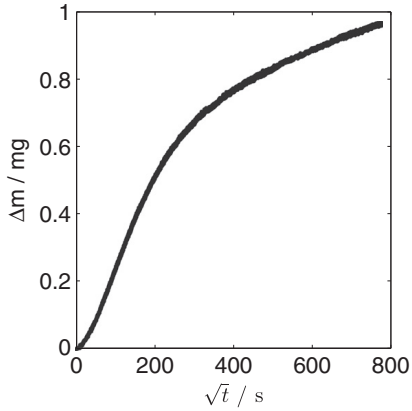

Fig. 6. Results from a long sorption measurement on a 2 mm thick sample of OPC paste for 80–70% RH. The step before this step was equilibrated for 6000 min.

5.9. Inhomogeneous initial moisture content distribution

It is known that capillary saturation does not fully saturate a sample and that the moisture distribution may become inhomogeneous. However, our samples are small (1–2 mm thickness) and it is unlikely that the initial moisture content is not uniform, and as we perform many successive steps an initial inhomogeneous moisture content would be evened out.

5.10. Vapor-tight surface

When cement paste samples are cast against another material – in this case a polyethylene foil – their surface will be different from the

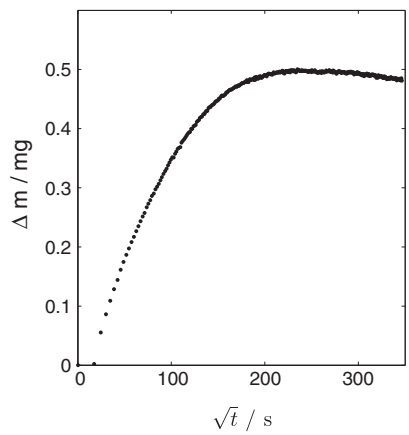

Fig. 7. An example of mass decrease in changing from desorption to absorption 40–50% RH.

bulk. Two reasons for this is that the particle packing is different at an interface and that substances such as $Ca(OH)_2$ may accumulate at the interface. If the surface had a lower conductivity than the bulk, the result would be a sigmoidal sorption curve similar to the effect of an external mass transfer coefficient (Fig. 1) and this is not seen in our results. The anomalous sorption behavior is also seen in crushed samples that does not have a casting surface.

5.11. Carbonation

Thin samples of cement based materials can carbonate (react with the carbon dioxide in the air) in a short time if kept at optimal relative humidity for carbonation. Then the surface of an OPC-based material will become less permeable than the bulk [33]. In the sorption balance the carbon dioxide level is low, so in our case the carbonation would have to take place before the measurement. However, during hydration the samples were kept in containers with a surplus of same binder and any leakage of air (CO_2) into the container would tend to react with that instead of with the samples, and during the saturation the RH is high so that the carbonation is negligible.

6. Origin of anomalous sorption

The original aim of the present measurements was to simultaneously measure sorption isotherms and concentration dependent diffusivities of cement pastes with the method described in reference [29]. The measurements gave the unexpected result that is reported in this paper.

Sorption curves are expected to have an initial linear part, possibly more or less corrupted by a sigmoidal start (Fig. 1). In the following we assume that the initial linear part of our sorption curves is associated with the mass flow into the sample, and we call this macrodiffusion. The second slope or the latter slow attainment of equilibrium (Fig. 2B–C) is caused by other processes not associated with the transport of water vapor through the sample. The second process takes place on shorter length scales and with longer time scales. For the initial rapid process there is local equilibrium between the relative humidity in the porous system and easily accessible sorption sites; for the second process other sorption sites throughout the material successively become available through some time dependent process. The latter is in the polymer literature attributed to “relaxation”, but it is not known what the corresponding processes in cement based materials are.

We see two principal mechanisms that can be responsible for the slow anomalous sorption. The first mechanism is transport limitations. The macrodiffusion takes place in easy accessible diffusion paths and give water molecules access to those parts of the material that are close to the macrodiffusion paths. However, there can also be other sorption sites that can be reached – on a longer time scale – through restricted diffusion paths. For cement based materials such transport rate limitations could possibly be found in the connected nano-porous structure of the CSH.

In the second mechanism the rate limiting process is not transport, but a phenomenon that creates or opens up hidden sorption sites as a function of time. Such a mechanism has been proposed for anomalous sorption in for example wood in which the swelling of amorphous cellulose can expose new sorption sites. Possibly, similar processes can take place within CSH or other hydrated phases in cement based materials.

7. Evaluation of the diffusivity from anomalous sorption curves

Calculating the diffusivity requires that $dE/d\sqrt{t}$ is known (Eq. (8)), but for anomalous results we only know $dm/d\sqrt{t}$ unless we can find a method for assessing at what final mass change that our initial diffusion-related mass change will end. To evaluate the diffusivity we therefore separate the Fickian part of the curve from the non-Fickian as shown in the example in Fig. 8 following a procedure described by

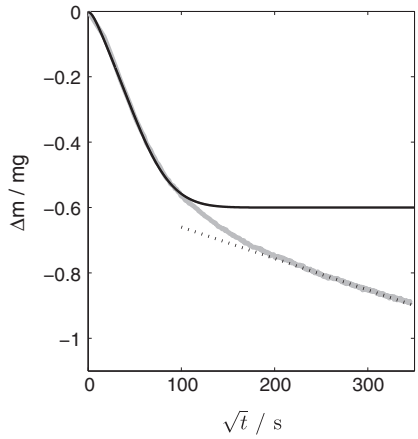

Fig. 8. The sorption curve seen in Fig. 1B (OPC paste sample RH = 90–80%) (thick gray line) overlaid with a calculated Fickian sorption curve (solid line) and a non-Fickian slope (dashed line).

Berens and Hopfenberg [13]. This gave a diffusivity of $D_c = 1.4 \cdot 10^{-10}$ m^2 s^{-1} from the initial slope of Fickian part of the curve, when the final mass change of the Fickian part was assumed to be −0.6 mg. Errors in the assumed final mass change of 10 and 20% give about 20 and 40% error in the calculated diffusivity, respectively. This procedure is therefore rather robust for calculating approximate diffusivities. We have also measured steady-state transport coefficients using the cup method for same cement paste in desorption. In this method a potential difference (vapor content) is applied over a certain thickness of a sample until a steady state flow rate has been reached. Our result from this method expressed using vapor content as potential was $D_v = 3 \cdot 10^{-7}$ m^2 s^{-1} in the range of 75–84% RH and $D_v = 4.5 \cdot 10^{-7}$ m^2 s^{-1} in the range of 84–94% RH. Note that the steady-state measurement only measures the macrodiffusion as the diffusion coefficient is evaluated by Fick's first law (Eq. (1)) after long time (typically 2 months) when the measured moisture flow through the sample is constant, indicating that anomalous sorption is negligible. The diffusivity $D_c = 1.4 \cdot 10^{-10}$ m^2 s^{-1} was recalculated to a diffusion coefficient $D_v = 8.8 \cdot 10^{-7}$ m^2 s^{-1} using the slope of the sorption isotherm, similarly as was described by Eq. (10). There is a reasonable agreement between these values, considering that the two methods are based on different principles and that one of the results is recalculated to the other potential.

Some of our sorption curves show a second linear part, cf. Fig. 2B. As we do not know at what length scale such a process takes place we cannot calculate a corresponding diffusivity, but we can define a time scale for each process, for example a time to half sorption, which for a Fickian process is about $0.2L^2/D$. For the twopart-processes in Fig. 8, $0.2L^2/D$ is about 2000 s and >60 ks, respectively (the value 60 ks is calculated using the final mass loss in the diagram; the actual final mass loss is higher so the time scale is higher than 60 ks). The processes are thus well separated in time. If the length scale of the slower process was known, it would be possible to calculate its associated diffusivity. For length scales (L) of 1 μm and 10 nm, calculated D_c is about 10^{-19} and 10^{-23} m^2 s^{-1}, respectively. However, it can be a coincidence that the second part of some of our sorption curves looks linear. More generally, both linear (Fig. 2B) and non-linear (Fig. 2C) second parts can be modeled by for example a sum of exponential terms.

It is interesting to note that the present anomalous results are clearly seen as the samples are so thin. If thicker samples had been used, the two parts would have merged and it would not been possible to see that there are two active processes. The time scales of the two processes would have been the same if our samples would have been five times as thick ($L = 5$ mm instead of 1 mm).

8. Conclusions

The kinetics of the water vapor sorption on cement paste cannot be fully described by Fick's law. The sorption curves indicate that the water vapor sorption (both absorption and desorption) takes place through two processes. One of these is macrodiffusion into the sample that can be evaluated from the first linear part of sorption curve. The second process takes place on longer time scales and it is related to the availability of sorption sites inside the material.

Acknowledgements

The research leading to these results has received funding from the European Union Seventh Framework Program (FP7/2007–2013) under grant agreement 264448. We thank Min Wu who prepared the material for the cup samples.

References

[1] A. Fick, Ueber diffusion, Ann. Phys. Chem. 114 (1855) 59–86.
[2] V. Baroghel-Bouny, M. Mainguy, T. Lassabatere, O. Coussy, Characterization and identification of equilibrium and transfer moisture properties for ordinary and high-performance cementitious materials, Cem. Concr. Res. 29 (1999) 1225–1238.
[3] R. Luo, J.L. Niu, Determination of water vapor diffusion and partition coefficients in cement using one FLEC, Int. J. Heat Mass Transf. 47 (2004) 2061–2072.
[4] S. Desobry, E. Arab-Tehrany, 4.20 – diffusion barrier layers for edible food packaging, in: S. Hashmi, G.F. Batalha, C.J.V. Tyne, B. Yilbas (Eds.), Comprehensive Materials Processing, Elsevier, Oxford, 2014, pp. 499–518.
[5] E. Besbes, V. Jury, J.Y. Monteau, A. Le Bail, Water vapor transport properties during staling of bread crumb and crust as affected by heating rate, Food Res. Int. 50 (2013) 10–19.
[6] R.L. Jerzewski, N.G. Lordi, Water vapor diffusion in model tablet systems: I. Design of a diffusion apparatus, Int. J. Pharm. 101 (1994) 35–44.
[7] G. Zografi, G.P. Grandolfi, M.J. Kontny, D.W. Mendenhall, Prediction of moisture transfer in mixtures of solids: transfer via the vapor phase, Int. J. Pharm. 42 (1988) 77–88.
[8] G. Zografi, M. Kontny, The interactions of water with cellulose- and starch-derived pharmaceutical excipients, Pharm. Res. 3 (1986) 187–194.
[9] V. Murikipudi, P. Gupta, V. Sihorkar, Efficient throughput method for hygroscopicity classification of active and inactive pharmaceutical ingredients by water vapor sorption analysis, Pharm. Dev. Technol. 18 (2013) 348–358.
[10] J.H. Petropoulos, M. Sanopoulou, K.G. Papadokostaki, Physically insightful modeling of non-Fickian kinetic regimes encountered in fundamental studies of isothermal sorption of swelling agents in polymeric media, Eur. Polym. J. 47 (2011) 2053–2062.
[11] C.M. Hansen, Diffusion in polymers, Polym. Eng. Sci. 20 (1980) 252–258.
[12] C.M. Hansen, The significance of the surface condition in solutions to the diffusion equation: explaining "anomalous" sigmoidal, Case II, and Super Case II absorption behavior, Eur. Polym. J. 46 (2010) 651–662.
[13] A.R. Berens, H.B. Hopfenberg, Diffusion and relaxation in glassy polymer powders: 2. Separation of diffusion and relaxation parameters, Polymer 19 (1978) 489–496.
[14] A.R. Berens, H.B. Hopfenberg, Diffusion of organic vapors at low concentrations in glassy PVC, polystyrene, and PMMA, J. Membr. Sci. 10 (1982) 283–303.
[15] O. Bley, J. Siepmann, R. Bodmeier, Characterization of moisture-protective polymer coatings using differential scanning calorimetry and dynamic vapor sorption, J. Pharm. Sci. 98 (2009) 651–664.
[16] L. Wadsö, Describing non-Fickian water-vapour sorption in wood, J. Mater. Sci. 29 (1994) 2367–2372.
[17] G.N. Christensen, K.E. Kelsey, Die Geschwindigkeit der Wasserdampfsorption durch Holz, Holz Roh Werkst. 17 (1959) 178–188.
[18] T. Alfrey, E.F. Gurnee, W.G. Lloyd, Diffusion in glassy polymers, J. Polym. Sci., Part C: Polym. Lett. 12 (1966) 249–261.
[19] L. Wadsö, Measurements of water vapour sorption in wood, Wood Sci. Technol. 28 (1993) 59–65.
[20] G.N. Christensen, Kinetics of sorption of water vapour by wood: I. The effect of sample thickness, Aust. J. Sci. 11 (1960) 295–304.
[21] N.L. Thomas, A.H. Windle, A deformation model for Case II diffusion, Polymer 21 (1980) 613–619.
[22] N.L. Thomas, A.H. Windle, A theory of Case II diffusion, Polymer 23 (1982) 529–542.
[23] C. Hall, Anomalous diffusion in unsaturated flow: fact or fiction? Cem. Concr. Res. 37 (2007) 378–385.
[24] S. Gál, Über die Ausdrucksweisen der Konzentration des Wasserdampfes bei Wasserdampf-Sorptionsmessungen, Helv. Chim. Acta 55 (1972) 1752–1757.
[25] J. Crank, The Mathematics of Diffusion, Oxford University Press, Oxford, 1975.
[26] L. Wadsö, A test of different methods to evaluate the diffusivity from unsteady-state sorption measurements, Drying Technol. 12 (1994) 1863–1876.
[27] B.E. 196-1, Methods of Testing Cement Determination of Strength, 2005.
[28] A. Anderberg, L. Wadsö, Moisture in self-levelling flooring compounds, Part I. Water Vapour Diffusion Coefficients [Elektronisk resurs], Nordic Concrete Research (NCR), 2004.
[29] A. Anderberg, L. Wadsö, Method for simultaneous determination of the sorption isotherm and the diffusivity of cement-based materials, Cem. Concr. Res. 38 (2007) 89–94.
[30] W.M. Haynes, Handbook of Chemistry and Physics, 93rd edition CRC Press, 2012.
[31] F.W. Murray, On the computation of saturation vapor pressure, J. Appl. Meteorol. 6 (1967) 203–204.
[32] T.C. Powers, A Discussion of Cement Hydration in Relation to the Curing of Concrete, Portland Cement Association, 1947.
[33] N. De Belie, J. Kratky, S. Van Vlierberghe, Influence of pozzolans and slag on the microstructure of partially carbonated cement paste by means of water vapour and nitrogen sorption experiments and BET calculations, Cem. Concr. Res. 40 (2010) 1723–1733.

Paper III

Moisture diffusion coefficients of mortars in absorption and desorption

Mahsa Saeidpour[1], Lars Wadsö

Building Materials, Lund University, Lund, Sweden

Abstract

Water vapor diffusion coefficients have been determined with a new set-up of the cup method for mortars with three binders (OPC, OPC+70% slag, OPC+10% silica fume) and two water/binder-ratios (0.4, 0.5). The measurements were made as a function of relative humidity with samples on both the absorption and desorption limbs of the sorption isotherm. For OPC samples the results show a clear difference between absorption and desorption. For the samples with supplementary cementitious materials the dependence on RH is small.

Keywords: Transport Properties (C); Diffusion (C); Durability (C); Supplementary cementitious materials; cycles (C); Mortar (E)

1. Introduction

As nearly all degradation issues with concrete and other cement based materials are relates to water, moisture transport properties are among of the most important parameters in durability models of such materials [1]. Water transport through porous materials can be described in different ways; the most fundamental division is into liquid water transport described with Darcy's law and water vapor transport described with Fick's law. The transport coefficient is normally called permeability in Darcy's law and diffusion coefficient in Fick's law. The driving force in Darcy's law is the total pressure in the liquid water [2], while transport in Fick's law is written in terms of diffusion, the tendency of random motion of molecules to

[1] Corresponding author. Tel: +462227786
E-mail address: mahsa.saeidpour@byggtek.lth.se

even out concentration differences. In porous materials it is a common situation that there are both large pores that are filled with air and water vapor and smaller pores that are filled with liquid water, and it is customary to use Fick's law even if part of the transport takes place in the liquid phase. One of the main reasons for this is that boundary conditions are usually expressed in terms of relative humidity (vapor content). In cement based materials diffusion coefficients are function of the moisture condition of the sample [3, 4].

In some studies of cementitious materials the total moisture diffusion is separated into two terms, vapor flow with vapor content or vapor pressure as gradient and liquid water transport with pore water pressure as gradient [5]. This approach has some practical advantages for modeling, but although the amount of vapor and liquid water can be accurately determined, it is not trivial to experimentally separate the two types of transport in a meaningful way as they – from a macroscopic perspective – are not spatially separated, but take place in a complex way in every point in a material. We have therefore chosen to work with diffusion coefficients that include both types of transport. In addition, in cementitious materials other mechanisms such as the flow of adsorbed water may also contribute to the transport.

A common method to measure steady-state diffusion coefficients is the cup method. In this method a disk-shaped specimen with a certain thickness is exposed to different relative humidities (RHs) on its two surfaces. The RH inside the cup is normally generated by a saturated salt solution and the external RH is that of ambient air. The moisture flux through the specimen is calculated from the mass change rate of whole cup. With this method it is possible to evaluate diffusion coefficients as a function of RH by making measurements in different RH intervals.

It is well known that cementitious materials – as most other materials – show sorption hysteresis [6-9]. For cementitious materials this is thought to have its origin in the fine porous

structure of these materials. The sorption – the physically bound water – is of two types: adsorption and capillary condensation [10]. Adsorption is the coverage of surfaces with a thicker and thicker layer of water molecules with increasing RH. This starts at low RHs and continuous through the whole RH range up to saturation. Capillary condensation is the filling of pores by thermodynamic driving forces; a filled pore has a curved meniscus at the water-air interface and thus a lower pressure (a suction pressure) which thermodynamically is equal to a lowered RH of the water in the pore (lower than the standard RH of bulk water of 100%). Capillary condensation in the smallest pores in a cementitious materials with a radius of about 2 nm takes place at about 50% RH; below this value there is only adsorption [11, 12].

The reason for this hysteresis in the capillary condensation range is (at least) two-fold. Firstly, as the pore structure is complex with small and large pores being mixed, when a large pore is placed inside small pores the large pore will not be emptied until the small pores are emptied (the ink-bottle effect) [8]. Secondly, the filling of cylindrical pores takes place on the radius of curvature of the circumference of the pore, while its emptying is from the two radii of curvature of the water meniscus [9]. It is thus natural that we end up with higher moisture content at desorption than at absorption (at the same RH).

As mentioned above, transport of water in cementitious materials occurs by vapor diffusion in empty pores and by capillary transport in filled pores. It is at present not possible to make a comprehensive model of water vapor transport in cementitious materials. The system is complex in that pores of different sizes are connected in three dimensions [13]. However, it is clear that pores with capillary condensed water have much higher water transport capacity than air filled pores with water vapor diffusion [5, 14], and it is probable that transport of adsorbed water (surface flow) is only a minor contributor to the total flow[15].

Based on the above discussion we can state the following hypothesis: samples in desorption show higher transport rates than samples in absorption when measured in the same RH range above 60% RH (transport coefficient hysteresis). As transport of water through materials in the hygroscopic range normally is measured with different static RH-levels this effect should be seen in studies made in both absorption and desorption. This is true both for the cup method where the flow is measured through specimens kept between two RH-levels, and for the sorption method where the mass increase of a sample is measured as it goes from equilibrium with one RH to a second RH [5, 16]. As we have not found any studies of this in the literature, we have made the experiments presented in this paper, in which diffusion coefficient for mortars with 3 different binders (OPC, OPC+70% slag and OPC+10% silica fume) were determined for samples on the absorption and desorption limbs on the sorption isotherm. We also describe a new cup method set up to avoid carbonation in cementitious samples during measurement, and discuss transport coefficient hysteresis.

2. Experimental

2.1. Materials

The materials used in this study were mortars with three different binders and two water/binder-ratios 0.4 and 0.5. The binders were ordinary Portland cement OPC (CEM I), OPC with 10% silica fume, and OPC with 70% slag (CEM III). The chemical compositions of the cements and the silica fume are given in Table 1 in reference [12]. The CEM III was premixed, but silica fume slurry was added to the OPC for the material with silica fume. The sand used in this study was standard sand EN 196-1 [17] with a maximum particle size of 2 mm.

The mortar materials were mixed with water according to EN 196-1 and cast in a 40×10×10 cm^3 steel mold. The mold was placed in a 20 °C climate room and cooled with fans during

first 24 hours of hydration to keep the temperature of hydration constant around 20 °C. Temperature was measured with thermocouples on the surface and in the center of the steel mold during the first 24 hours of hydration. The maximum temperature measured in the center was 24 °C (for samples with 10% silica fume). The samples were seal-cured for 90 days at 20 °C. After that, cylindrical specimens with a diameter of 64 mm and a thickness of 12-13 mm were wet cut from the blocks. A specimen thickness of at least six times the maximum sand diameter was used to give specimens whose properties are representative for the material. Before the measurements, the samples were in contact with wet cloth in sealed containers for one month to become capillary saturated and avoid carbonation.

2.2. The new cup method set up

The water vapor diffusion coefficients with vapor content as potential (D_v) of the mortars was measured with a new set-up developed in our laboratory based on the standard cup test [18]. In this method the samples are placed as lids on cups containing saturated salt solutions with different constant RHs. In our set-up there are different RHs inside the cups, but they are all placed in sealed boxes with NaCl saturated solution with 75.5% RH at 20 ˚C (Fig. 1). Fans circulate the air to keep the RH constant and to decrease the external moisture transfer resistance. To avoid carbonation in the samples during the relatively long measurements, the saturated NaCl solutions that fill the bottom of the boxes are complemented with small containers of unsaturated NaOH-solutions that have the same RH as saturated NaCl solutions. Values for the RH of unsaturated NaOH solutions as a function of their molarity were taken from reference [19]. The hydroxide solutions thus absorb carbon dioxide, but do not interfere with the RH in the boxes. The RH of the boxes was regularly checked with relative humidity sensors and found to be ±1% accurate. The RH-sensors were calibrated with salt solution every month.

The boxes are made of high density polyethylene (HDPE) and they are covered with a glass plate that rests on an EPDM sealing. There is a hole above each cup on the glass plate; these holes are normally covered with silicon stoppers. The steel wire that goes through each stopper has a hook at each end so that the cups can be lifted and hanged in the balance placed over the box (the stopper is then lifted out of its hole). The cups are equipped with steel hang-downs. This set-up makes it possible to measure the mass of the cups without taking them out from the box and expose them to the CO_2 in the air (see Fig.1). When weighing is to be made, the box with the cups is placed on a movable plate under the balance. As the plate has four wheels that can roll in any direction on a glass plate, it is easy to position the box so that the cup to be weighed comes right under the balance.

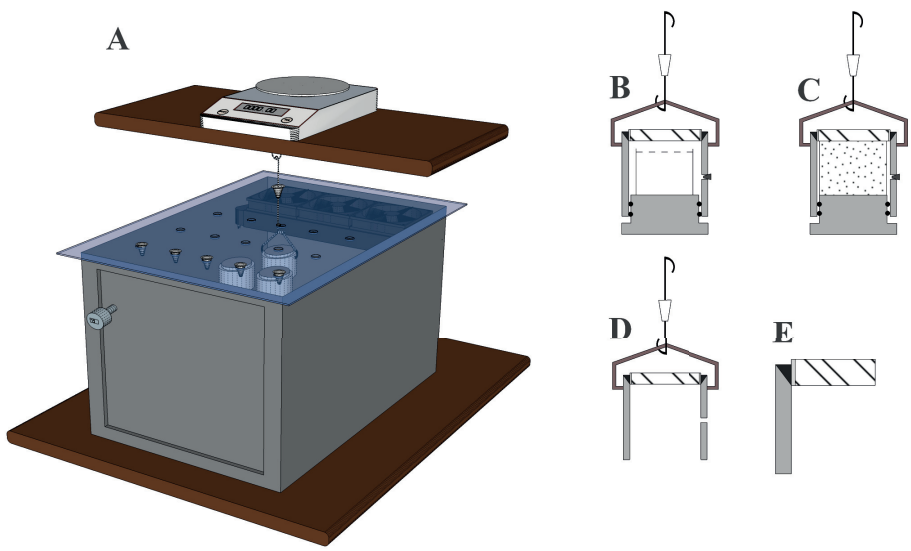

Figure 1. A: Cup method set-up. The cups are placed in boxes with saturated NaCl that are equipped with RH sensors, fans and CO_2 absorbents. To weigh the samples, they are hanged from a balance with steel wires that go through silicon stoppers that seal the holes in the glass plate between the

measurements. B: A cup with salt solution. Each cup is equipped with a steel wire with hooks in both ends; this goes through the stopper so that they both can be lifted and hanged from the balance. The bottom of the cup is removable and when it is closed it is sealed with two o-rings (black). C: A cup with saturated sponge (CAP100%), which is the contact with the sample surface. D: The cups were opened after the first measurements in desorption and the salt solutions and the bottom parts were removed. The cups were then placed in 33% RH before starting the experiment in absorption. E: How a specimen is fastened to the cup. The over-tape is light grey and the sealing tape is shown in black, filling up the space between sample and edge of the cup.

The cup measurements were carried out in two steps. First initially capillary saturated samples were measured in desorption, and then samples initially dried to 33.1% RH were measured in absorption. The diffusion coefficients were in both cases measured at 20±0.5 ˚C with an outer RH of 75.5% (in the boxes). The RHs inside the cups were generated by saturated salt solutions (Table 1) kept in cups (Fig. 1B) so that the distance between the salt solutions and the samples were 15 mm. The salt solutions were prepared by mixing salts (Merck, pA quality) and deionized water (Table 1). Three replicates were used for each combination of material and RH condition. In addition, cups with water (called VAP100%) and cups in which the samples were in contact with liquid water (called CAP100%) were used (Fig. 1C). In the latter a water saturated sponge gave a constant supply of moisture to the surface of a sample. Both the VAP100% and the CAP100% specimens gave large spread in the results and are therefore reported and discussed separately.

Table 1. The salts used and the relative humidity of their saturated salt solutions [20].

Salt Solutions	**RH (%)**
$MgCl_2$	33.1±0.2
NaBr	57.6±0.4
NaCl	75.5±0.14
KCl	85.1±0.3
KNO_3	94.6±0.7
K_2SO_4	97.6±0.4

The masses of the cups were measured regularly on a balance with 1 mg resolution. The moisture flux was calculated as the mass change rate divided by the externally exposed surface area of the samples. Steady-state was considered to be reached when the mass rate was less than 0.002 g per day.

After the samples reached steady state flow in desorption, the measurements were stopped. The cups were then opened and the salt solutions and the bottom parts of the cups with the salt solutions were removed (Fig. 1D). The samples were then dried in boxes with 33.1% RH until they reached a mass change rate of less than 0.003 g per day. In the second absorption-part of the study these dried samples were again placed in the cups with the same RHs as for the desorption measurements and then placed in the boxes with 75.5% RH. The measured diffusion coefficients in the two parts of the study are reported as diffusion coefficients in desorption and absorption, respectively. The whole study took two years to perform.

The cups used are similar to those described by Hedenblad [21, 22] and Anderberg and Wadsö [23]. They are made of polypropylene with EPDM o-rings, and the sealants were two butyl-tapes products (Isola AS, Norway). The first type was a butyl-tape with polyethylene (PE) foil on one side (Platon over-tape). The over-tape is only sticky on one side. The other type was butyl-tape, which is sticky on both sides (Platon sealing tape). The disk-shaped specimens were sealed along the perimeter with the over-tape and then were fitted on the rim inside the cups using the sealing tape to fix the specimen in the cup and to insure a vapor-tight connection between cup and specimen.

2.3. Evaluation

The steady-state vapor flux through a diffusion cup is determined from the measured mass change rate

$$q_m = \frac{\Delta m}{A \cdot \Delta t}. \qquad (1)$$

Here q_m (g m^{-2} s^{-1}) is moisture flux, A (m^2) is surface area of sample, $\Delta m/\Delta t$ (g s^{-1}) is mass change rate.

The aim of cup measurements is to calculate the diffusion coefficient. To do this we need to use Fick's law that is formulated as follows with vapor content as potential:

$$q_m = -D_v \frac{dv}{dx}, \qquad (2)$$

where D_v (m^2 s^{-1}) is diffusion coefficient, v (g m^{-3}) is vapor content and x (m) is the distance. However, as we do not measure the gradient dv/dx, we instead use the integrated form of Eq. 2:

$$q_m = -\overline{D}_v \frac{\Delta v}{\Delta x}, \quad (3)$$

where $\overline{D}_v$ is the mean diffusion coefficient in the measurement interval.

Cup measurements are normally evaluated by finding the slope of the final linear part of the curve of mass as a function of time. This works well if many measurements with low uncertainty can be made at the latter part of a measurement, but in many cases – such as the present measurements – the available data is both quantitatively and qualitatively limited. The quantitative limitations come from that a relatively large test matrix was used and the resources to measure the cups were limited, as was the duration of the measurements; the qualitative limitations have their origin in that the mass measurements are accompanied by uncertainties. In measurements such as the present ones, it would have been optimal to use different sample thicknesses for different samples. Thinner samples could have been used for materials with lower diffusion coefficients (so that all samples would show a similar mass change rate at steady-state), but this is not practical as it is not possible to know the diffusion coefficient before the measurements. As all samples are made to the same thickness, some cups will show low mass changes and are thus more difficult to evaluate with respect to the mass change rate of the final linear part. To improve the situation we have developed an evaluation method that uses all the available data, i.e., also the initial transient data.

Figure 2 shows results of four measurements in the present study. It is seen that mass as a function of time can be continuously increasing or decreasing, or first decrease and then increase, or vice versa. In all cases the final part of the measurement – that we want to evaluate – is linear, but with a significant noise in some cases. We have curve-fitted each measurement to a sum of a straight line and an exponential function:

$$m = at + b + c \cdot \exp\left[-d(t-e)\right], \quad (4)$$

where t is time, m is mass, and a-e are fitting parameters. The parameter a is the slope of the linear part that we want to evaluate. As is seen in Fig. 2 the curve fits are reasonably good.

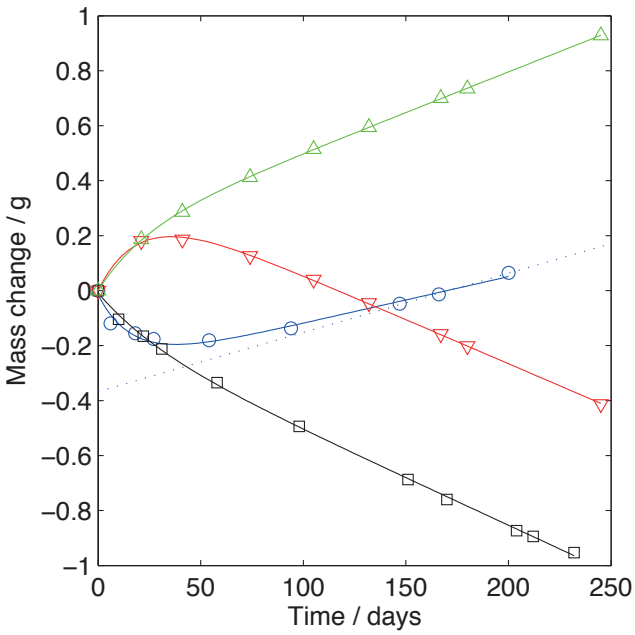

Figure 2. Results for four cups and the corresponding curve fits. The data is for the following measurements: (circles) OPC+slag in desorption with RH=33% inside; (squares) OPC+slag in desorption with RH= 98% inside; (triangles pointing down) OPC in absorption with RH=85% inside; (triangles pointing up) OPC in absorption with RH=58% inside. The dotted line is the linear curve fit to the last three points on one of the data sets (discussed in the text).

The main advantage with the proposed method is that it is not dependent on any subjective judgment and that it improves the accuracy of measurements with few data point at the end of the measurement. The latter is exemplified by the data for "OPC+70% slag in desorption with RH= 33% inside" shown in Fig. 2. If only the three last data points would have been used a 27% higher slope would have been found because of the random scatter in these data points.

With the curve fit method all data points are used and such random scatter does not influence the result as much.

The curve fitting has been made with fminsearch (the simplex method) in MATLAB. As it was difficult to make the curve fit work for all cases based on a general guess of the parameter values, the curve fit was made in two steps. First an exponential curve fit is made to the first four data points and a linear curve fit is made to the last four data points. Based on the coefficients from these curve fits a good guess of the five parameters in Eq. 4 can be made. This results in a robust curve fitting method.

From the flux measurement we evaluate the mean diffusion coefficients in the measurement intervals. For experimental convenience these intervals all have 75% RH on one side, so the primary result shown in Fig. 4 does not give the diffusion coefficient as a function of the RH. However, we can calculate the mean diffusion coefficients in the difference intervals to get results such as those shown in Fig. 5. Consider two cup measurements that have been made on the same sample and with the same external vapor content v_0, but with two different internal vapor contents v_1 and v_2, with the corresponding mean diffusion coefficients D_{v01} and D_{v02} (we now skip the bar over the symbols for diffusion coefficients as all such values given in this paper are mean values in different RH intervals). The mean diffusion coefficient in the difference interval between v_1 and v_2 (D_{v12}) then can be calculated with Eq. 7.

$$D_{v12} = \frac{D_{v02}(v_2 - v_0) - D_{v01}(v_1 - v_0)}{(v_2 - v_1)} \qquad (7)$$

This equation can be developed by writing Eq. 3 for a whole specimen and for a lower and an upper part of the same specimen, all with the same boundary conditions on the outer surfaces (and thus the same flux).

2.4 Error analysis

A complication with cup measurements is that the vapor contents on the two sides of a sample are not the same as the vapor contents of the RHs of the salt solutions inside and outside the cups. On the lower side there is a gap of still air between the saturated salt solution and the sample, and on the top side there is a boundary layer close to the surface. Both the air gap and the boundary layer contribute to the overall resistance to moisture flow, and should be included in the evaluation unless they can be proved to be small. In the following we discuss these in terms of internal and external mass transfer coefficients k_{vi} and k_{ve} (m s^{-1}) (see Fig. 3). For the gap of still air the mass transfer coefficient is a function of the diffusion coefficient of water vapor in air ($D_{v,H2O\text{-}air}$=24.2·10^{-6} m^2s^{-1} [24]) and the thickness of the air gap d (m):

$$k_{vi} = \frac{D_{v,H2O-air}}{d}. \qquad (5)$$

In the present case the air gap is approx.15 mm, which gives a k_{vi} value of approx. 1700 m s^{-1}.

The mass transfer coefficient of the boundary layer is a function of the air speed, the surface roughness and the size of the sample. In the present case the air speed over the cups was about 1 m s^{-1}. A typical literature-value for the mass transfer coefficient for sample of the size of our cup specimens is k_p=50·10^{-9} s m^{-1} which is approx. k_{ve}=0.007 m s^{-1} (recalculated from k_p in reference [25]) .

If the external and internal mass transport coefficients are included in the evaluation, Eq. 3 changes to Eq. 6:

$$q_m = \frac{v_2 - v_1}{\frac{d}{\overline{D}_v} + \frac{1}{k_{vi}} + \frac{1}{k_{ve}}}. \qquad (6)$$

According to this equation, the case with highest D_v of the tested materials will be the most influenced by external resistance. For the present measurements, the moisture flux will be changed by 2% in this case: we therefore neglect the effect of internal and external mass transfer coefficients.

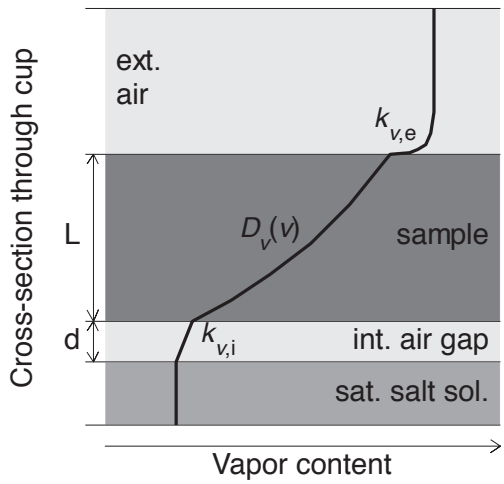

Figure 3. Schematic cross section of a cup considering the mass transfer coefficients of the air gap between salt surface and sample ($k_{v,i}$) inside the cup and the external mass resistance ($k_{v,e}$).

It is important to check the tightness of sealant materials before their use in cup measurements; note that such products can change their properties even if they have the same trade name. The tightness of the sealants was therefore measured in cup measurement in which the sealant covered holes in an aluminum plate on top of a glass cup with a saturated K_2SO_4 (97.6% RH). These cups were placed in a room with 55% RH and 20 °C. The water vapor diffusion coefficient of the sealant with vapor content as potential was about $5 \cdot 10^{-9}$ $m^2 s^{-1}$. This is about 100 times lower than the diffusion coefficient of the materials investigated in

this study (in same RH interval). In this study the effect of vapor flow through the sealant has therefore not been taken into account.

The transport through the edge of the sample is two dimensional as the outer 1 mm of the top surface is covered by sealant. The flow through the sample will then be lower than it should have been if the sample had not had a masked edge (the exposed surface is used in the evaluation. The masked edge effect of the sealant in cup measurements and related correction for diffusion coefficient of samples are discussed in reference [26]. In our cups this correction will increase the calculated flux by about 5%, but as this is small compared to other uncertainties it is not corrected for our cups.

The thickness (12-13 mm) of each specimen was measured in four positions and an average of these values were used in the evaluation. Thicknesses were accurate to within ±0.5 mm.

3. Results

Diffusion coefficients were first calculated for the measurements intervals between inside the cups and in the boxes (RH=75.5%). The results of these calculations are shown in Fig. 4. The error bars are the standard deviations of the three replicates.

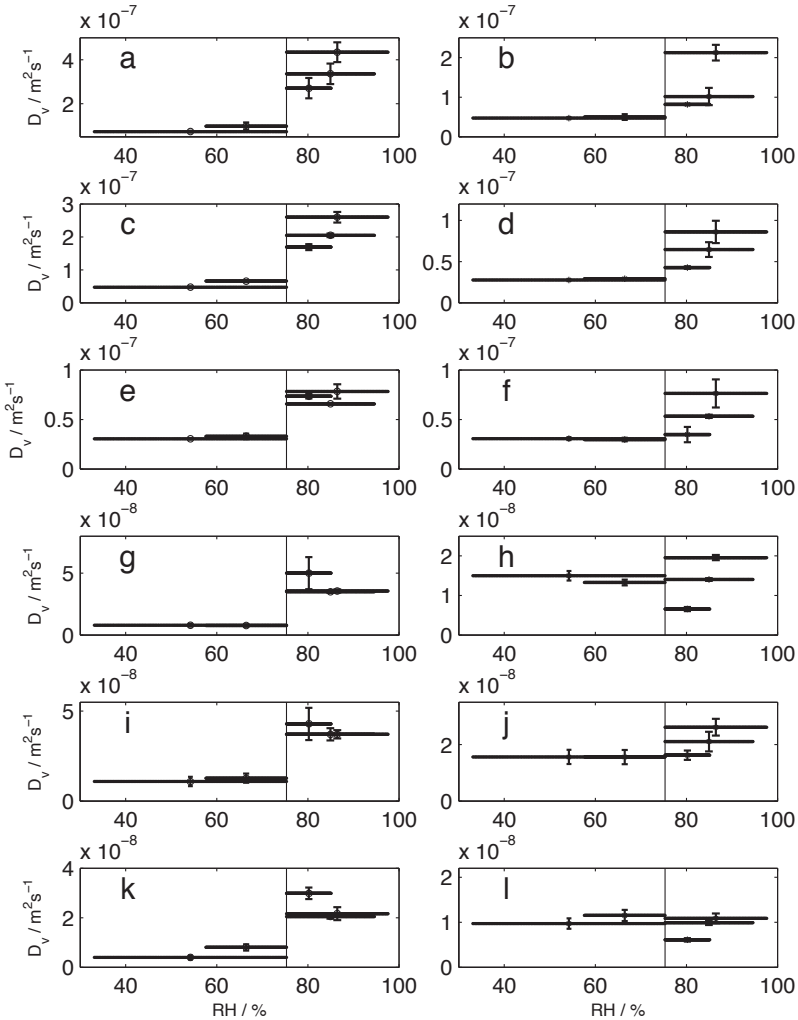

Figure 4. Mortar diffusion coefficients (D_v) measured for (a): OPC mortar w/b=0.5 in desorption, (b): OPC mortar w/b=0.5 in absorption, (c): OPC mortar w/b=0.4 in desorption, (d): OPC mortar w/b=0.4 in absorption, (e): OPC+10% SF mortar w/b=0.5 in desorption, (f): OPC+10% SF mortar w/b=0.5 in absorption, (g): OPC+10% SF mortar w/b=0.4 in desorption, (h): OPC+10% SF mortar w/b=0.4 in absorption, (i): OPC+70% slag mortar w/b=0.5 in desorption, (j): OPC+70% slag mortar w/b=0.5 in

absorption, (k): OPC+70% slag mortar w/b=0.4 in desorption, (l): OPC+70% slag mortar w/b=0.4 in absorption, for intervals of RH inside the cups (97.6, 94.6,85.1,57.6,33.1 %) and climate chamber (75.5%). The error bars show the standard deviation of three replicates.

Table 2. Measured diffusion coefficients for cups with water vapor (VAP100%) and liquid water (CAP100%) inside and 75.5% RH outside the cups (the interval of measurement is 75.5%-100%). The standard deviations given after ± are calculated from three replicates.

Mortar sample	**VAP100%**	**CAP100% cups**
OPC, w/b=0.5 desorption	$(4.8 \pm 0.78)\cdot 10^{-7}$	$(4.7 \pm 1.9)\cdot 10^{-7}$
OPC, w/b=0.5 absorption	$(3.6 \pm 0.4)\cdot 10^{-7}$	$(3.2 \pm 0.19)\cdot 10^{-7}$
OPC, w/b=0.4 desorption	$(2.5 \pm 0.29)\cdot 10^{-7}$	$(3.0 \pm 0.36)\cdot 10^{-7}$
OPC, w/b=0.4 absorption	$(1.52 \pm 0.2)\cdot 10^{-7}$	$(3.1 \pm 0.19)\cdot 10^{-7}$
OPC+10% SF, w/b=0.5 desorption	$(7.1 \pm 0.19)\cdot 10^{-8}$	$(8.5 \pm 0.07)\cdot 10^{-8}$
OPC+10% SF, w/b=0.5 absorption	$(1.1 \pm 0.45)\cdot 10^{-7}$	$(8.1 \pm 1.3)\cdot 10^{-7}$
OPC+10% SF, w/b=0.4 desorption	$(3.5 \pm 0.53)\cdot 10^{-8}$	$(3.9 \pm 0.22)\cdot 10^{-8}$
OPC+10% SF, w/b=0.4 absorption	$(2.9 \pm 0.07)\cdot 10^{-8}$	$(2.1 \pm 0.42)\cdot 10^{-8}$
OPC+70% slag, w/b=0.5 desorption	$(4.7 \pm 0.27)\cdot 10^{-8}$	$(5.9 \pm 1.4)\cdot 10^{-8}$
OPC+70% slag, w/b=0.5 absorption	$(4.9 \pm 0.16)\cdot 10^{-8}$	$(2.6 \pm 0.34)\cdot 10^{-8}$
OPC+70% slag, w/b=0.4 desorption	$(2.9 \pm 0.22)\cdot 10^{-8}$	$(3.2 \pm 0.81)\cdot 10^{-8}$
OPC+70% slag, w/b=0.4 absorption	$(2.6 \pm 0.91)\cdot 10^{-8}$	$(1.2 \pm 0.21)\cdot 10^{-8}$

We have calculated the mean diffusion coefficients for the RH intervals using Eq. 7. Figure 5 shows the result for all materials. The error bars are calculated using Monte Carlo simulations with normally distributed values of D_{01} and D_{02} in Eq. 7 with the measured standard deviations.

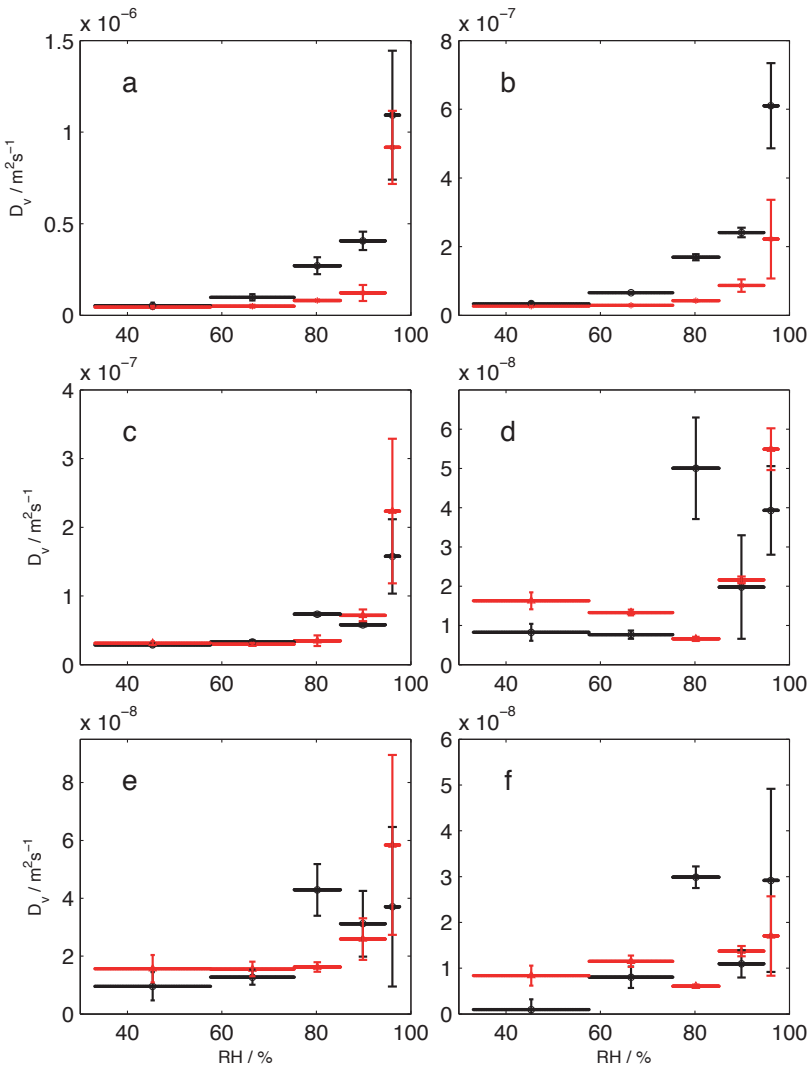

Figure 5. Average moisture diffusion coefficients (D_v) calculated for (a): OPC mortar w/b=0.5, (b): OPC mortar w/b=0.4, (c): OPC+10% SF mortar w/b=0.5, (d): OPC+10% SF mortar w/b=0.4 (e): OPC+70% slag mortar w/b=0.5 in desorption, (f): OPC+70% slag mortar w/b=0.5.The black lines are desorption and the red lines are absorption.

4. Discussion

The discussion part is divided in two main parts. In the first part the differences between diffusion coefficients in desorption and absorption are discussed, followed by a discussion of the effect of the w/b-ratio. In the second part experimental limitations of the used method are discussed.

4.1. Diffusion coefficients in absorption and desorption

In the introduction it was hypothesized that when we have sorption hysteresis – especially in the range of capillary condensation – we should also find that the diffusion coefficient D_v should be higher for desorption than for absorption (at the same RH). In the present results this is clearly seen for samples made with OPC, but less clearly for blended cements (with supplementary cementitious materials, SCMs) that in some cases seem to follow a different trend. We will in the following discuss this.

Our results can be discussed in terms of sorption isotherms, sorption hysteresis, and transport. The sorption isotherm is the relation between the moisture content and the relative humidity at equilibrium. Sorption for a porous cement based material is a combination of adsorption (sorption on the inner surface) and capillary condensation in the porous system. Adsorption starts at low RHs and continues in the whole RH-range with thicker layers of water at higher RH. It is typically modeled with the BET-equation [27] at low RH (<45%) or by other equations (GAB [28], Dent [29] etc) in a larger range. Capillary condensation is the filling of a pore when a certain RH is reached. The RH at which the filling takes place is a function of

the pore size and pore shape. In practice capillary condensation starts at 50% RH in pores of 2 nm radius and continues up to RHs close to 100% (at 99% RH cylindrical pores of 100 nm radius are filled).

Sorption hysteresis is the difference in moisture content depending on if an RH has been reached through absorption or desorption (or a combination of these two modes). Hysteresis in the capillary range can be caused by different factors; two causes commonly discussed are the ink bottle effect (when small pores protect large pores from being emptied during desorption) and the difference in radius of curvature for absorption and desorption in cylindrical pores and slit-shaped pores [8, 9]. The sorption hysteresis for cement based materials is significant; as an example, the moisture content in absorption is only about 65% of that for desorption for an OPC cement paste with w/b=0.6 [12].

The transport in a porous network is mainly through vapor diffusion in gas-filled pores and capillary flow in water-filled pores (we neglect surface flow). In gas filled pores the transport is by Fick's law (here written for a cylindrical pore and with vapor content as potential; vapor content is relative humidity multiplied by saturation vapor content):

$$Q = D_v \cdot \pi \cdot r^2 \cdot \frac{dv}{dx}. \qquad (8)$$

Here, Q (g s^{-1}) is the flow rate in a single pore, D_v (m^2 s^{-1}) is the diffusion coefficient, r (m) is the radius of the pore, v (g m^{-3}) is the vapor content, and x (m) is distance in the flow direction. Transport in water-filled pores is by pressure driven flow according to Hagen-Poiseues law:

$$Q = \frac{\pi \cdot r^4 \cdot \rho}{8\mu} \cdot \frac{dP}{dx}. \qquad (9)$$

Here, ρ (g m^{-3}) is the water density, μ (Pa s) is the dynamic viscosity of water, and P (Pa) is the pressure of the pore water. The above two equations are naturally given in terms of different potentials, but the pore water pressure can be written in terms of the vapor content through the Kelvin equation:

$$\ln\left(\frac{v}{v_s}\right) = \frac{V}{RT}P, \qquad (10)$$

Where v_s (g m^{-3}) is the saturation vapor content, V (m^3 mol^{-1}) is the molar volume of water, R is the gas constant, and T (K) is temperature.

To illustrate that the transport is higher in pores filled with water, than in vapor-filled pores, we have made calculations of the flow rate in a single cylindrical pore using the above three equations. In all cases the length of the pore was 1 μm and the difference in RH over the pore was 0.01% at 20˚C; the results would have been similar with other pore sizes and RH-differences. We made the calculations for different RHs and at each RH we used the radii corresponding to the filling and emptying of pores at this RH (an adsorbed layer was not accounted for). These RH/radii-combinations are the ones where the change from an empty pore to a filled pore (or vice versa) takes place. The results are shown in Fig. 6. According to Eq. 8, the vapor flow in a pore of a certain size is not a function of the RH as long as the RH-difference over the pore is the same. As the transformation from pressure to vapor contents is not linear, the liquid flow in a pore decreases when the RH increases when the vapor content difference over the pore is constant. However, this decrease is small and can almost not be seen in Fig. 6. There is only a major change in flow rate when a pore is filled or emptied, but this change is on the other hand four orders of magnitude.

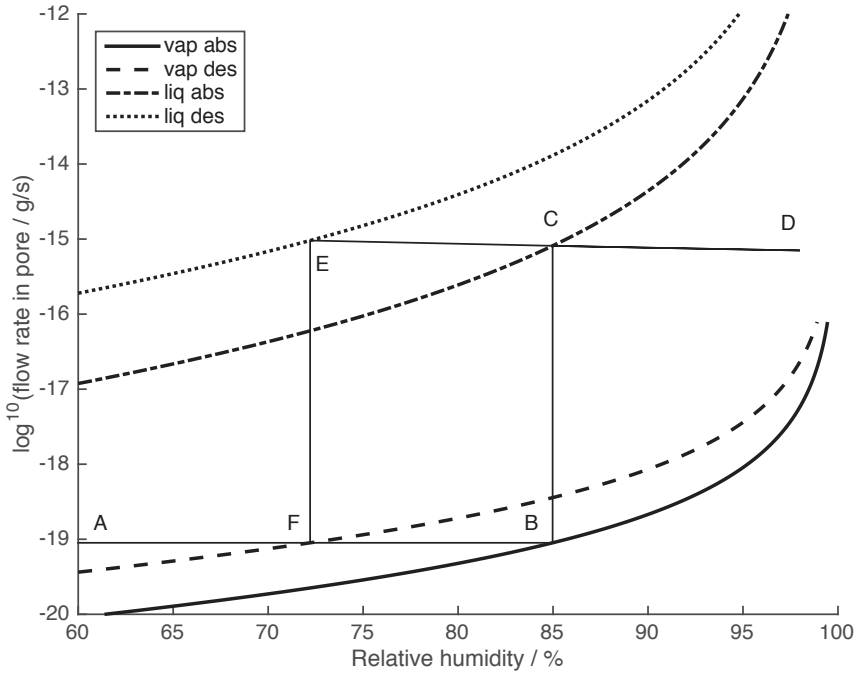

Figure 6. Water flow rates at 20 °C in a cylindrical pore of length 1 μm over which there is an RH-difference of 0.01%. The thick curves give the flow rates in gas (vap) and liquid (liq) filled pores at the RH of filling (abs) or emptying (des) of a pore. Note that the flow rate through a pore of a certain size only has two values; one for vapor flow and one for liquid flow. See the text for a further discussion. Standard values of the parameters in Eqs. 8-10 at 20 °C have been used.

An absorption-desorption process can be followed in the figure in the following way. We chose a pore that is filled by capillary condensation at 85% (it has a radius of 3.4 nm). From low RH up to the point of filling (A-B in the figure) the vapor flow rate is constant at about 10^{-19} g s^{-1}. At 85% RH the pore is filled (B-C) and the liquid flow rate is about 10^{-15} g s^{-1}. If the RH is increased the flow rate will stay at about the same high level (C-D); if the RH is then decreased the flow rate will once again stay almost constant (D-C-E), and the pore will

not empty until at an RH of 72.2% (E-F). Then we again have a vapor filled pore and a flow rate of 10^{-19} g s^{-1}.

The above calculations were made under the assumption that the RH-difference over a pore was constant. This may seem as an arbitrary assumption, but it is not. As we use these calculations in the discussion of diffusion coefficients D_v, the difference in RH is the driving potential for transport under isothermal conditions (when vapor content is proportional to RH). Results such as the ones shown in Fig. 6 are thus proportional to the diffusion coefficient D_v for a material with only parallel pores of one size. They then serve as an explanation of why we expect to have low and quite constant D_v at low RHs, and then get rapid increase in D_v when capillary condensation starts. However, note that the internal structure of cement based materials is very complex, both because the widely different length-scales involved, and because the pore system is complex at all levels (pore shape, pore connectivity).

Looking at only the diffusion coefficients as a function of RH, we see the expected increase in D_v at higher RHs for the OPC materials. This is similar to results from Hedenblad [22, 30]. However, the results from materials with slag and silica fume are more complex. Although they all show an increase in D_v at high RHs, below that they show mixed results. The samples with w/b-ratio 0.4 have minima at RH=75.5-85.1%. This cannot be explained by the reasoning above, according to which an increased moisture content always should give higher D_v. The qualitative difference between the diffusion coefficients in absorption and desorption is also according to the above reasoning for the OPC materials, while it is more complex for the slag and silica fume containing materials. The presence of silica fume and slag decreased the diffusion coefficient by a factor 10 at high RHs (RH>75.5%). A previous study showed [12] that samples with slag and silica fume has higher amount of gel pores and lower amount of capillary pores in comparison with OPC samples. The transport in OPC samples, especially

in samples with lower w/b-ratio, is controlled by the gel pores. Capillary pores are involved only at high RHs, and even then the amount of these pores is small and does not affect the transport significantly. As the gel pores are filled with water the transport is not strongly effected by increasing RH; it is only when the capillary pores are filled at high RHs that there is a significant increase in D_v.

One important conclusion from this study is that it is important to control the sorption state of samples to measure transport coefficients on. If this is not done the results can be quite wrong. As an example, if a cup measurement on an OPC-material in absorption in the range 84-94% RH is compared to a desorption result in the lower range 75-84% RH, the coefficient is higher in the lower range; an odd result that is the result of comparing results from different sorption directions. Problems can also arise when samples are not in pure absorption or desorption, but in a mixed state.

The results of the present study – at least concerning the OPC materials – naturally raises the question of whether hysteresis would decrease or disappear if the transport coefficient D_v would be drawn as a function of the moisture content, or if D_v should be recalculated to diffusion coefficient with moisture concentration as potential D_c (diffusivity).

The results for OPC samples (Fig. 5) show at RH<75% the effect of w/b-ratio is small, both in absorption and desorption. At RH>75% the sample with higher w/b-ratio has higher D_v. The diffusion coefficient D_v can change by a factor 2 when the w/b-ratio changes from 0.4 to 0.5 at the highest RH-interval for OPC samples in this study (RH=94.6-97.6%). The moisture transport is increased with an increase of RH especially for samples with w/b-ratio 0.5 but for w/b=0.4 the dependency is small. Similar behavior has been reported for concrete samples by Nilsson [31].

4.2. Experimental limitations

4.2.1. Pore solution effect

In a previous paper we discussed the influence of the dissolved ions in the pore solution on the sorption isotherms at high RHs [12]. We came to the conclusion that the strength of the pore solution limits the high end RH of a sorption isotherm to a certain value which is lower for stronger pore solutions (typically cementitious materials with high alkali content). When a sample of a cementitious material has taken up so much water so that its pore system is filled with pore solution, this pore solution has a certain water activity, which translates into a similar value of the RH of the air in contact with the solution. If the RH is increased above this 'critical value' the material will absorb more water from the air which will dilute the pore solution, and at the same time force part of the solution to end up on the outside of the sample. We are then not any longer talking about material properties, and such complex phenomena cannot be described by a sorption isotherm only.

With the above reasoning in mind, using 100% RH on one side in a cup measurement is clearly an undefined situation. What will happen is that the whole pore system on the 100% side will be filled with pore solution, and as liquid water transport is generally much higher than vapor transport, a wet front will travel from the 100% RH side towards the lower RH side. Whether it will reach the other side (wet the drier surface of the sample) depends on the transport parameters (this did not happen in our samples), but it will at least travel some distance into the material. A second thing that is likely to happen is that ions from the internal pore solution will leak out from the sample, collect water vapor and form droplets on the 100% RH side of the sample (this was seen in our measurements); this will tend to happen for all high RHs that are higher than the 'critical RH'. Because of this we have chosen not to discuss the 100CAP and 100RH results together with the other results. The values measured with water should simply not be evaluated in terms of diffusion coefficients as they are from a significantly more complex measurement situation than can be evaluated by Fick's law only.

A possible problem with our measurements is that the highest RHs lower than 100% used may be higher than the critical RH of the materials. The critical RH is a function of the strength of the pore solution, which mainly is a function of the concentrations of alkali (Na, K). This is because the main ion pairs in solution are NaOH and KOH as $Ca(OH)_2$ has a much lower solubility (and Si, Al, Fe and SO_4 are bound in different hydrated phases). Methods for the calculation of ionic strengths of in materials with both OPC [32-34] and SCMs [35] have been published, and these values can be converted to RH [21]. The RH (water activity) for known concentrations of alkali ions can be calculated using the concentration of alkali with Eq. 10 [36].

$$\ln(a_w) = -v \cdot m \cdot M_w \cdot \phi \qquad (11)$$

Here a_w is water activity in solution; v is number of ions per salt molecules, m (mol g^{-1}) is molality (number of moles of solute per kg of solvent), M_w (g mol^{-1}) is molecular weight of water and ϕ is an 'osmotic coefficient'.

In the extreme case when none of the alkali ions (Na^+, K^+) of the cement powder is bound, the volume of pore solution (v^p) can be calculated by Eq. 12 [32].

$$v^p = (\frac{w}{c} - 0.19\alpha)c \qquad (12)$$

Where w/c is water to cement ratio, α is degree of hydration, and c is amount of cement. From this it is possible to calculate the molality of alkalis (Na, K) (m) using total amount of Na and K in the cement powder analysis (K_2O=0.7, 0.6, 0.3% and Na_2O= 0.2, 0.2, 0.09% for our CEM I 32,5 R, CEM III/B 42,5 N and silica fume). From this the critical RH can be calculated using Eq. 11. The total degree of hydrations of the samples was measured using a

combination of X-ray diffraction (XRD) and thermal gravimetric analysis (TGA) [37]. The results are given in Table 3.

Table 3. Critical RH calculated for extreme case were none of the alkali is bound

Sample	w/b- ratio	Total degree of hydration (%)	Critical RH (%)
OPC mortar	0.5	93	97.7
OPC mortar	0.4	88	96.8
OPC+70% slag mortar	0.5	92	97
OPC+ 70% slag mortar	0.4	89	96
OPC+10% SF mortar	0.5	82	97.5
OPC+ 10% SF mortar	0.4	71	96.7

However, in real cement pastes a significant part of the alkalis are bound in hydration products [38] and the concentration is then lower in the pore solution. This leads to higher values of the critical RH than the ones in Table 3. We conclude that the RH inside the 100VAP cups is higher than the critical RH, which leads to other transport phenomena and high spread in our results, but that the lower RHs used probably are below the critical limit. This is supported by that the primary results (Fig. 3) for the 97.6% cups do not show increased standard deviations (as did the 100VAP cups).

4.2.2. Mass change rate limitation

In the 75.5-85.1% range there is a minimum in D_v on the absorption limb for samples with 10% silica fume and slag with w/b- ratio of 0.4. The corresponding cups show a different behavior during measurements than do the other cups. The masses of these cups vs. time show very small changes at the end of our measurements. Figure 7 shows an example of the mass vs. time for OPC+70% slag samples with w/b-ratio 0.4 for two different cups. The first cup is with 85% RH and the second one is with 97.6% RH inside and both placed in 75.5% RH. For the sample with 85.1% RH inside, the final mass change is very slow; from the maximum point of the graph to the end of measurement the duration is more than 5 months while the mass change is only 0.124 g (0.03% of total mass). There is a possibility that if we had continued the measurement for longer time the mass change rate would have increased and changed the D_v is increased in this range. Note that in the evaluation method that we use, D_v is calculated from two D_v:s measured in different intervals, and that this added evaluation step – compared to directly measuring in each interval – does bring added uncertainty into the results. However, the minima at 75.6-85.1% is a result of very low slope measured in this interval.

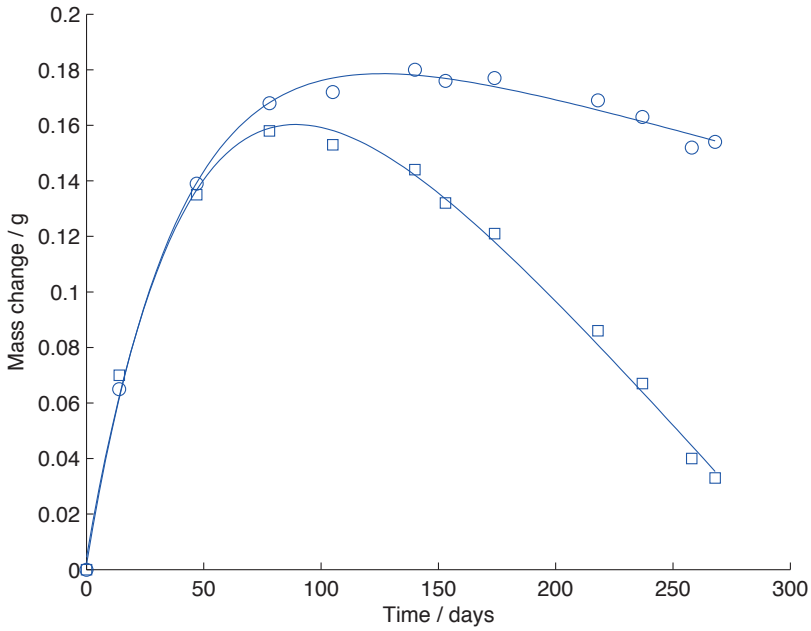

Figure 7. Examples of mass of cups vs. time for OPC+70% slag samples with w/b-ratio 0.4. The cups are in absorption with 75.5% RH outside and 85.1% (circles) and 97.6% RH (squares) inside the cup.

5. Conclusions

A new cup method set-up was designed to avoid carbonation during long-term measurements. A new systematic evaluation method was also developed. The results generally showed different D_v for absorption and desorption. For OPC samples the D_v is increasing with RH and there is a very clear hysteresis in D_v. Samples in desorption have higher D_v than samples in absorption, especially at RH>60%. The presence of slag and silica fume decreases D_v by approximately a factor 10. In these samples the dependence of D_v on RH is small and the influence of hysteresis is more complex.

Acknowledgment

The research leading to these results has received funding from the European Union Seventh Framework Program (FP7/2007-2013) under grant agreement 264448.

References

1. Nilsson, L.O., *On the role of moisture in degradation of concrete structures*, in *International Congress - Global Construction: Ultimate Concrete Opportunities*. 2005: Dundee, Scotland, United Kingdom. p. 15 - 24.
2. Nilsson, L.-O., *8 - Durability concept; pore structure and transport processes*, in *Advanced Concrete Technology Set*, N. John, et al., Editors. 2003, Butterworth-Heinemann: Oxford. p. 3-29.
3. Bažant, Z.P. and L.J. Najjar, *Nonlinear water diffusion in nonsaturated concrete.* Matériaux et Construction, 1972. **5**(1): p. 3-20.
4. Arfvidsson, J. and J. Claesson, *Isothermal moisture flow in building materials:: modelling, measurements and calculations based on Kirchhoff's potential.* Building and Environment, 2000. **35**(6): p. 519-536.
5. Baroghel-Bouny, V., *Water vapour sorption experiments on hardened cementitious materials. Part II: Essential tool for assessment of transport properties and for durability prediction.* Cement and Concrete Research, 2007. **37**(3): p. 438-454.
6. Baroghel-Bouny, V., *Water vapour sorption experiments on hardened cementitious materials: Part I: Essential tool for analysis of hygral behaviour and its relation to pore structure.* Cement and Concrete Research, 2007. **37**(3): p. 414-437.
7. De Belie, N., J. Kratky, and S. Van Vlierberghe, *Influence of pozzolans and slag on the microstructure of partially carbonated cement paste by means of water vapour and nitrogen sorption experiments and BET calculations.* Cement and Concrete Research, 2010. **40**(12): p. 1723-1733.
8. Espinosa, R.M. and L. Franke, *Inkbottle Pore-Method: Prediction of hygroscopic water content in hardened cement paste at variable climatic conditions.* Cement and Concrete Research, 2006. **36**(10): p. 1954-1968.
9. Espinosa, R.M. and L. Franke, *Influence of the age and drying process on pore structure and sorption isotherms of hardened cement paste.* Cement and Concrete Research, 2006. **36**(10): p. 1969-1984.
10. Sing, K.S.W., *Adsorption methods for the characterization of porous materials.* Advances in Colloid and Interface Science, 1998. **76–77**(0): p. 3-11.
11. Haul, R., *S. J. Gregg, K. S. W. Sing: Adsorption, Surface Area and Porosity. 2. Auflage, Academic Press, London 1982. 303 Seiten, Preis: $ 49.50.* Berichte der Bunsengesellschaft für physikalische Chemie, 1982. **86**(10): p. 957-957.
12. Saeidpour, M. and L. Wadsö, *Moisture equilibrium of cement based materials containing slag or silica fume and exposed to repeated sorption cycles.* Cement and Concrete Research, 2015. **69**(0): p. 88-95.
13. Quenard, D., et al., *Microstructure and transport properties of porous building materials.* Materials and structures, 1998. **31**(5): p. 317-324.
14. Zhang, Z., M. Thiery, and V. Baroghel-Bouny, *Numerical modelling of moisture transfers with hysteresis within cementitious materials: Verification and investigation of the effects of repeated wetting-drying boundary conditions.* Cement and Concrete Research, 2014. **68**: p. 10-23.
15. Quenard, D. and H. Sallee, *Water vapour adsorption and transfer in cement-based materials: a network simulation.* Materials and Structures, 1992. **25**(9): p. 515-522.

16. Anderberg, A. and L. Wadsö, *Method for simultaneous determination of sorption isotherms and diffusivity of cement-based materials.* Cement Concrete Res., 2008. **38**(1): p. 89-94.
17. 196-1, B.E., *Methods of testing cement Determination of strength.* 2005.
18. ASTM, *E 96-90*, in *Standard test method for water vapor transmission of materials*. 1990, ASTM: Philadelphia. p. 685-695.
19. Balej, J., *Water vapour partial pressures and water activities in potassium and sodium hydroxide solutions over wide concentration and temperature ranges.* International Journal of Hydrogen Energy, 1985. **10**(4): p. 233-243.
20. Greenspan, L., *Humidity fixed points of binary saturated aqueous solutions.* Journal of Research of the National Bureau of Standards, 1977. **81**(1).
21. Hedenblad, G. and W. Roszak, *SCIENCE - project : Characterisation of microstructure as a tool for prediction of moisture transfer in porous materials : moisture permeability for clay-brick and lime sandstone*. Rapport TVBM: 7034. 1992: Lund, 1992.
22. Hedenblad, G., *Moisture permeability of mature concrete and cemnet paste materials*, in *Microstructure of cement based systems, bonding and interfaces in cements*, M.r.s.s. Proceedings, Editor. 1994: Boston, USA. p. 443-448.
23. Anderberg, A. and L. Wadsö, *Moisture in Self-levelling Flooring Compounds. Part I. Water Vapour Diffusion Coefficients [Elektronisk resurs]*. 2004, Nordic Concrete Research (NCR).
24. Lide, D., ed. *Handbook of chemistry and physics*. 1993, CRC Press: Boca Raton FL, USA.
25. Wadso, L., *SURFACE MASS TRANSFER COEFFICIENTS FOR WOOD.* Drying Technology, 1993. **11**(6): p. 1227-1249.
26. Claesson, J., C.E. Hagentoft, and L. Wadsö, *Masked edge effects when measuring diffusion coefficients with the cup method.* Polymer Engineering & Science, 1994. **34**(10): p. 821-826.
27. Brunauer, S., P.H. Emmett, and E. Teller, *Adsorption of Gases in Multimolecular Layers.* Journal of the American Chemical Society, 1938. **60**(2): p. 309-319.
28. Timmermann, E.O., *Multilayer sorption parameters: BET or GAB values?* Colloid Surf. A, 2003. **220**: p. 235-260.
29. Dent, R.W., *A multilayer theory for gas sorption. Part I: Sorption of a single gas.* textile Res. J., 1977: p. 145-152.
30. Hedenblad, G., *Moisture permeability of mature concrete, cement mortar and cement paste*, in *Div of Building Materials LTH*. 1993, Lund University.
31. Nilsson, L.O., *Long-term moisture transport in high performance concrete.* Materials and Structures, 2002. **35**(10): p. 641-649.
32. Taylor, H.F.W., *A method for predicting alkazi ion concentrations in cement pore solutions.* Advances in Cement Research, 1987. **1**(1): p. 5-17.
33. Chen, W. and H.J.H. Brouwers, *Alkali binding in hydrated Portland cement paste.* Cement and Concrete Research, 2010. **40**(5): p. 716-722.
34. Brouwers, H.J.H. and R.J. vanEijk, *Alkali concentrations of pore solution in hydrating OPC.* Cement and Concrete Research, 2003. **33**(2): p. 191-196.
35. Chen, W. and H.J.H. Brouwers, *A method for predicting the alkali concentrations in pore solution of hydrated slag cement paste.* Journal of Materials Science, 2011. **46**(10): p. 3622-3631.
36. R. A. Robinson and R.H. Stokes, *Electrolyte Solutions*. 2 ed. 1955, New York: Wiley Subscription Services, Inc., A Wiley Company.
37. Scrivener, K.L., et al., *Quantitative study of Portland cement hydration by X-ray diffraction/Rietveld analysis and independent methods.* Cement and Concrete Research, 2004. **34**(9): p. 1541-1547.
38. Taylor, H.F.W., *A method for predicting alkali ion concentration in cement pore solutions.* Advances in cement research, 1997. **1**(1): p. 5-16.

Paper IV

The influence of sorption hysteresis on diffusion coefficients represented with different moisture potentials

Mahsa Saeidpour, Lars Wadsö

Building Materials, Lund University, Lund, Sweden

Abstract

This paper continues the discussion in a previous paper where a clear effect of sorption hysteresis was seen in moisture diffusion coefficients for cement-based materials. Coefficients with vapor content as a potential (D_v) had different values depending on whether the sample was in absorption or in desorption. In this paper we recalculate these D_v coefficients into coefficients with other water potentials and draw them as a function of different water potentials. The aim is to see if the effect of hysteresis disappears with an optimal choice of representation. The best choice was to draw D_v is as a function of the degree of saturation (concentration, moisture content).

1. Introduction

A common approach in the study of transport of water vapor in cement-based materials is to combine a sorption isotherm with a transport coefficient. Cement-based materials are known to show hysteresis behavior in sorption and a significant effort has been put into describing hysteresis – including scanning – as this is a complex path (history) dependent property [1-5]. In addition, transport coefficients (diffusion coefficient and permeability) are functions of the moisture state, for example of relative humidity (RH) or moisture content (MC) [6-9] rather than a constant number. In a recent paper [10] we also showed that at least for cement mortars made with ordinary Portland cement (OPC) there is a significant difference between the moisture diffusion coefficients when the mortar is on the absorption or on the desorption limbs of the sorption isotherm, even if the two values are taken in the same RH interval. We then expressed the diffusion coefficient with vapor content as potential as this is most natural for the steady-state cup measurements that we did.

A problem with moisture transport coefficients is that they can be expressed using many different potentials. This is in contrast with for example heat transport which is always treated using temperature as potential; or diffusion of chloride ions in concrete where concentration (mass of ions per volume material) is the preferred potential. For moisture transport we can use vapor content (v, mass vapor per volume air), moisture content (c, mass of moisture per volume material) or a dozen other potentials. This opens for the question of which of these possibilities that is best in the sense that it gives the smallest dependence of the transport coefficient on the potential on whether the system is in absorption or desorption. Our previous results [10] show an effect of sorption hysteresis for D_v as a function of RH (the diffusion coefficient is higher in desorption than absorption in same RH interval).

It is well known that sorption hysteresis above 50% RH is caused by that capillary condensation do not take place at the same RH during absorption and desorption [1, 5, 11];

the RH for emptying of a pore is lower than the RH at which the same pore is filled. This will also affect the transport, as the rate of transport is significantly higher in a water filled pore than in a pore in which vapor diffuses [10]. As there are many different pore sizes, pore shapes, pore connections etc in cement based materials, the sorption situation is complex, and it is not possible to theoretically determine the values of transport coefficients with different potentials and on different limbs of the sorption isotherm.

It is the aim of this work to determine how the transport coefficients should be represented to introduce a minimum of sorption hysteresis in the transport coefficient. This includes both the potential used for the coefficient and what potential it should be a function of. Originally we evaluated $D_v(\varphi)$, where φ is the relative humidity, i.e., v/v_{sat}, which at isothermal conditions essentially equals $D_v(v)$. Some examples of other alternatives are $D_v(c)$, $D_c(v)$ and $D_c(c)$. In this study we recalculate D_v to other potentials and present these transport coefficients as function of different potentials.

2. Experimental

The experimental results that we use in the present paper are from two standard mortars of ordinary Portland cement (OPC) with water/cement-ratios (w/c) of 0.5 and 0.4. The sample preparation is described in reference [3] and the transport measurements with the cup method and the evaluation of D_v as a function of RH are discussed in detail reference [10]. The measurement was done in two steps. First water saturated disk-shaped samples were placed on cups with salt solutions with RH=33.1, 57.6, 85.1, 94.6 and 97.6%. The RH outside the cups was 75.5%, so this part of the measurement gave values measured in desorption. The samples were weighed regularly until constant mass change rates (flow) were reached, from which D_v(RH) was calculated. In a second step the cups were opened and the salt solutions were removed. The samples were then dried in 33.1% RH, after which the cups were closed again (with the same salt solutions as mentioned above) and the measurement continued. From this step of the measurement D_v(RH) in absorption was calculated when the flow reached steady-state. The sorption isotherms needed for the recalculations between different potentials were determined using a sorption balance and taken from reference [3].

3. Evaluation

In the cup method the vapor content is the natural potential (driving force) to use to calculate diffusion coefficients [10], but it is also possible to use other potentials to calculate diffusion coefficients. One example is using volumetric moisture content (concentration) as this is the natural potential in the dynamic sorption method to measure transport coefficients [2, 12]. It is possible to recalculate from coefficients based on one potential to coefficients based on another potential is the relationship between the potentials is known. Changing the potential gives other numerical values and (in most cases) other units of the transport coefficient.

These recalculations are based on viewing a steady-state transport case from the viewpoint of the two potentials of interest. If we have the transport coefficient for potential a and wants to have the transport coefficient for potential b, we state Fick's law with these two potentials (the recalculations could also have been made using Δ instead of differential d:s):

$$q_m = -D_a \frac{da}{dx} \tag{1}$$

$$q_m = -D_b \frac{db}{dx} \tag{2}$$

Here, q_m (g s^{-1} m^{-2}) is the mass flux, which must be equal in the two equations as the above two equations are for the same transport case. We can this equate the right sides of the two equations and rewrite to

$$D_b = D_a \frac{da}{db} \tag{3}$$

We can thus recalculate transport coefficients from one potential to another if we know how one of the potentials changes when the other changes. For the trivial case of vapor content v and relative humidity φ, we get

$$D_\varphi = D_v \frac{dv}{d\varphi}, \tag{4}$$

where

$$\frac{dv}{d\varphi} = v_s, \tag{5}$$

as the relative humidity is the vapor content divided by the saturation vapor content v_s.

For the more complex case of vapor content v (g m^{-3}) and volumetric moisture content (concentration) c (g m^{-3}) we get the following relation:

$$D_c = D_v \frac{dv}{dc}, \tag{6}$$

where

$$\frac{dv}{dc} = \frac{v_s}{\rho \frac{du}{d\varphi}}. \tag{7}$$

Here, D_v (m^2 s^{-1}) and D_c (m^2 s^{-1}) are transport coefficients with vapor content and concentration as potentials, respectively, ρ is density of the material (g m^{-3}) and du/dφ is the slope of sorption isotherm, where u (g g^{-1}) is the specific moisture content and φ (1) is the relative humidity.

In this paper we have also used the degree of saturation S (1) as potential. This is the fraction of the pore volume that is filled with moisture. The degree of saturation is related to the concentration as follows:

$$S = \frac{c}{p \cdot \rho_w}, \tag{8}$$

where p (1) is the porosity and ρ_w (g m^{-3}) is the density of liquid water. It can also be calculated from the volumetric moisture content and the maximal volumetric moisture content (when the pore system is assumed to be completely filled):

$$S = \frac{c}{c_{\max}}. \tag{9}$$

As both porosity and water density are constants, the degree of saturation is proportional to concentration for a certain material and at a certain temperature.

Finally, we have used the fundamental potential Ψ (g s^{-1} m^{-1}), which can be seen as the potential defined in such a way that the transport coefficient always is unity:

$$q_m = \frac{d\Psi}{dx}. \tag{10}$$

This potential has found use in building physics calculations (see for example reference [8]) and has an advantage when calculations are based on transport data from cup measurements, as these measured data can be used directly in the calculations without the calculation of transport coefficients. It may seem odd to include this potential with a diffusion constant coefficient in a paper on diffusion coefficients, but the moisture dependence is here built into the potential and not the coefficient. Therefore, to see if the fundamental potential will reduce the influence of hysteresis we have to look at the fundamental potential itself as a function of different other potentials.

The fundamental potential can be evaluated directly from our cup results (reference [8], p. 525). For each internal RH (φ) in the cups the fundamental potential is

$$\Psi(\varphi) = q_m \cdot L, \tag{10}$$

where L (m) is the thickness of the cup sample. Note that from this definition we find that the fundamental potential for the common RH outside the cups is by definition zero as we have zero flux when the internal and external RHs are the same. The reference point of the fundamental is thus dependent on how the experiment is conducted, but this is of no importance as only differences between different Ψ-values are used (cf. height and enthalpy where the mean sea level and the value at 25 °C and 1 atm are common reference values). In the present measurements the reference (zero) point is at 75.5% RH.

4. Results and discussions

In the following we use the following symbols for the discussed potentials: v for vapor content; c for concentration (volumetric moisture content); S for degree of saturation; and Ψ

for the fundamental potential discussed above. Diffusion coefficients are called D with a sub-index for the potential used.

4.1. D_v and Ψ as a function of RH

The D_v and Ψ as a function of RH for OPC samples are shown in Fig. 1. The black lines are for samples on the desorption curve and the red lines are for samples on the absorption curve. Note that D_v are evaluated as mean values in different RH intervals, while each cup measurement interval gives one Ψ-value at the end of the interval.

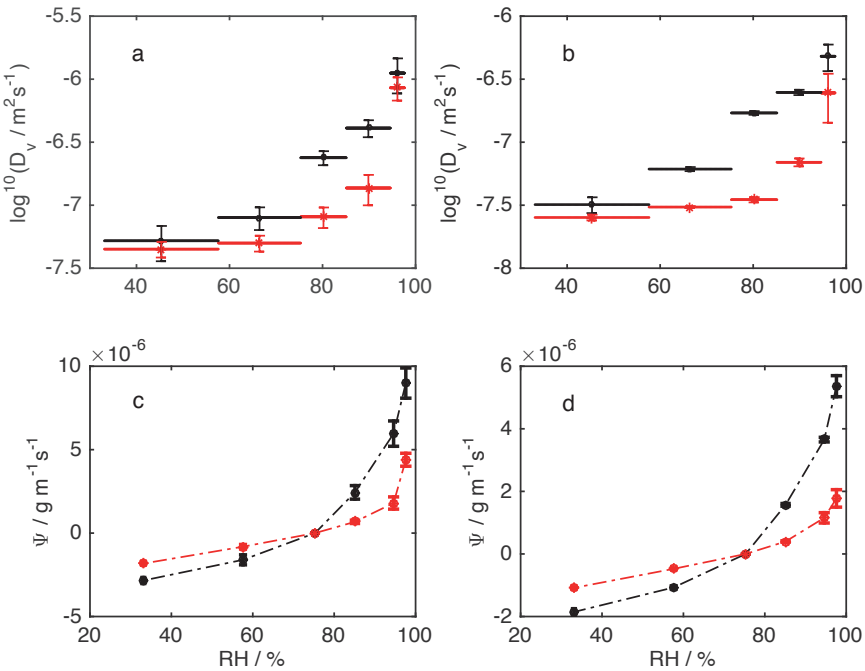

Figure 1. Diffusion coefficients (D_v) as a function of RH (a): OPC mortar w/b=0.5, (b): OPC mortar w/b=0.4, Ψ as a function of RH (c): OPC mortar w/b=0.5, (d): OPC mortar w/b=0.4.The black lines are on the desorption curve and the red lines are on the absorption curve. The error bars are the standard deviations calculated from three replicates.

4.2. D_v and Ψ as a function of S

The diffusion coefficient D_v of OPC samples as a function of S is shown in Fig. 2. Sorption isotherms for same materials were measured [3] and are used here to calculate moisture content. The degree of saturation was not measured, but is calculated as moisture content divided by the moisture content at 97.6% RH (the degree of saturation at 97.6% RH is assumed as 1.0) as 97.6% is the highest value in our transport measurements and close to the

critical RH where all pores are filled by pore solution [3]. As the sorption isotherms were not measured over RH=95%, the moisture content at RH=97.6%, was assessed by assuming that the slope of each sorption isotherm is constant from 85% RH to 97.6% RH. The values of the moisture content at saturation were 0.075 and 0.052 $g_{water}\ g_{mortar}^{-1}$ for w/c 0.5 and 0.4, respectively. This compares reasonably well with values calculated using Powers' model of cement paste porosity given in Eqs. 21-22 in reference [13]. The cement composition was (fractional mass) 0.527, 0.193, 0.106, and 0.074 for C_3S, C_2S, C_3A and C_4AF; we used a specific volume of non-evaporable water of 0.72 [14]: 0.067 and 0.055 $g_{water}\ g_{mortar}^{-1}$. However, note that the results are not critically dependent on the value of the maximal moisture content as both absorption and desorption are scaled with the same factor.

In Figs. 2a and 2b the difference between the results in absorption and desorption is smaller than in other representations tested.

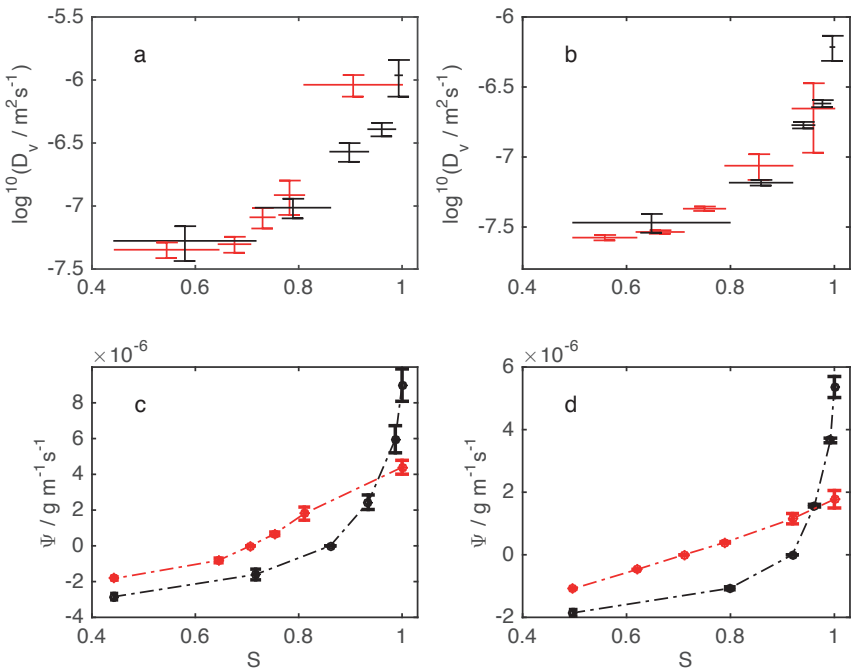

Figure 2. D_v as a function of degree of saturation (S) (a): OPC mortar w/b=0.5, (b): OPC mortar w/b=0.4. Ψ as a function of S (c): OPC mortar w/b=0.5, (d): OPC mortar w/b=0.4 The black lines are on the desorption curve and the red lines are on the absorption curve. The error bars are the standard deviations calculated from three replicates.

4.3.D_c as a function of RH and *S*

Figure 3 shows D_c (calculated from D_v by Eqs. 6-7) for samples in absorption and desorption as a function of RH and *S*. The results show similar influence of hysteresis as D_v as a function of RH. Note that the calculations with Eqs. 6-7 brings an added uncertainty into these coefficients; especially from the slope of the sorption isotherm.

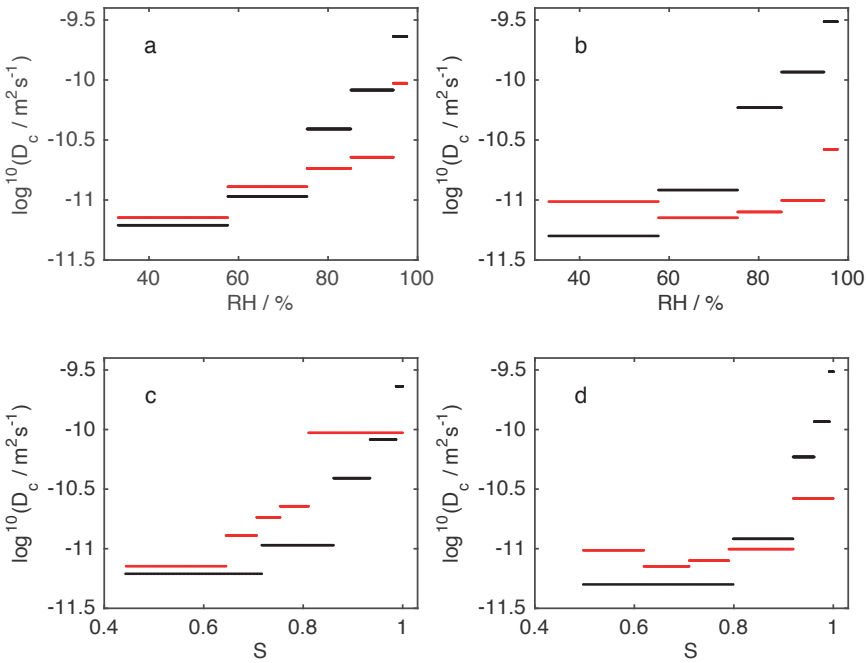

Figure 3. Moisture diffusivity D_c as a function of RH (a): OPC mortar w/b=0.5, (b): OPC mortar w/b=0.4. D_c as a function of *S* (c): OPC w/b=0.5, (d): OPC mortar w/b=0.4. The black lines are on the desorption curve and the red lines are on the absorption curve. Note the logarithmic y-axes.

4.4 General discussion

Looking at the results in Figs. 1-3, it is seen that Fig. 2b shows the smallest difference between absorption and desorption, closely followed by 2a. This indicates that if the diffusion coefficient with vapor content as potential (D_v) is used as a function of the degree of saturation (or moisture content or concentration) the effect of absorption/desorption does not need to be taken into account. However, as this study was rather limited and this tentative conclusion should be further tested.

It may seem odd that a transport coefficient using one potential (vapor content) should be used together with another potential (degree of saturation) describing the state of the water.

However, it may be natural that two potentials are used together to reduce the effect of hysteresis, one to describe the conductivity and one to describe how the conductivity changes with a change in moisture content/state. Below we give some arguments for that the best choice of potentials that we have indicated above, is the best representation also in terms of the physics of the processes. However, these arguments are rather weak and should only be seen as the start of a discussion about this.

Moisture transport in porous materials is a combination of vapor and liquids flow. The most physical way of representing the vapor transport part (Fick's law) is probably by using vapor pressure, which is equivalent to using vapor content. When it comes to liquid flow (Hagen-Poisseuilles and Darcy's laws), this is treated in terms of pressure of the liquid. In porous systems where the pressures originate from the capillary action (not from external pressure), the pressure can be written in terms of relative humidity by the Kelvin equation. As vapor content and relative humidity are equivalent under isothermal conditions, we can conclude that both the vapor and the liquid flow components naturally can be written in terms of vapor content in our case. Although one can use concentration based moisture potentials, these will not have the same strong connection to the physics of the transport processes.

The situation is possibly different when it comes to how the moisture state influences the value of a transport coefficient. It is generally believed that at low moisture levels there is mainly vapor flow and at higher moisture levels there is a combination of vapor and liquid flow. At least above 50% RH the liquid part is the most important as liquid flow is so much higher than vapor flow, all other parameters kept equal. If we look at a porous material at two moisture states with different amounts of liquid water, it does seem natural that the state with a higher moisture level (higher moisture concentration) will correspond to a higher flow rate; so that concentration should be a more proper potential to judge the variations in transport coefficients than, e.g., RH. We can envisage a porous material with no pores in a certain pore radii range. If the moisture state is increased through this area where there are no pores, the RH will increase, but very little moisture will be taken up and the transport coefficient will not change. It may thus be natural that transport coefficients are represented as a function of concentration based potentials, like the degree of saturation.

The above reasoning is not a rigorous argumentation and one problem that is relevant in the context of this paper is of course that because of sorption hysteresis one RH can correspond to two quite different concentrations, and vice versa. It is also probable that it is a too limited approach to look at the potential of the coefficient and the potential it is a function of as two separate problems.

4. Conclusions

Expressing the transport coefficients using vapor content as a function of degree of saturation (essentially moisture content) gave the lowest difference between data in absorption and desorption in our study, but the transport coefficient with vapor concentration as potential as a function of degree of saturation was almost as good.

References

1. Baroghel-Bouny, V., *Water vapour sorption experiments on hardened cementitious materials: Part I: Essential tool for analysis of hygral behaviour and its relation to pore structure.* Cement and Concrete Research, 2007. **37**(3): p. 414-437.
2. Baroghel-Bouny, V., *Water vapour sorption experiments on hardened cementitious materials. Part II: Essential tool for assessment of transport properties and for durability prediction.* Cement and Concrete Research, 2007. **37**(3): p. 438-454.
3. Saeidpour, M. and L. Wadsö, *Moisture equilibrium of cement based materials containing slag or silica fume and exposed to repeated sorption cycles.* Cement and Concrete Research, 2015. **69**: p. 88-95.
4. Espinosa, R.M. and L. Franke, *Inkbottle Pore-Method: Prediction of hygroscopic water content in hardened cement paste at variable climatic conditions.* Cement and Concrete Research, 2006. **36**(10): p. 1954-1968.
5. Espinosa, R.M. and L. Franke, *Influence of the age and drying process on pore structure and sorption isotherms of hardened cement paste.* Cement and Concrete Research, 2006. **36**(10): p. 1969-1984.
6. Zalzale, M. and P.J. McDonald, *Lattice Boltzmann simulations of the permeability and capillary adsorption of cement model microstructures.* Cement and Concrete Research, 2012. **42**(12): p. 1601-1610.
7. Bažant, Z.P. and L.J. Najjar, *Nonlinear water diffusion in nonsaturated concrete.* Matériaux et Construction, 1972. **5**(1): p. 3-20.
8. Arfvidsson, J. and J. Claesson, *Isothermal moisture flow in building materials:: modelling, measurements and calculations based on Kirchhoff's potential.* Building and Environment, 2000. **35**(6): p. 519-536.
9. Nilsson, L.O., *Long-term moisture transport in high performance concrete.* Materials and Structures, 2002. **35**(10): p. 641-649.
10. saeidpour, M. and L. wadsö, *Moisture diffusion coefficients of mortars in absorption and desorption* 2015.
11. Hagymassy Jr, J., et al., *Pore structure analysis by water vapor adsorption. III. Analysis of hydrated calcium silicates and portland cements.* Journal of Colloid and Interface Science, 1972. **38**(1): p. 20-34.
12. Anderberg, A. and L. Wadsö, *Method for simultaneous determination of sorption isotherms and diffusivity of cement-based materials.* Cement Concrete Res., 2008. **38**(1): p. 89-94.
13. Hansen, T.C., *The physical struture of hardened cements paste. A classical approach,* Materials and Structures, 1986. **19**(6): p. 423-436.
14. Brouwers, H.J.H., *The work of Powers and Brownyard revisited: Part 1.* Cement Concrete Res., 2004. **34**: p. 1697-1716.

Paper V

Cement and Concrete Research 65 (2014) 85–95

Contents lists available at ScienceDirect

Cement and Concrete Research

journal homepage: http://ees.elsevier.com/CEMCON/default.asp

Methods to determine hydration states of minerals and cement hydrates

Luis G. Baquerizo [a,*], Thomas Matschei [a], Karen L. Scrivener [b], Mahsa Saeidpour [c], Alva Thorell [c], Lars Wadsö [c]

[a] Innovation, Holcim Technology Ltd., CH-5113 Holderbank, Switzerland
[b] Laboratory of Construction Materials, Ecole Polytechnique Fédérale de Lausanne, CH-1015 Lausanne, Switzerland
[c] Building Materials, Lund University, Box 124, 221 000 Lund, Sweden

ARTICLE INFO

Article history:
Received 28 April 2014
Accepted 18 July 2014
Available online 12 August 2014

Keywords:
Cement hydrates (B)
Monosulfoaluminate (D)
Hydration states (D)
Thermodynamic properties (C)
Characterization techniques (B)

ABSTRACT

This paper describes a novel approach to the quantitative investigation of the impact of varying relative humidity (RH) and temperature on the structure and thermodynamic properties of salts and crystalline cement hydrates in different hydration states (i.e. varying molar water contents). The multi-method approach developed here is capable of deriving physico-chemical boundary conditions and the thermodynamic properties of hydrated phases, many of which are currently missing from or insufficiently reported in the literature. As an example the approach was applied to monosulfoaluminate, a phase typically found in hydrated cement pastes. New data on the dehydration and rehydration of monosulfoaluminate are presented. Some of the methods used were validated with the system Na_2SO_4–H_2O and new data related to the absorption of water by anhydrous sodium sulfate are presented. The methodology and data reported here should permit better modeling of the volume stability of cementitious systems exposed to various different climatic conditions.

1. Introduction

1.1. General

Varying hydration states of minerals and hydrated phases and their associated changes in molar volume (i.e. density) are a common cause of failure in porous materials. Two mechanisms can be distinguished: i) crystals that can precipitate from a saturated solution and grow in confined spaces such as porous media due to changes in temperature and relative humidity RH and ii) hydrated minerals such as clays that can absorb or release water from their structure depending on the external conditions producing swelling or shrinkage directly without full dissolution and recrystallization.

The first mechanism, commonly called salt damage, is one of the main reported causes of failure in stones, cultural heritage buildings and any porous building material [1–3]. The growth of salts produces a crystallization pressure which can exceed the tensile strength of a porous material causing its rupture. Most cases of the damage are the consequence of unfavorable conditions of temperature and RH that result in repeated cycles of dissolution and crystallization, or hydration and dehydration [3]. Sodium sulfate is very well known for its ability to cause damage to porous media such as building stone. This is usually attributed to the growth of $Na_2SO_4 \cdot 10H_2O$ (mirabilite) from a supersaturated solution [1]. In relation to Portland cement-based concretes, the crystallization of ettringite due to external sulfate attack or autogenous delayed ettringite formation can cause complete failure of structures [4,5].

The second mechanism is related to the ability of layered minerals such as smectite clays and layered double hydroxides (LDH) to absorb or release water from the interlayer space depending on the external conditions, especially varying temperature and RH [6,7]. Ca^{2+}-montmorillonite, for instance, shows an increase of basal space d(001) from ~0.97 nm in the anhydrous state up to ~1.8 nm in the three-layer hydrate, which is associated with considerable changes in molar volume [8]. LDH are lamellar materials with positively charged layers and charge-balancing anions in the interlayer and they have many physical and chemical properties in common with those of clay minerals such as ion-exchange properties and swelling in water [7]. Several phases formed during hydration of cement belong to this family and each of these can exist in several different well-defined hydration states.

1.2. Hydration states of crystalline cement hydrates

Cement clinker phases react chemically with water to form cement hydrates. Some of these hydrates are crystalline phases with LDH- or ettringite-type structures. These so called Alumino-Ferrite mono- and tri-phases (AFm and AFt) show different hydration states depending on the temperature and relative humidity (RH) to which they are exposed, similar to what is observed in many clay minerals. Varying the hydration states of these phases can have a significant impact on the density of cement paste. The molar volume of some AFm phases can decrease by as much as 20% during drying [9], strongly influencing the porosity and performance of cementitious systems.

The most important AFm and AFt phases and their reported water contents are presented in Table 1. Water molecules can be incorporated in the interlayer in AFm phases (LDH-type) or in the interchannel in AFt

* Corresponding author. Tel.: +41 58 858 64 31.
E-mail address: luis.baquerizoibarra@holcim.com (L.G. Baquerizo).

http://dx.doi.org/10.1016/j.cemconres.2014.07.009
0008-8846/

phases (ettringite type). In the case of AFm phases different types of interlayer water can be identified: water molecules strongly bound to the calcium cations of the main layer, and space filling water molecules which are lost first during an increase in temperature or a decrease in RH [10].

There is presently no systematic approach to assessing the stability range (as a function of temperature and RH) of cement hydrates which takes into account the impact of different hydration states. Moreover, a complete database of thermodynamic properties related to the absorption/desorption of water from the crystal structures of such hydrates is not yet available.

The aim of this study is to examine a set of characterization techniques intended for to the determination of the hydration states of minerals such as cement hydrates and see how these methods correlate with or complement each other. Some of the techniques studied have already been widely used, such as X-ray diffraction (XRD) and thermogravimetric analysis (TGA), but others, for instance the sorption balance technique and sorption calorimetry, are less well known. Subsequently, measurements and calculations of enthalpies related to the absorption/desorption processes are described using results from sorption calorimetry and from a novel hydrate pair–humidity buffer method that makes use of phase rule constraints [24,25]. A similar approach was used by Chou et al. to study the stability of hydrated sulfate salts [26–30]. The experimental results from sorption balance, sorption calorimetry and the hydrate pair–humidity buffer method were validated on the relatively well described system Na_2SO_4–H_2O, including the salts thenardite and mirabilite.

At the end of the paper the stability ranges of the different hydration states of monosulfoaluminate (Ms) are presented, as well as the thermodynamic properties associated with these changes. Monosulfoaluminate was chosen to test the methodology as it is one of the most common AFm cement hydrates which can make up to 10% by volume of a hydrated cement paste. This hydrate contains a sulfate anion (SO_4^{2-}) in its interlayer and exists in different hydration states.

2. Materials and conditioning

2.1. Reference material

The hydrate pair–humidity buffer method, the sorption balance and sorption calorimetry experiments were validated on thenardite and mirabilite: salts with known RH and temperature stability. Reagent grade thenardite was obtained from Sigma Aldrich,>99% pure, and mirabilite $Na_2SO_4 \cdot 10H_2O$ was prepared by wetting thenardite with degassed and deionized water.

2.2. Cement hydrate preparation

All syntheses were done from analytical grade reagents. For the synthesis of monosulfoaluminate tricalcium aluminate (C_3A) and anhydrite were used as precursors. C_3A was prepared from a 3:1 molar ratio of $CaCO_3$ and Al_2O_3 at 1400 °C, based on the procedure given by Matschei [31]. Anhydrite $CaSO_4$ was prepared by dehydration of gypsum in a muffle furnace at 550 °C overnight. Double distilled CO_2 free water was used in the synthesis of the hydrates. Monosulfoaluminate $C_4A\hat{S}H_{14}$ was prepared by suspending a 1:1 molar mixture of C_3A and $CaSO_4$ with a water/solid ratio (w/s) of 20 at 85 °C during 14 days in a PTFE bottle. Once purity has been confirmed by XRD, the solid was vacuum filtered under N_2 atmosphere in a glove box and subsequently aged at 25 °C (20 months) inside hermetically sealed glass bottles equilibrated at different RHs using saturated salt solutions [32] as shown in Table 2. The RH was periodically checked using a Testo 174H humidity probe. Monosulfoaluminate synthesis was also carried out at 5 °C to study the impact of low temperatures on the hydration states.

3. Experimental methods and analysis

3.1. X-ray diffraction (XRD)

This characterization technique was used to analyze the crystal structure, e.g. space group and lattice parameters of synthetic cement hydrates, as well as to identify possible impurities precipitated during the synthesis. Then, changes of the unit cell volume can be calculated when samples are exposed to different temperatures and RHs.

X-ray analyses of monosulfoaluminate wet and dried to different RHs were carried out at room temperature (unless otherwise stated) with a Bruker D8 Advance diffractometer (CuKα radiation, 45 mA, 35 kV) equipped with a Super Speed detector, in the 2θ range 5–70°, with a step size and time per step of 0.02° and 0.5 s, respectively. Samples were prepared inside a glove box filled with N_2. A low background-airtight specimen holder (Bruker AXS) was used to avoid carbonation and drying during testing. The peak profile and lattice parameters were determined by a Le Bail fit [33] using TOPAS 4.2 (Bruker AXS). When the crystal structure of a specific hydration state was not known, assumptions such as space group and initial lattice parameters were made in order to obtain relevant data. In the case of monosulfoaluminate the crystal structure of kuzelite was used as a starting model [34].

In addition to conventional XRD, a humidity chamber CHC plus$^+$ from Anton Paar coupled to a Bruker D8 Advance diffractometer (CuKα radiation, 45 mA, 35 kV) was used to determine lattice parameters of the lowest hydration state of monosulfoaluminate under dry N_2 flow at 90 °C.

3.2. Thermogravimetric analysis (TGA)

Thermogravimetry measurements were carried out with a Mettler Toledo TGA/SDTA 851^e under N_2 flux, over the temperature range 25–1200 °C with a heating rate of 20 K/min. Measurements were done on samples dried at different RHs once the presence of a single hydration state was confirmed by XRD. This data enabled us to measure the water content of pure hydrates. Together with the volume information obtained by XRD, the density of a cement hydrate dried at a specific temperature and RH can be calculated.

Table 1
Most important AFm and AFt phases and reported water content.

	Phase name	Chemical formula	Cement notation[a]
AFm	Monosulfoaluminate [11–19]	$[Ca_4(Al)_2(OH)_{12}]^{2+}\,[SO_4 \cdot nH_2O]^{2-}$ $n = 4–10$	$C_4A\hat{S}H_{6+n}$
	Hydroxy-AFm [11,12,14,18–20]	$[Ca_4(Al)_2(OH)_{12}]^{2+}\,[(OH)_2 \cdot nH_2O]^{2-}$ $n = 4–12$	C_4AH_{7+n}
	Monocarboaluminate [11,12,14,18–21]	$[Ca_4(Al)_2(OH)_{12}]^{2+}\,[CO_3 \cdot nH_2O]^{2-}$ $n = 5$	$C_4A\hat{C}H_{6+n}$
	Hemicarboaluminate [11,12,14,18–20,22]	$[Ca_4(Al)_2(OH)_{12}]^{2+}\,[1/2CO_3\,(OH) \cdot nH_2O]^{2-}$ $n = 0–5.5$	$C_4A\hat{C}_{0.5}H_{6.5+n}$
AFt	Ettringite [11–13,23]	$[Ca_6(Al)_2(OH)_{12} \cdot 24H_2O]^{3+}\,[3SO_4 \cdot nH_2O]^{3-}$ $n = 0–6$	$C_6A\hat{S}_3H_{30+n}$

[a] $A = Al_2O_3$, $C = CaO$, $H = H_2O$, $\hat{S} = SO_3$, $\hat{C} = CO_2$.

Table 2
Equilibrium RH of selected saturated salt solutions at 25 °C [32].

Salt used	RH (%)
Na(OH)	8.2
CH_3CO_2K	22.5
$MgCl_2$	32.8
$Mg(NO_3)_2$	52.9
NaCl	75.3
KCl	84.3
K_2SO_4	97.3

3.3. Hydrate pair–humidity buffer method

This method was developed to determine the RH at which a change in hydration state occurs. It applies the salt–hydrate pair principle which considers a thermodynamic equilibrium between hydrate pairs, i.e. two hydration states of the same salt, and the water vapour pressure of the surrounding gas. Similar methods have been used before mainly as humidity calibrators [24] and to control RH in confined environments [25,35].

The technique is based on simple phase rule restrictions. Consider a chemical system with 2 components (C), a solid of chemical composition **A** and water H_2O. As shown in the imaginary RH/T phase diagram in Fig. 1, component **A** may take up water and exist with different hydration states x and y hence forming the phases $\mathbf{A}\cdot xH_2O$ and $\mathbf{A}\cdot yH_2O$ (consider that $x \geq 0$ and $y > x$) or dissolve to form a solution. If we consider the line *b* there are 3 phases (P) coexisting: $\mathbf{A}\cdot xH_2O$, $\mathbf{A}\cdot yH_2O$ and water vapour. Using the phase rule the number of degrees of freedom (F) of the system is then 1 ($F = C - P + 2$; $C = 2$; $P = 3$ therefore $F = 1$). Hence at every temperature the system will have a fixed vapour pressure (or RH). Under these conditions the system is buffered, which means that under isothermal conditions the RH of the system will not change as long as the 3 phases are present.

The thermodynamic properties of the de/rehydration process $\mathbf{A}\cdot yH_2O \leftrightarrow \mathbf{A}\cdot xH_2O$ can be calculated as follows.

For the reaction

$$\mathbf{A}\cdot yH_2O\,(s) \rightarrow \mathbf{A}\cdot xH_2O\,(s) + (y-x)H_2O(g), \quad (1)$$

where s and g are solid and gas, respectively, the Gibbs free energy of reaction is given by:

$$\Delta G_r^\circ = -RT\ln K = -RT\ln\frac{a(\mathbf{A}\cdot xH_2O)\,a(H_2O)^{y-x}}{a(\mathbf{A}\cdot yH_2O)} \quad (2)$$

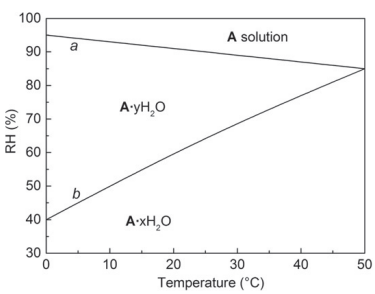

Fig. 1. RH/T phase diagram of the system A–H_2O.

By defining the activity of all pure solid phases as 1, then:

$$\Delta G_r^\circ = -RT\ln\left[a(H_2O)^{y-x}\right] = (x-y)RT\ln\left[f(H_2O)\right] = (x-y)RT\ln\frac{f^*(H_2O)RH}{100} \quad (3)$$

where ΔG_r° is the standard Gibbs free energy of the reaction (1), *T* is the absolute temperature, *K* is the equilibrium constant, *R* is the gas constant, $a(H_2O)$ is the activity of H_2O in vapour, $f(H_2O)$ is the equilibrium fugacity, $f^*(H_2O)$ is the fugacity of pure H_2O at *T* and *RH* is the equilibrium relative humidity [27–30]. Since ln*K* can be calculated at any temperature for the reaction (1) according to Eq. (3) then the standard enthalpy of reaction ΔH_r° can be calculated with the van't Hoff equation:

$$\frac{\partial(\ln K)}{\partial(1/T)} = -\frac{\Delta H_r^\circ}{R}. \quad (4)$$

The standard entropy of reaction ΔS_r° can be calculated from the following equation:

$$\Delta G_r^\circ = \Delta H_r^\circ - T\Delta S_r^\circ. \quad (5)$$

Experimentally a mixture of two phases with different hydration states was placed inside a small container (30 mL bottles of HDPE) and the RH at which the combined system reached equilibrium recorded with a tightly fitted pen hygrometer (Testo 605-H1, accuracy ± 3% RH). The hygrometer was tightened to the container by using a plastic cable gland thread PG16 which was also wrapped with Parafilm to avoid any leakage. Since the system is closed and there is no exchange of water with the exterior (diffusion of water through the bottle is negligible), the RH inside will be forced to be at equilibrium with the two hydrate phases at the given temperature. The same type of measurement can be made for a phase in equilibrium with its saturated aqueous solution (see line *a* Fig. 1). By varying the temperature during the experiments it is possible to assess phase boundary curves, which can then be used to construct RH–T phase diagrams. With Eqs. (3)–(5) the thermodynamic properties of the studied phases can be assessed.

3.4. Sorption balance

The sorption balance is commonly used in the pharmaceutical industry to study sorption behavior. In the present study a DVS Advantage (Surface Measurement Systems, London, UK) was used [37]. A schematic picture of this sorption balance is shown in Fig. 2. The mass of the small (5–100 mg) sample is continuously measured with an analytical balance while it is exposed to a program which varies RH. The desired RH is reached by mixing different proportions of dry and water vapour saturated nitrogen gas streams. The accuracy of the generated RH is better than 1.5%.

With the sorption balance the mass of water taken up or released during a hydration/dehydration phase transformation or deliquescence and the water activity at which the process takes place can both be quantified. The mass is directly measured by the balance. To determine the water activity (RH/100) of a specific transformation one has to run either a ramp or a step method [38,39]. The step method is less sensitive to disturbances and less time consuming than the ramp method and therefore this regime was chosen for testing the samples. If the (constant) mass change rate dm/dt at each RH level is plotted as a function of the RH of the gas stream, a linear curve fit intersects $dm/dt = 0$ at the water activity at which an absorption/desorption process takes place.

3.5. Sorption calorimetry

This technique provides the means to continuously scan water activity of a small sample, while simultaneously measuring water activity,

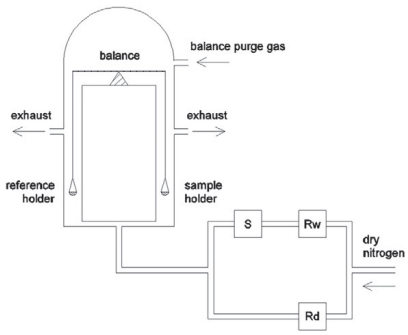

Fig. 2. Schematic picture of the sorption balance. Rw and Rd are mass flow controllers for the saturated and dry gas; S is the saturator.

moisture content and sorption enthalpy during an ad/absorption process.

The double twin isothermal sorption calorimeter used in this study is described in detail elsewhere [40]. It has two measuring positions placed 90 mm apart. The ampoule where the diffusion–sorption process takes place is schematically shown in Fig. 3. When introduced into the calorimeter, thermal power of evaporation (P_{vap}) and thermal power of sorption (P_{sorp}) are continuously measured by two twin microcalorimeters at the top and bottom chambers of the ampoule, respectively. The dry sample is loaded in the bottom chamber, after which water is injected in the top and is transported by diffusion to the sample during the measurement. The diffusion rate depends on the geometry of the connecting tube and the water activity over the sample. The water diffusion rate, and thus the rate of change of moisture content of the sample, is proportional to P_{vap}. The water activity is calculated from the evaporation rate, and the mixing enthalpy is calculated by comparing the thermal powers of sorption and vaporization (more details about the method can be found in [41]).

The enthalpy measured from the sorption microcalorimeter is normally presented as a mixing enthalpy, i.e., the difference between the enthalpy of the sorption process and that of condensation of liquid water. The mixing enthalpy can be seen as an "excess enthalpy" indicating how much additional heat is obtained from a sorption process compared to condensation of water. Sorption enthalpy, condensation enthalpy and the mixing enthalpy are related as follows:

$$\Delta H_{sorp} = \Delta H_{cond} + \Delta H_{mix}. \quad (6)$$

Note, that the sorption enthalpy and the mixing enthalpy are properties of the moisture state at which the sorption/mixing takes place, while the condensation enthalpy of water is constant under isothermal conditions with a value of −2440 J/g H_2O at 25 °C. The thermodynamic sign convention used in this work states that processes are considered from the system viewpoint, i.e., if heat is lost by the system to the surroundings (heat is produced) the enthalpy change is negative. Enthalpies of sorption, condensation and mixing are therefore all negative.

4. Results

4.1. Validation

Before testing cement hydrates the hydrate pair–humidity buffer method, sorption balance and sorption calorimetry were validated with the system Na_2SO_4–H_2O which is relatively well described in the literature.

4.1.1. Hydrate pair–humidity buffer method

Consider the RH/T phase diagram of the system Na_2SO_4–H_2O as shown in Fig. 4 taken from Linnow [36]. Phase boundaries are shown with the lines *a*, *b* and *c*. Line b is the boundary between thenardite (Na_2SO_4) and mirabilite ($Na_2SO_4 \cdot 10H_2O$), both of them in the solid state. Above and below this line $Na_2SO_4 \cdot 10H_2O$ and Na_2SO_4 are the stable phases, respectively, but both phases can coexist on the line. The dotted line corresponds to a solution in metastable equilibrium with respect to thenardite and supersaturated with respect to mirabilite [1]. To validate the method three different mixes were prepared: one mix of 80%–20% thenardite–mirabilite and two mixes of 50%–50%. A few measurements were done using saturated solutions in order to measure the solid–liquid lines *a* and *c*. The measured RH for the thenardite–mirabilite equilibrium (filled dots) as well as the mirabilite or thenardite-saturated solution phase boundaries (open dots) are

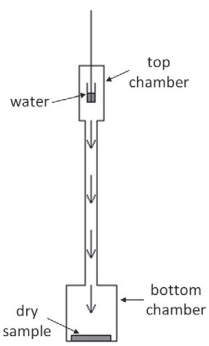

Fig. 3. Schematic graphic of the sorption ampoule. A dry sample is loaded in the bottom chamber and water is injected in the top chamber, where thermal power of sorption (P_{sorp}) and thermal power of evaporation (P_{vap}) are continuously measured by two twin microcalorimeters, respectively.

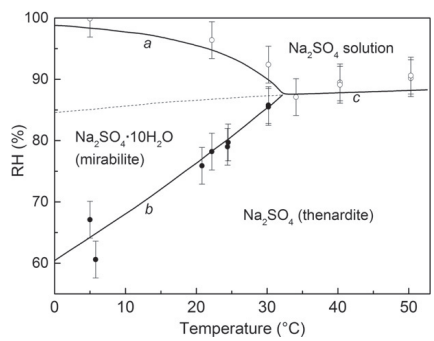

Fig. 4. RH/T phase diagram of the system Na_2SO_4 + H_2O at 0.1 MPa. The filled and open dots are our experimental results using the hydrate pair–humidity buffer method. Taken from Linnow [36].

shown in Fig. 4, respectively. As can be seen there is a good agreement with the phase diagram published by Linnow [36], which is based on thermodynamic data of aqueous Na_2SO_4 and the crystalline phases. Measurements done at around 5 °C on the thenardite–mirabilite boundary were rather scattered which might be due to low accuracy of the hygrometers at low temperature or the occurrence of other metastable equilibria including Na_2SO_4(III) and $Na_2SO_4 \cdot 7H_2O$ [3]. Since the purpose of this work was not to study in the detail the equilibrium of the system Na_2SO_4–H_2O no further analysis was carried out in these samples.

In a next step the related thermodynamic relations are cross-checked. For the reaction:

$$\underset{\text{mirabilite}}{Na_2SO_4 \cdot 10H_2O(s)} \rightarrow \underset{\text{thenardite}}{Na_2SO_4(s)} + 10H_2O(g) \quad (7)$$

The Gibbs free energy of reaction was calculated according to Eq. (3):

$$\Delta G_r^\circ = -RT \ln\left[a(H_2O)^{10}\right] - 10RT \ln \frac{f^*(H_2O)RH}{100}. \quad (8)$$

Fig. 5 shows the relation between ln$K$ and 1 / T. The error considered in the graph is due to the accuracy of the hygrometer (±3%) and the plotted 95% prediction bands were calculated using Origin Pro 8.5. Finally, ln$K$ can be obtained at any temperature according to the following equation:

$$\ln K(\pm 0.8) = 174.2 - \frac{62797.0}{T}. \quad (9)$$

The standard enthalpy of reaction ΔH_r° was calculated with help of the van't Hoff equation (Eq. (4)) using the slope value $\partial(\ln K)/\partial(1/T)$ obtained from Fig. 5. The standard entropy of reaction ΔS_r° was calculated from Eq. (5). Finally the calculated values of ΔG_r°, ΔH_r° and ΔS_r° for reaction (7) are summarized in Table 3. The results are in a very good agreement with previously reported values although the uncertainty in our data is probably larger in comparison to other techniques when we take the accuracy of the hygrometer as given by the manufacturer (+/− 3% RH) into account. Nevertheless the results underline that even with the use of a simple experimental setup, as used here, it is possible to derive relatively complex phase diagrams and related thermodynamic data.

Table 3
Derived Thermodynamic data for reaction (7) at 25 °C and 0.1 MPa.[a]

ΔG_r° [kJ/mol]	ΔH_r° [kJ mol^{-1}][b]	ΔH_r° [kJ mol^{-1}][c]	ΔS_r° [J mol^{-1} K^{-1}]	Ref.
90.3 ± 1.9	522.1 ± 9.8	82.1	1448.4 ± 39.6	This study
90.6	521.8	81.8	1444.7	[42]
	521.6	81.6		[43]

[a] Errors were calculated considering the accuracy of the hygrometers, the calculated 95% prediction band and the error in the calculated slope of the curve in Fig. 5.
[b] Calculated considering H_2O as a gas.
[c] Calculated considering H_2O as a liquid (for reaction (7) substract the heat of evaporation of 10 mol of H_2O, ΔH°_{evap} = 44 kJ mol^{-1}).

4.1.2. Sorption balance

To validate the operation of the sorption balance, Na_2SO_4 powder vacuum dried at 100 °C for 24 h was used. The measurements were carried out at 25 °C. Fig. 6a and b show the applied RH ramp program and the related evolution of sample mass, respectively. From 0% to 85% RH no water was absorbed by the sample. At RH > 85% we observed a linear mass increase, corresponding to a constant water uptake rate. During drying a linear mass decrease was observed at RH < 85%. In Fig. 6c the mass change rate versus time is plotted and dm/dt at the final 10 min of each step was used to derive Fig. 7. The line fitted to these points passes dm/dt = 0 at a RH of 88.3%, which means that Na_2SO_4 absorbs water vapour until the sample reaches a metastable equilibrium with its saturated solution at a water activity of about 0.88 or 88% RH rather than precipitating as mirabilite, despite an obvious supersaturation with respect to this phase. This value is in agreement with the 87% RH shown in Fig. 4 (metastability line). Since no equilibrium was reached in any of the set RH the sorption isotherm could not be plotted.

4.1.3. Sorption calorimetry

The validation experiments were conducted at 25 °C on sodium sulfate dried as described in the previous section. Two measurements were carried out using different sample sizes.

Fig. 8 shows that both the sorption isotherm and the mixing enthalpy plot can be divided into two parts. First there is a constant water activity that ends at a moisture content of about 2.0 g H_2O/g Na_2SO_4; secondly a process with gradually increasing water activity. Note that

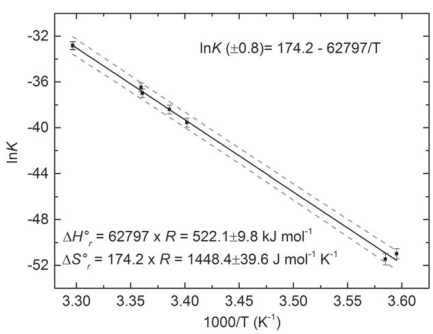

Fig. 5. van't Hoff plot of our experimental results at different temperatures for reaction (7). Dashed line represents the 95% prediction band calculated with Origin Pro 8.5.

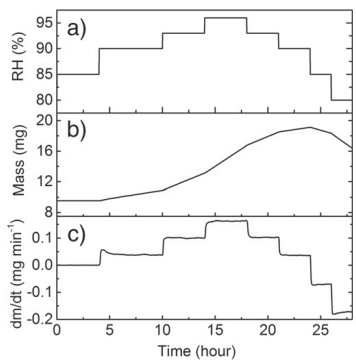

Fig. 6. a) RH step-wised program for the sorption balance. b) Mass change of sample. (c) dm/dt of sample.

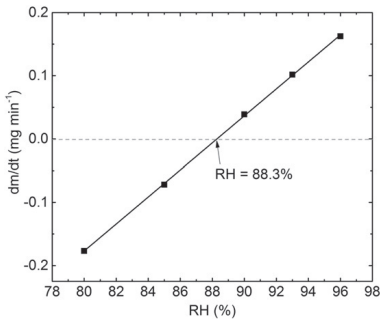

Fig. 7. Calculated RH of deliquescence of Na_2SO_4.

the water activity only changes a few tenths of a percent during the period of constant water activity. Fig. 8 can be interpreted as follows.

- The initial water activity is ~0.87 (or 87% RH) in both measurements and this is in agreement with both the literature [3,36] and the sorption balance measurement done in this study for a solution in metastable equilibrium with respect to thenardite (supersaturated with respect to mirabilite) (the dotted line in Fig. 4). Thenardite is thus dissolved to form a (metastable) saturated solution, similar to what happens at equilibrium above 32 °C where mirabilite is not stable.
- The moisture content increases at constant water activity up to a value of about 2.0 g H_2O/g Na_2SO_4 or 3.52 mol Na_2SO_4/kg H_2O, which agrees with the reported solubility of thenardite [3,43].
- The mixing enthalpy for a dissolution process should be constant and the measurement on the larger sample indicates that the value is about −125 J/g H_2O. The measurement on the smaller sample shows a drifting value, possibly because as the dissolution of the thenardite particles proceeds, a thicker and ticker layer of saturated solution is formed, the outer parts of which are more dilute (also seen in the slight increase in the water activity during the measurement). We have not found any values in literature to validate this metastable dissolution enthalpy.

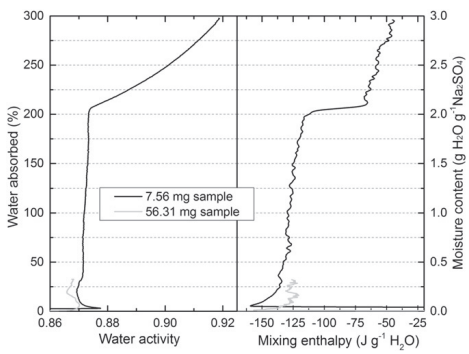

Fig. 8. The results of two measurements on thenardite with sorption calorimetry. The left diagram shows the sorption isotherm and the right one the mixing enthalpy as function of the moisture content (note that this graph is plotted with the mixing enthalpy on the x axis in order to compare it with the sorption isotherm graph). The y axes water absorbed and moisture content are proportional.

- At moisture contents above about 2.0 g H_2O/g Na_2SO_4 the water activity starts to shift to higher values. At this point the last thenardite crystals have dissolved and as the measurement continues, the solution gets increasingly more and more diluted by the absorption of water. This is substantiated by the fact that the sample is a transparent liquid after the measurement. At a moisture content of 3.0 g H_2O/g Na_2SO_4, where the measurement on the smaller sample ends, the system is still within the supersaturated region of the phase diagram with respect to mirabilite. However, there is no indication that any mirabilite forms during our measurements.
- Above a moisture content of 2.0 g H_2O/g Na_2SO_4 the measured enthalpy is due to the dilution of the aqueous solution. At increased moisture contents this will approach zero (pure water). Note the step in the mixing enthalpy from about −120 to −60 J/g H_2O when the last thenardite crystal is dissolved.

The three measured parameters have quite different errors. The moisture content is the most robust result, while the measurement of water activity can be disturbed by slow kinetics of absorption in some systems — even if this does not seem to be the case for the present measurements. The mixing enthalpy results become increasingly more uncertain at high RHs. Although we cannot at present make confident uncertainty calculations, a tentative estimate is that the error of the mixing enthalpies is at least ±10, ±20, and ±30 J/g H_2O at 80, 90 and 95% RHs, respectively.

4.2. Results of monosulfoaluminate measurements

During cement hydration C_3A reacts with calcium sulfate (gypsum, hemihydrate or anhydrite) to produce ettringite, which subsequently reacts with the remaining C_3A to form monosulfoaluminate, an LDH-type AFm phase. This cement hydrate is known to present different hydration states and has a characteristic hexagonal morphology as shown in Fig. 9. In this section the results obtained on synthetic monosulfoaluminate (Ms) using the aforementioned characterization techniques are presented.

4.2.1. XRD and TGA

As shown in the X-ray diffractograms in Fig. 10 at 25 °C, Ms14 (the index 14 gives the water content of the phase in moles) is the hydration state observed under saturated conditions (100% RH) but it dehydrates at 97% RH to Ms12 which is found until 23% RH (the water content of Ms12 was verified by TGA, see Fig. 12). At 8% RH an even lower hydration state appears, which according to Dosch et al. [14] corresponds to Ms10, but according to our TGA results it is more likely to be Ms10.5, which agrees with results presented by Pöllmann [13]. An additional lower hydration state was obtained by vacuum drying the sample.

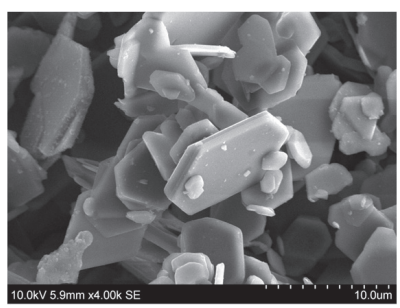

Fig. 9. SEM picture of monosulfoaluminate.

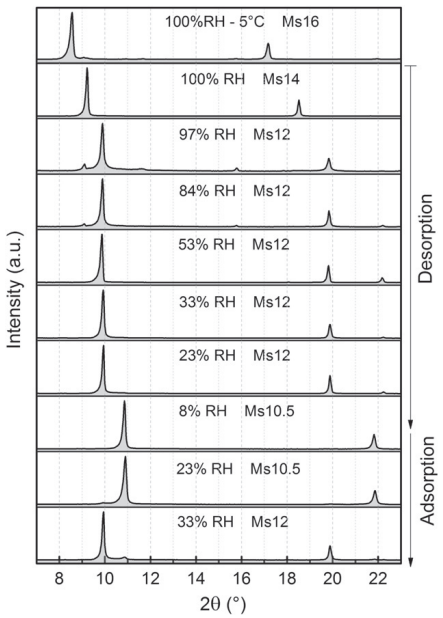

Fig. 10. XRD patterns of monosulfoaluminate dried at different RHs at 25 °C (unless otherwise stated).

According to TGA measurements this corresponds to Ms9. Since this hydration state tends to rehydrate fast at RH > 2%, XRD measurements were done using a sample dried in situ at 90 °C under N_2 flux in the humidity chamber. As no other hydration state was observed from 25 °C to 90 °C during the in-situ drying we assumed that this hydration state is the same one observed close to 0% RH at room temperature during vacuum drying. The exact RHs at which changes of hydration states take place were determined using sorption balance, sorption calorimetry and the hydrate pair–humidity buffer method, which gave comparable results.

An adsorption experiment was carried out after the desorption experiment, as shown in Fig. 10. After 1 year exposure of Ms10.5 to 23% and 33% RHs, respectively, rehydration to Ms12 is only observed at 33% RH. Also when Ms12 is rewetted (immersed in water) it does not rehydrate to Ms14 at 25 °C. This hysteretic behavior will be further discussed in the coming sections.

In order to study the stability of Ms14 a series of in situ tests using the humidity chamber were carried out at temperatures > 50 °C and high RHs. Rehydration Ms12 → Ms14 takes place at around 90, 85 and 78% RHs at 50, 65 and 75 °C.

A water rich hydration state was obtained by wet synthesis at 5 °C. According to several references it corresponds to Ms16 [13,14]. Nevertheless, most of the time the sample contained traces of Ms14, making the study of its stability difficult. For this reason, and because Ms16 was never observed from 25 °C to 85 °C in wet conditions, this hydration state was not considered during our stability and thermodynamic properties derivation analysis.

Attempts to index the diffraction patterns of the different hydration states were unsuccessful due to impurities, mainly small traces of ettringite and carbonates. For this reason the structure used for the refinement of the different hydration states of monosulfoaluminate was the kuzelite refined crystal structure published by Allmann [34] (ICSD# 100138, PDF# 41-0477) using the Le Bail method [33]. The refined lattice parameters and volume of the different hydration states of monosulfoaluminate are given in Fig. 11. Ms16 refined lattice parameters are also included in this graph. It is worth noting that a decrease of RH can often lead to a very significant reduction in molar volume, in this case (i.e. for Ms14 → Ms9) approximately 17% as shown in Fig. 11.

Fig. 12 shows the TGA curves of four different hydration states of monosulfoaluminate. The derivative plot shows similar weight losses at temperatures > 175 °C. The main differences are observed below this temperature. Ms12 shows two well defined water losses at 90 °C and 140 °C and Ms10.5 only a single water loss at 140 °C. In order to verify the water content of Ms14, a TGA test was carried out on a sample dried at 97% RH for two months. Unfortunately the sample was composed of Ms14 + Ms12, so, for this reason, and because a considerable amount of condensed water is also present in the sample at this RH, it was not possible to determine the precise water content of this hydration state. A similar problem occurred for Ms16. It was therefore simply assumed that the widely reported water contents of Ms14 and Ms16 were correct.

4.2.2. Hydrate pair–humidity buffer method

This method was used to determine the equilibrium Ms10.5–Ms12 according to the reaction:

$$C_4A\hat{S}H_{12}(s) \rightarrow C_4A\hat{S}H_{10.5}(s) + 1.5H_2O(g) \text{ or } Ms12(s) \rightarrow Ms10.5(s) + 1.5H_2O(g). \quad (10)$$

Experimentally a mixture of Ms10.5 and Ms12 was placed inside a small container and the equilibrium RH at different temperatures was recorded. The measurements were repeated 3 times for each RH point at the same temperatures from 19 °C to 50 °C in order to obtain

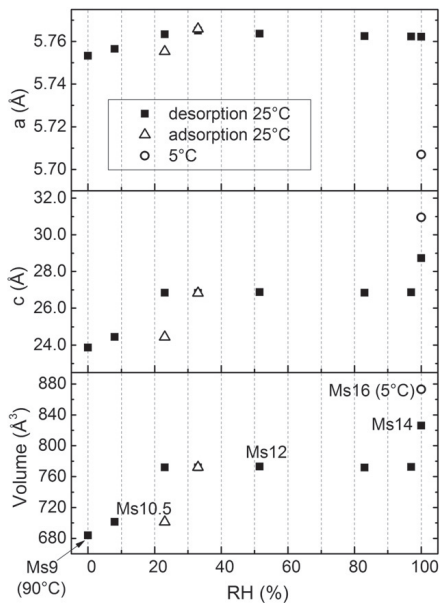

Fig. 11. Refined lattice parameter and volume of the lattice of monosulfoaluminate dried at different RHs at 25 °C (unless otherwise stated).

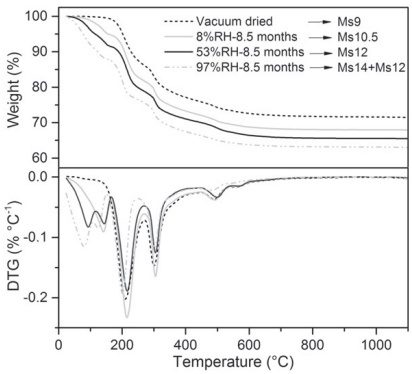

Fig. 12. TGA of monosulfoaluminate dried at different conditions at 25 °C.

representative results. One of the mixes was rejected due to large differences in recorded RH, probably due to leakage during the testing. The accuracy of the hygrometers (±3% RH) was considered in the graphs and in the calculations. A diagram presenting the measured critical RH of phase transition between Ms10.5 and Ms12 as function of temperature is shown in Fig. 13.

For reaction (10) we can write:

$$\Delta G_r^\circ = -RT\ln K = -RT\ln\left[f(H_2O)^{1.5}\right] = -1.5RT\ln\frac{f^*(H_2O)RH}{100}. \quad (11)$$

From Eq. (11) and the data presented in Fig. 13 a linear van't Hoff plot (Fig. 14) can be derived. Then ln*K* follows Eq. (12):

$$\ln K(\pm 0.1) = 26.2 - \frac{9895.8}{T}. \quad (12)$$

The standard thermodynamic properties ΔG_r°, ΔH_r° and ΔS_r° were calculated using Eqs. (3), (4) and (5), respectively and are shown in Fig. 14. The values are positive because reaction (10) shows a dehydration process; however, assuming a rehydration process these values would be negative.

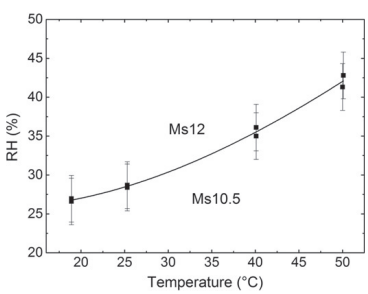

Fig. 13. Ms10.5–Ms12 equilibria at 0.1 MPa.

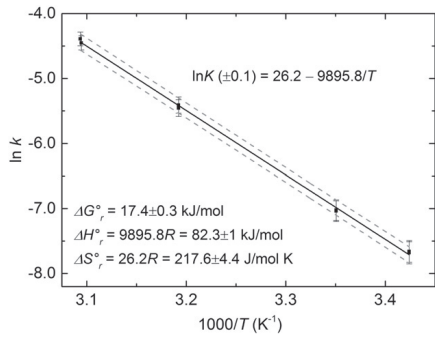

Fig. 14. van't Hoff plot for Ms10.5–Ms12 equilibria. The dashed lines represent the 95% prediction band.

4.2.3. Sorption balance

A sorption balance measurement was carried out on a monosulfoaluminate sample aged at 33% RH for 12 months, thus the initial hydration state was Ms12. The sample (10.1 mg) was initially equilibrated at 30% RH, followed by a desorption down to 0% RH, absorption up to 97% RH and finally desorption down to the initial state (30% RH). The test lasted about 92 h and the RH at each step was kept constant during 2 to 3 h (12 h in the case of 0% RH). In contrast to the validation test done on Na_2SO_4 a constant mass was achieved in almost all the steps during this experiment and thus the mass change rate could not be used to determine the RH at which a change of hydration state took place. Nevertheless we could determine the complete sorption isotherm (Fig. 15) which is also useful to determine sudden changes of mass and thus of hydration states.

4.2.4. Sorption calorimetry

A sorption calorimetry measurement was done on monosulfoaluminate at 25 °C. The sample was initially vacuum-dried for 24 h at room temperature, which means that at the beginning of the test the hydration state was Ms9 (as found by TGA). The initial mass of the sample was 89.6 mg.

Two hydration processes were observed (labelled 1 and 2 in Fig. 16). The calculated sorption isotherm is shown in Fig. 16 and is in good agreement with the isotherm measured by sorption balance.

Process 1 refers to the hydration step of Ms9 to Ms10.5 which is in very good agreement with the sorption balance measurements.

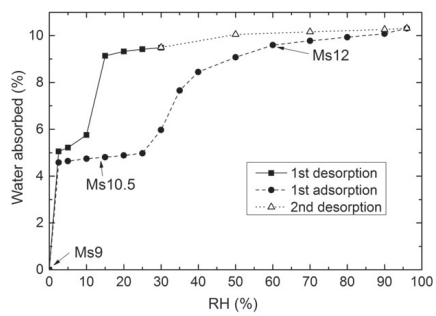

Fig. 15. Sorption isotherm of monosulfoaluminate at 25 °C.

Stoichiometrically this process can be described by the following reaction:

$$Ms9(s) + 1.5H_2O(g) \rightarrow Ms10.5(s). \quad (13)$$

This process starts and finishes in points *a* and *b*, respectively (see Fig. 16). As the hydrate pair–humidity buffer method could not be used to calculate the thermodynamic properties of this reaction/process, the experimental findings of the calorimetry measurements show that the critical RH for the transformation of Ms9 to Ms10.5 is at around 2% RH. Thus the Gibbs free energy of reaction ΔG_r° of reaction (13) can be calculated according to Eq. (3), giving a value of 27.3 kJ/mol. As shown in Fig. 17 the mixing enthalpy of this process is not completely constant, having an average value of −1365 J/g H_2O. The related sorption enthalpy ΔH_{sorp} for reaction (13) can now be calculated according to Eq. (6):

$$\Delta H_{sorp} = \Delta H_{cond} + \Delta H_{mix} = -2440 \text{ J/g } H_2O - 1365 \text{ J/g } H_2O = -3805 \text{ J/g } H_2O = -68.6 \text{ kJ/mol } H_2O.$$

Since 1.5 mol of H_2O are needed to complete hydration reaction (13), the total standard enthalpy of this reaction can be calculated as:

$$\Delta H_r^\circ = -68.6 \text{ kJ/mol } H_2O \times 1.5 = -102.8 \text{ kJ/mol}.$$

Process 2 follows hydration reaction (14):

$$Ms10.5(s) + 1.5H_2O(g) \rightarrow Ms12(s). \quad (14)$$

This reaction was also studied with the invariant point method. As seen in Fig. 16 this process starts in point *b* and finish approximately in point *c* where the mixing enthalpy is close to zero. The mixing enthalpy of this second process is around −670 J g^{-1} H_2O in the constant region. Following the same procedure as shown in process 1 the corresponding standard enthalpy of reaction (14) is:

$$\Delta H_{sorp} = \Delta H_{cond} + \Delta H_{mix} = -2440 \text{ J/g } H_2O - 670 \text{ J/g } H_2O = -3110 \text{ J/g } H_2O = -56.0 \text{ kJ/mol } H_2O$$

$$\Delta H_r^\circ = -56.0 \text{ kJ/mol } H_2O \times 1.5 = -84.0 \text{ kJ/mol}.$$

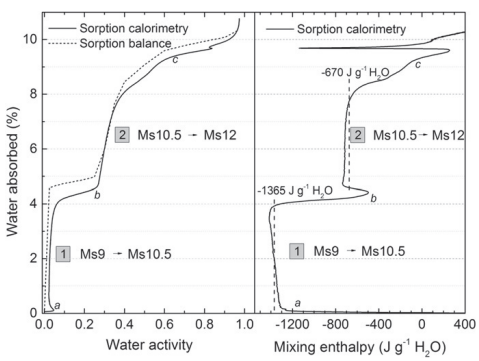

Fig. 16. Sorption calorimetry results on initially vacuum dried monosulfoaluminate at 25 °C. The left graph shows the calculated sorption isotherm (for comparison the isotherm obtained with sorption balance is superposed). The right graph presents the mixing enthalpy measured on the sample (the dashed lines represent the mean mixing enthalpies for the two observed processes).

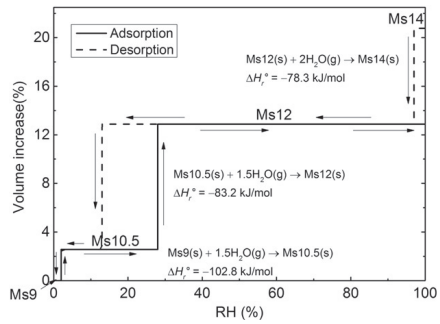

Fig. 17. Volume changes of monosulfoaluminate vs RH and related enthalpies of reaction at 25 °C.

This value is in good agreement to the enthalpy of reaction calculated from the invariant point method, 82.3 kJ/mol. Please note that the enthalpy value calculated with sorption calorimetry is negative because the test measures an absorption process which is exothermic.

In addition to processes 1 and 2, an endothermic process followed by an exothermic peak is observed after point *c*. As there is no significant increase in moisture content corresponding to this event, it seems that it has its origin in, for example, a conformational/morphological change that may be initiated by the increase in moisture content, but does in itself not involve uptake of water. It should be noted that although the thermal effect of this event is clearly seen, the uncertainty in the absolute values increases significantly at high RH; thus the increase of the mixing enthalpy to positive values after the sharp exothermal peak is probably an artefact as the RH then approaches 100%.

The very good agreement between the sorption isotherm measured on monosulfoaluminate by sorption balance and the one calculated by sorption calorimetry as shown in Fig. 16 is worth noticing. This clearly shows the power and reliability of this technique, which can also be used to study ad/absorption processes in salts, minerals, proteins, pharmaceutical products, etc.

4.2.5. Summary of results

A summary of results obtained for monosulfoaluminate is shown in Fig. 17 and Table 4. The hysteretic behavior observed in the sorption balance and XRD measurements is represented by a dashed-line. In the experimental studies Ms12 is observed when Ms14 is dried at 97% RH, for this reason the dehydration process Ms14 → Ms12 was assumed to take place at this RH. The rehydration Ms12 → Ms14 at 25 °C was not observed by any of the techniques used in this study.

Table 4
Derived thermodynamic data for the changes of hydration states of monosulfoaluminate at 25 °C and 0.1 MPa.

Reaction	Change of hyd. state (% RH)	ΔG_r° (kJ/mol)	ΔH_r° (kJ/mol)	ΔS_r° (J/mol K)
Ms14(s) → Ms12(s) + 2H_2O(g)	97	17.2	78.3[a]	205.2
Ms12(s) → Ms10.5(s) + 1.5H_2O(g)	28.5[b]	17.4	83.2[c]	220.5
Ms10.5(s) → Ms9(s) + 1.5H_2O(g)	2[d]	27.3	102.8[e]	253.3

[a] Calculated considering a change of hydration state at 97, 90, 85 and 78% RHs at 25, 50, 65 and 75 °C, respectively.
[b] From hydrate pair–humidity buffer method.
[c] Average value from sorption calorimetry and hydrate pair–humidity buffer method.
[d] From sorption balance.
[e] From sorption calorimetry.

Thermodynamic properties of Ms16 found at 5 °C in wet conditions were not calculated due to lack of data. The density values of the different hydration states of monosulfoaluminate are shown in Table 5 and were calculated with Eq. (15):

$$D = ZM/N_A V \quad (15)$$

where D is the density, Z is the number of formula units per unit cell (which is 1.5 in our case), M is the molecular weight of the hydration state, V is the unit cell volume obtained from the XRD lattice parameter refinement and N_A is the Avogadro's number.

To show how critical may be the changes of hydration states, a short experiment was carried out on a sample initially dried at 8% RH and 25 °C. This powder sample was then compacted to form a small disk (Φ: 15 mm and thickness: 3 mm) and subsequently exposed to 97% RH and 25 °C during 5 days. The results can be observed in Video 1 and clearly show the expansion and cracking of the sample due to the rehydration reaction Ms10.5(s) + 1.5H_2O(g) → Ms12(s).

5. Discussion

5.1. Correlation between the methods and accuracy

The complementarity of the different methods shown in this work is evident. While XRD and TGA provide important structural data about the different hydration states, they cannot derive information about critical de/rehydration RH and thermodynamic properties. These were instead obtained by sorption calorimetry, sorption balance and the hydrate pair–humidity buffer method.

Sorption calorimetry was demonstrated to be a powerful tool which can give an almost complete thermodynamic description of a sorption process, although part of a measurement or a whole measurement may take place at metastable conditions. This has to be kept in mind when such experiments are evaluated. When calculating thermodynamic properties with the hydrate pair–humidity buffer method one has to consider that the accuracy of this method is determined by the hygrometers used to record RH and thus it is recommended to crosscheck the results with, for instance, sorption calorimetry measurements. Nevertheless average values calculated agrees well with previously reported data on Na_2SO_4, so despite the accuracy issue the hydrate pairs–humidity buffer method proved to be a simple, reliable and fast technique to determine stability ranges of different hydration states of minerals and thermodynamic properties of de/rehydration.

5.2. Interactions between Na_2SO_4 and water vapour

Na_2SO_4 (thenardite) and $Na_2SO_4 \cdot 10H_2O$ (mirabilite) were used to validate sorption balance, sorption calorimetry and the hydrate pair–humidity buffer method. The thenardite–mirabilite equilibrium RH as function of temperature and the enthalpy of reaction (7) determined by the humidity buffer method was in agreement with previously published data.

However, during sorption balance and sorption calorimetry tests the critical RH at which the first absorption process occurred on thenardite was about 87% RH (no water was absorbed below this RH) which corresponds to a solution in metastable equilibrium with respect to thenardite and supersaturated with respect to mirabilite [1,3,36]. The presence of a solution at the end of the calorimetry test confirmed the dissolution of thenardite during the measurement. This means that during an absorption process thenardite will tend to dissolve into a metastable solution with no precipitation of mirabilite. This behavior was also observed by Rodriguez-Navarro et al. [2] with in situ environmental scanning electron microscopy (ESEM) showing no hydration of thenardite into mirabilite but dissolution; during drying they observed crystallization of both thenardite and mirabilite. It has to be considered that our absorption tests took place under unconstrained conditions in a free non-confined space, opposite to what happens in real conditions where the deliquescence and crystallization of salts happen in porous media such as stone and building materials. In those cases a reduction of water activity and different supersaturation levels due to pore size can alter the dissolution behavior observed in our tests and mirabilite might precipitate upon hydration of thenardite.

At the end of the first absorption process at 87% RH (as measured by sorption calorimetry) the sample has absorbed 2 g H_2O/g Na_2SO_4, which agrees perfectly with reported values of thenardite solubility [3,43]. The second process observed in the sorption calorimetry test, which starts once all the initial salt has been dissolved, is dilution of the initially saturated solution into a more and more dilute solution. This shows a lower mixing enthalpy compared to the dissolution process. Unfortunately, we have not found literature values to compare our enthalpy results because of the metastable nature of the processes.

Table 5
Molar volume and density of monosulfoaluminate hydration states.

Hydration state	Formula	V° (cm^3/mol)	Density (kg/m^3)
Ms16	$[Ca_4(Al)_2(OH)_{12}]^{2+}[SO_4 \cdot 10H_2O]^{2-}$	350.5	1981.7
Ms14	$[Ca_4(Al)_2(OH)_{12}]^{2+}[SO_4 \cdot 8H_2O]^{2-}$	331.6	1985.9
Ms12	$[Ca_4(Al)_2(OH)_{12}]^{2+}[SO_4 \cdot 6H_2O]^{2-}$	310.1	2007.7
Ms10.5	$[Ca_4(Al)_2(OH)_{12}]^{2+}[SO_4 \cdot 4.5H_2O]^{2-}$	281.6	2114.9
Ms9	$[Ca_4(Al)_2(OH)_{12}]^{2+}[SO_4 \cdot 3H_2O]^{2-}$	274.6	2070.2

5.3. Interactions between LDH-type cement hydrates and water vapour

Five hydration states of monosulfoaluminate were found in this study: Ms16, Ms14, Ms12, Ms10.5 and Ms9. Ms14 is stable under saturated conditions over 20 °C and once it dehydrates to Ms12 it does not rehydrate to Ms14 at room temperature. Ms9 was obtained at a water activity close to zero. A hysteresis in the equilibria Ms10.5–Ms12 and Ms12–Ms14 was observed with XRD and sorption balance measurements, probably due to kinetic constraints or crystal size; it is believed that the larger the crystal size the longer it would take to absorb water within the structure. Another possibility for the hysteretic behavior is a related activation energy of de/rehydration which might be needed to remove/introduce water within the hydrate. In minerals such as clays, hysteresis can occur due to a non-reversible orderliness due to changes that occur in the structure of the material while water is being absorbed [44]. However during the hydrate pair–humidity buffer method the equilibrium RH between Ms10.5 and Ms12 agrees with the adsorption regime. This suggests that the adsorption results correspond to the real equilibrium between two coexisting hydration states. Enthalpy of sorption for the reaction Ms9 → Ms10.5 was calculated from sorption calorimetry results, while the reaction Ms10.5 → Ms12 was evaluated from both sorption calorimetry and the humidity buffer method, resulting in similar values. The sorption isotherms measured with sorption balance and sorption calorimetry were qualitatively and quantitatively similar. A water rich hydration state, Ms16, was found in wet conditions at low temperatures (5 °C) by XRD. Thermodynamic properties of the dehydration for the reaction Ms16 → Ms14 were not calculated due to lack of stability even in wet state. Our research indicates that Ms16 can occur at low temperatures, which agrees with observations done by Dosch et al. [14]. Further research is required to find out under which conditions this hydration state is stable.

The results clearly show the impact of drying condition on crystalline cement hydrates. At room temperature monosulfoaluminate will decrease about 17% in volume from Ms14 to Ms9. Although in real conditions the dehydration Ms14 → Ms12 can occur, it is unlikely for a concrete structure to reach humidities where Ms10.5 and Ms9 are stable, 28.5% and 2% RH, respectively. Nevertheless, these low humidities are easily obtained during sample preparation prior to characterization, which includes vacuum drying, P-drying, solvent exchange and so on,

which highlight the importance of our results in connection to the analysis of a hydrated cement paste.

5.4. Practical implications

The thermodynamic properties obtained on monosulfoaluminate are the first to be reported. This methodology will be subsequently used to derive stability conditions and thermodynamic properties of the different hydration states of the most important AFm and AFt phases present in ordinary Portland cement (OPC) and calcium aluminate cement (CAC) blended systems. This data will enable the modelling of the mineralogy and volume changes of a hydrated cementitious system exposed to different drying conditions. This opens the possibility to engineer cement mixes containing hydrate phase assemblages which are less sensitive to changing exposure conditions which can positively impact the performance and durability of cement based materials.

Supplementary data to this article can be found online at http://dx.doi.org/10.1016/j.cemconres.2014.07.009.

Acknowledgements

The research leading to these results has received funding from the European Union Seventh Framework Programme (FP7/2007–2013) under grant agreement 264448. We would like to thank Holcim Technology Ltd. for actively promoting cement research, especially the Innovation Function and the Analytical Lab of the Cement Manufacturing Function.

References

[1] R. Flatt, Salt damage in porous materials: how high supersaturations are generated, J. Cryst. Growth 242 (2002) 435–454.
[2] C. Rodriguez-Navarro, E. Doehne, E. Sebastian, How does sodium sulfate crystallize? Implications for the decay and testing of building materials, Cem. Concr. Res. 30 (2000) 1527–1534.
[3] M. Steiger, S. Asmussen, Crystallization of sodium sulfate phases in porous materials: the phase diagram Na_2SO_4–H_2O and the generation of stress, Geochim. Cosmochim. Acta 72 (2008) 4291–4306.
[4] M. Collepardi, A state-of-the-art review on delayed ettringite attack on concrete, Cem. Concr. Compos. 25 (2003) 401–407.
[5] H.F.W. Taylor, C. Famy, K.L. Scrivener, Delayed ettringite formation, Cem. Concr. Res. 31 (2001) 683–693.
[6] F. Bergaya, G. Lagaly, Chapter 1 - General Introduction: Clays, Clay Minerals, and Clay Science, in: F. Bergaya, G. Lagaly (Eds.), Developments in Clay Science, Elsevier, 2013, pp. 1–19.
[7] C. Forano, U. Costantino, V. Prévot, C. Taviot Gueho, Chapter 14.1 - Layered Double Hydroxides (LDH), in: F. Bergaya, G. Lagaly (Eds.), Developments in Clay Science, Elsevier, 2013, pp. 745–782.
[8] M.F. Brigatti, E. Galan, B.K.G. Theng, Structure and mineralogy of clay minerals, Chapter 2 in: F. Bergaya, G. Lagaly (Eds.), Developments in Clay Science, Elsevier, 2013, pp. 21–81.
[9] L. Baquerizo, T. Matschei, K. Scrivener, The impact of water chemical potential on the hydration states of Monosulfoaluminate, Proceedings of the 31th Cem. Concr. Science Conference, London, England, 2011.
[10] H. Pöllmann, T. Runcevski, R. Dinnebier, Synthesis and characterization of layered carbonated calcium aluminate hydroxi carbonate hydrates, IV Int. Work Layered Materials, Campinas SP, Brazil, 2012.
[11] H.F.W. Taylor, Cement Chemistry, second ed. Thomas Telford, London, 1997.
[12] H.E. Schwiete, U. Ludwig, Crystal structures and properties of cement hydration products (hydrated calcium aluminates and ferrites), 5th ISCC, vol. 2, 1968, pp. 37–67.
[13] H. Pöllmann, Characterization of different water contents of ettringite and kuzelite, Proceeding of the XII Int. Congress on the Chemistry of Cement, Montreal, Canada, 2007.
[14] W. Dosch, H. Keller, H. Strassen, 5th ISCC, vol. 21968. 72–77.
[15] D. Damidot, F.P. Glasser, Thermodynamic investigation of the CaO–Al_2O_3–$CaSO_4$–H_2O at 50 °C and 85 °C, Cem. Concr. Res. 22 (1992) 1179–1191.
[16] I. Kaprálik, F. Hanic, Phase relations in the subsystem C_4A_3S–CS–H_2–CH–H_2O of the system CaO–Al_2O_3–CS–H_2O referred to hydration of sulphoaluminate cement, Cem. Concr. Res. 19 (1989) 89–102.
[17] H.J. Kuzel, Initial hydration reactions and mechanisms of delayed ettringite formation in Portland cements, Cem. Concr. Compos. 18 (1996) 195–203.
[18] H. Pöllmann, Die Kristallchemie der Neubildungen bei Einwirkung von Schadstoffen auf hydraulische Bindemittel, (PhD Dissertation) University of Erlangen-Nuernberg, 1984.
[19] M.H. Robert, Calcium aluminate hydrates and related basic salt solid solutions, 5th ISCC, vol. 2, 1968, pp. 104–117.
[20] R. Fischer, H.J. Kuzel, Reinvestigation of the system $C_4A{\cdot}nH_2O$–$C_4A{\cdot}CO_2{\cdot}nH_2O$, Cem. Concr. Res. 12 (1982) 517–526.
[21] M. Francois, G. Renaudin, O. Evrard, A cementitious compound with composition $3CaO{\cdot}Al_2O_3{\cdot}CaCO_3{\cdot}1H_2O$, Acta Crystallogr. C54 (1998) 1214–1217.
[22] T. Runcevski, R.E. Dinnebier, O.V. Magdysyuk, H. Pöllmann, Crystal structures of calcium hemicarboaluminate and carbonated calcium hemicarboaluminate from synchrotron powder diffraction data, Acta Crystallogr. B68 (2012) 493–500.
[23] G. Renaudin, Y. Filinchuk, J. Neubauer, F. Goetz-Neunhoeffer, A comparative structural study of wet and dried ettringite, Cem. Concr. Res. 40 (2010) 370–375.
[24] K.J. Parkinson, W. Day, Water vapour calibration using salt hydrate transitions, J. Exp. Bot. 32 (1981) 411–418.
[25] G.M. Richardson, R.S. Malthus, Salts for static control of humidity at relatively low levels, J. Appl. Chem. 5 (1955) 557–567.
[26] I.M. Chou, R.R. Seal II, B.S. Hemingway, Humidity buffers and their application to the studies of dehydration reactions of sulfate salts at 0.1 mPa, Trans. Am. Geophys. Union 79 (1998) S364.
[27] I.M. Chou, R.R. Seal II, B.S. Hemingway, Determination of melanterite–rozenite and chalcanthite–bonattite equilibria by humidity measurements at 0.1 MPa, Am. Mineral. 87 (2002) 108–114.
[28] I.M. Chou, R.R. Seal II, Determination of epsomite–hexahydrite equilibria by the humidity–buffer technique at 0.1 MPa with implications for phase equilibria in the system $MgSO_4$–H_2O, Astrobiology 3 (2003) 619–630.
[29] I.M. Chou, R.R. Seal II, Determination of goslarite–bianchite equilibria by the humidity–buffer technique at 0.1 MPa, Chem. Geol. 215 (2005) 517–523.
[30] I.M. Chou, R.R. Seal II, Acquisition and evaluation of thermodynamic data for morenosite–retgersite equilibria at 0.1 MPa, Am. Mineral. 88 (2003) 1943–1948.
[31] T. Matschei, Thermodynamics of Cement Hydration, (PhD Dissertation) University of Aberdeen, 2007.
[32] L. Greenspan, Humidity fixed points of binary saturated aqueous solutions, J. Res. Natl. Bur. Stand. Sect. A 81 (1977) 89–96.
[33] A. Le Bail, H. Duroy, J.L. Fourquet, Ab-initio structure determination of $LiSbWO_6$ by X-ray powder diffraction, Mater. Res. Bull. 23 (1988) 447–452.
[34] R. Allmann, Refinement of the hybrid layer structure $[Ca_2Al(OH)_6]^+{\cdot}[1/2SO_4{\cdot}3H_2O]^-$, Neues Jb. Mineral. Monat. (1977) 136–144.
[35] J.F. Young, Humidity control in the laboratory using salt solutions — a review, J. Appl. Chem. 17 (1967) 241–245.
[36] K. Linnow, Salt Damage in Porous Materials: An XRD Investigation, (PhD dissertation) Universität Hamburg, 2007.
[37] D.R. Williams, The characterisation of powders by gravimetric water vapor sorption, Int. Labmate. 20 (1995) 40–42.
[38] L. Wadsö, A. Anderberg, I. Ålund, O. Söderman, An improved method to validate the relative humidity generation in sorption balances, Eur. J. Pharm. Biopharm. 72 (1) (2009) 99–104.
[39] L. Wadsö, N. Markova, Comparison of three methods to find the vapor activity of a hydration step, Eur. J. Pharm. Biopharm. 51 (1) (2001) 77–81.
[40] L. Wadsö, N. Markova, A double twin isothermal microcalorimeter, Thermochim. Acta 360 (2000) 101–107.
[41] L. Wadsö, N. Markova, A method to simultaneously determine sorption isotherms and sorption enthalpies with a double twin microcalorimeter, Rev. Sci. Instrum. 73 (2002) 2743–2754.
[42] S.E.D. Hamad, A study of the reaction $Na_2SO_4{\cdot}10H_2O \rightarrow Na_2SO_4 + 10\ H_2O$ in the temperature range 0 to 25 °C, Thermochim. Acta 17 (1976) 85–96.
[43] P. Marliacy, R. Solimand, M. Bouroukb, L. Schuffenecker, Thermodynamics of crystallization of sodium sulfate decahydrate in H_2O–NaCl–Na_2SO_4: application to $Na_2SO_4{\cdot}10H_2O$-based latent heat storage materials, Thermochim. Acta 344 (2000) 85–94.
[44] M.H. Fu, Z. Zhang, P.F. Low, Changes in the properties of a montmorillonite–water system during the adsorption and desorption of water: hysteresis, Clays Clay Minerals 38 (1990) 485–492.

Paper VI

Cement and Concrete Research 73 (2015) 143–157

Contents lists available at ScienceDirect

Cement and Concrete Research

journal homepage: http://ees.elsevier.com/CEMCON/default.asp

Hydration states of AFm cement phases

Luis G. Baquerizo [a,*], Thomas Matschei [a], Karen L. Scrivener [b], Mahsa Saeidpour [c], Lars Wadsö [c]

[a] Innovation, Holcim Technology Ltd., CH-5113 Holderbank, Switzerland
[b] Laboratory of Construction Materials, Ecole Polytechnique Fédérale de Lausanne, CH-1015 Lausanne, Switzerland
[c] Building Materials, Lund University, Box 124, 221 000 Lund, Sweden

ARTICLE INFO

Article history:
Received 23 November 2014
Accepted 10 February 2015
Available online 27 March 2015

Keywords:
Cement hydrates (B)
AFm phases (D)
Hydration states (D)
Thermodynamic properties (C)
Characterization techniques (B)

ABSTRACT

The AFm phase, one of the main products formed during the hydration of Portland and calcium aluminate cement based systems, belongs to the layered double hydrate (LDH) family having positively charged layers and water plus charge-balancing anions in the interlayer. It is known that these phases present different hydration states (i.e. varying water content) depending on the relative humidity (RH), temperature and anion type, which might be linked to volume changes (swelling and shrinkage). Unfortunately the stability conditions of these phases are insufficiently reported. This paper presents novel experimental results on the different hydration states of the most important AFm phases: monocarboaluminate, hemicarboaluminate, strätlingite, hydroxy-AFm and monosulfoaluminate, and the thermodynamic properties associated with changes in their water content during absorption/desorption. This data opens the possibility to model the response of cementitious systems during drying and wetting and to engineer systems more resistant to harsh external conditions.

1. Introduction

AFm (Al_2O_3–Fe_2O_3–mono) phases are hydrated tetracalcium aluminate-ferrite compounds belonging to the lamellar double hydroxide family. They are formed during the hydration process of Portland and calcium aluminate cements. AFm phases are composed of positively charged main layers $[Ca_2(Al,Fe)(OH)_6]^+$ and negatively charged interlayers $[X.nH_2O]^-$ where X is either one monovalent anion or half a divalent anion. Since Fe substitution for Al is limited in cement paste [1], in this study we focus on the aluminium AFm phases. The general formulae (in cement notation[1]) $C_4AX_2H_n$ for monovalent anions (OH^-, NO_3^-) and C_4AXH_n for divalent anions (SO_4^{2-}, CO_3^{2-}) are generally used in cement chemistry [2]. The substitution of Ca by the smaller Al atoms (one Ca atom in three by one Al) distorts the structure of the principal layer which allows each Ca atom to coordinate the oxygen atom of an interlayer H_2O molecule in addition to its six OH^- groups [2]. A crystal may contain more than one species of X anions. The interlayer thickness depends on the nature of the X anion and the amount of interlayer water *n* [2,3]. Fig. 1 shows a schematic of the lamellar AFm structure.

The anion content depends on the cement composition. Thus in a typical Portland cement (PC) the common anions are hydroxide (OH^-) and sulfate (SO_4^{2-}). If PC is blended with limestone the anion will be a carbonate (CO_3^{2-}) and in case it is blended with slag or fly ash the interlayer anion might be an aluminosilicate ($AlSiO_8H_8^-$). The anion also depends on the service environment, e.g., in marine applications chloride (Cl^-) can displace other anions and form AFm phases such as Friedel's salt and Kuzel's salt [2,4]. A short summary of the phases studied in this paper and their different hydration states follows. The phases are denoted by an abbreviation[2] followed by an index which denotes the water content in moles, thus the 14 H_2O hydration state of monosulfoaluminate will be denoted as Ms14.

1.1. Monosulfoaluminate (Ms)

Monosulfoaluminate is a common cement hydrate formed during hydration of cements with $CaCO_3$ content < 1% [5] by reaction of the initially formed ettringite with the remaining tricalcium aluminate. It is an analogue of the natural occurring mineral kuzelite ($C_4A\hat{S}H_{12}$), whose crystal structure was refined by Allmann [6]. Its formula is $C_4A\hat{S}H_{6+x}$ (which we will denote as Ms($6+x$) in this study), where *x* is the interlayer water content, which according to several reference may vary from 2 to 10, depending on the exposure temperature and RH [2, 6–13]. However, there is no unified data showing the stability range of this hydrate except a recent study by Baquerizo et al. [14] that reports the hydration states Ms14, Ms12, Ms10.5 and Ms9, and the thermodynamic properties related to their formation. In the present study the previous results are complemented with low temperature studies investigating the stability of the water-rich hydration state Ms16.

* Corresponding author. Tel.: +41 58 858 64 31.
E-mail address: luis.baquerizoibarra@holcim.com (L.G. Baquerizo).

[1] Cement notation: C = CaO, A = Al_2O_3, S = SiO_2, $\hat{C}$ = CO_2, $\hat{S}$ = SO_3, H = H_2O.

[2] Abbreviation of phases: Ms = monosulfoaluminate, Mc = monocarboaluminate, Hc = hemicarboaluminate, cHc = carbonated hemicarboaluminate, OH-AFm = hydroxy-AFm, Str = strätlingite.

http://dx.doi.org/10.1016/j.cemconres.2015.02.011
0008-8846/

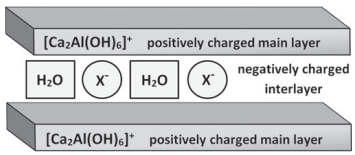

Fig. 1. Schematic figure of the lamellar structure of an AFm phase.

1.2. Hydroxy-AFm (OH-AFm)

The first studies related to the structural description of hydroxy-AFm (also called "C_4A hydrates") were published by Ahmed et al. [15] and Buttler et al. [16]. Its formula can be written as C_4AH_{7+x} (or OH-AFm$(7+x)$), where the anions are two $(OH)^-$ groups and the interlayer water content x varies from 0 to 12 according to the literature [2-3,9,12–17], although there are contradictions in terms of water content and the related layer thickness at different conditions. The occurrence of OH-AFm in hydrated Portland cement pastes is not likely, mainly due to the presence of sulfates and carbonates, favouring the precipitation of monosulfoaluminate, OH–SO_4–AFm solid solutions [18] and carboaluminate phases [19], and also because of its metastable nature with respect to hydrogarnet (C_3AH_6) and portlandite (CH) [20] at temperatures >20 °C.

1.3. Monocarboaluminate (Mc)

The crystal structure of monocarboaluminate $C_4A\hat{C}H_{11}$ was first determined by Fisher and Kuzel [17]. The lamellar structure contains only one type of structural element, with $[Ca_2(Al)(OH)_6]^+$ as the main layer and $[1/2CO_3^{2-}\cdot 2.5H_2O]^-$ as the interlayer content. Francois et al. [21] later refined the crystal structure of monocarboaluminate. Their results are well accepted, and basically state that the main difference with respect to other AFm phases is that one oxygen atom of the carbonate (CO_3^{2-}) group occupies the seventh coordination site of one out of four Ca atoms contained in the main layer. Additionally, every oxygen atom of the carbonate groups contributes to the formation of relatively strong hydrogen bonds with water molecules, providing a strong cohesion between the inter- and the main layer. This seems a plausible explanation for why monocarboaluminate is comparatively stable over a wide range of exposure condition. For this reason Mc11 is the only hydration state reported at 25 °C, although lower water contents have been reported with increasing temperature [12,17]. In a later work done by Renaudin et al. [22] two modifications of monocarboaluminate were reported, an ordered and a disordered structure with different stacking sequences of the layers. Another proof of the high stability of monocarboaluminate has been presented by Moon et al. [23] with synchrotron X-ray diffraction studies under high pressure (4.3 GPa), showing a perfectly reversible pressure-induced dehydration with no critical effect on the bulk modulus due to its strong framework.

1.4. Hemicarboaluminate (Hc)

Hemicarboaluminate ($C_4A\hat{C}_{0.5}H_{12}$ or Hc12) is a carbonated AFm phase similar to monocarboaluminate, where half a carbonate group ($0.5CO_3^{2-}$) has been replaced by an $(OH)^-$ group. Fisher and Kuzel [17] indexed the powder diffraction pattern but the crystal structure was not solved. In contrast to other AFm phases, Hc12 shows slight differences in basal spacing probably due to limited solid solutions and/or slight differences in interlayer water [2,12,17]. Other hydration states than Hc12 have been reported for higher temperatures [12,13,17]. Moon et al. [24] demonstrated that the application of pressures >0.5 GPa results in a volume contraction due to pressure-induced dehydration and partial removal of the weakly bound interlayer water.

Runcevski et al. [25] solved the crystal structure of synthetic hemicarboaluminate and refined it in the R3c space group of the trigonal crystal system. However, another phase, called carbonated hemicarboaluminate (cHc) was also found together with Hc due to partial carbonation. Its interlayer composition shows a slightly higher CO_3^{2-} content compared to that of Hc and lower water content. Its crystal structure was also solved, showing the same space group as Hc but with lower c lattice parameter. When Hc was exposed to increasing temperatures in an atmosphere with a reduced amount of CO_2, cHc was formed. It should be mentioned that this cHc has been previously reported as a lower hydration state of Hc rather than as a new phase [17].

1.5. Strätlingite (Str)

Strätlingite (C_2ASH_8), also called gehlenite hydrate, is a cement hydrate which can occur as a hydration product in slag-, metakaolin- or fly ash blended cements as well as in hydrated high alumina cements [26,27]. According to structural data published by Rinaldi et al. [28], strätlingite, with a formula $C_2ASH_{7.25}$, has the same principal layer constitution as other AFm phases, but with an aluminosilicate anion as interlayer, which is a double tetrahedral sheet of composition $[(T,\square)_4(OH,O)_8]^-$, where □ is a vacant tetrahedral site and T can be Si or Al. This phase is more complex than other AFm phases, due to the vacant sites and partial occupancy of some groups, including hydroxyl sites and water molecules, which can alter the water content of this phase. This is the likely reason why strätlingite is usually reported as Str8 although structural data by Rinaldi presents a total water content of 7.25 mol (Str7.25). Similar to hemicarboaluminate, strätlingite shows an abrupt contraction in volume when subjected to high pressures (up to 5 GPa) [24]. These volume changes can be associated with a structural transition or with the removal of weakly bound interlayer water.

1.6. Importance of this study

Presently there is neither complete experimental data nor thermodynamic properties associated with changes of hydration states on AFm phases. In the present paper these missing data are derived using the multi-method approach developed by Baquerizo at al. [14], which includes the combined use of X-ray diffraction (XRD), thermogravimetric analysis (TGA), sorption balance measurements, sorption calorimetry and the hydrate pair–humidity buffer method. The obtained information is important in order to assess the stability of complex cementitious systems containing, among others, AFm phases at unsaturated conditions, i.e. at <100% RH. In addition these data enable the prediction of the mineralogical constitution of cement pastes made from new binder combinations, and will further help to predict phase changes in concrete structures following environmental fluctuations (for example severe drying at high temperatures, etc.). Note that this paper only focusses on pure AFm hydrates. The study of the influence of solid solutions, e.g. SO_4–OH AFm, in their water content and stability has not been considered in this study.

2. Experimental procedure

2.1. Preparation of cement hydrates

In order to produce phase-pure synthetic AFm hydrates several precursors are required. All syntheses were done from analytical grade reagents. The main precursor in the synthesis of the studied AFm phases (excluding strätlingite) was tricalcium aluminate, C_3A ($3CaO\cdot Al_2O_3$), which was prepared from a 3:1 molar ratio of $CaCO_3$ and Al_2O_3 at 1400 °C, based on the procedure given by Matschei et al. [18]. Anhydrite

$CaSO_4$ was prepared by dehydration of gypsum in a muffle furnace at 550 °C overnight. CaO was prepared from $CaCO_3$ calcined at 900 °C overnight. Double distilled CO_2 free water with a water to solid ratio (w/s) of 20 was used in the synthesis of all hydrates. Monosulfoaluminate, monocarboaluminate and hydroxy-AFm were prepared by suspending a 1:1 molar mixture of C_3A and either $CaSO_4$, $CaCO_3$ or CaO, respectively. In the case of hemicarboaluminate, C_3A, $CaCO_3$ and CaO were used with molar ratios 2:1:1. For the synthesis of strätlingite a stoichiometric mix of CaO, $Na_2SiO_3 \cdot 5H_2O$ and $NaAlO_2$ was used. Since water content of the sodium silicate and sodium aluminate precursors might vary, the water content was measured on a TGA to correct the initial mix composition prior to synthesis. Monosulfoaluminate was prepared at 5 and 80 °C, while hydroxy-AFm was made at 5 °C. The other phases were kept at room temperature. The different mixtures were stirred using a magnetic stirrer for 3 days and then periodically agitated during 2 weeks. Once purity has been confirmed by XRD, the solids were vacuum filtered under N_2 atmosphere in a glove box and then placed inside small (open) plastic bottles, which were subsequently introduced inside hermetically sealed glass bottles containing salt solutions at the bottom in order to equilibrate the samples at different RHs [29] (see Table 1). Finally the glass bottles were conditioned at 5, 25 and 50 °C during different periods of time (from 8 to 30 months). The RH was periodically checked using a Testo 174H humidity probe.

The typical hexagonal morphology of the AFm phases studied is shown in Fig. 2.

2.2. Experimental methods

Different hydration states of the studied AFm phases as well as their thermodynamic properties were derived using the methodology developed by Baquerizo et al. [14]. Samples aged during different periods of time at different temperatures and RHs were characterized using XRD, TGA, sorption balance measurements, sorption calorimetry and the salt pair–humidity buffer method as described below.

XRD on samples aged at different conditions was carried out at room temperature (unless otherwise stated) with a Bruker D8 Advance diffractometer (CuKα radiation, 45 mA, 35 kV) equipped with a Super Speed detector, in the 2θ range 5–70°, with a step size and time per step of 0.02° and 0.5 s, respectively. Prior characterization the samples were prepared inside a glove box filled with N_2. A low background-airtight specimen holder (Bruker AXS) was used to avoid carbonation and drying during testing. Samples were mixed with small amounts of rutile in order to correct for pattern displacement due to variations in sample height. The lattice parameters were determined by a Le Bail fit [30] using TOPAS 4.2 (Bruker AXS). Phase quantification was carried out using Rietveld analysis implemented in TOPAS 4.2. A humidity chamber CHC plus$^+$ from Anton Paar coupled to the X-ray diffractometer was used to determine lattice parameters of some of the samples at low and high temperatures and different RHs. The lowest hydration states at room temperature were also studied in vacuum dried samples. In this work, when several XRDs are shown in one graph, their intensities axes are not the same (unless otherwise stated) because the samples tested were different and no spinning was possible during characterization due to the use of the airtight sample holder, which highly impacts the preferred orientation.

TGA measurements were carried out using a Mettler Toledo TGA/SDTA 851^e under N_2 flux, over the temperature range 25–1200 °C with a heating rate of 20 K/min. Measurements were done on samples dried at different RH usually after the presence of a single hydration state was confirmed by XRD.

Sorption balance measurements were carried out using a DVS Advantage system (Surface Measurement Systems, London, UK). The step method was the chosen regime to test the samples [31]. When using this method a specific RH is kept constant for certain time before being increased or decreased while the mass of the sample is continuously recorded. Sample masses were between 5 and 15 mg. The hydration state of the initial sample must be known and the sample chosen must be as pure as possible.

Sorption calorimetry was carried out using a state of the art calorimeter developed at Lund University capable of measuring water activity, moisture content and sorption enthalpy on initially dried samples during the sorption process [32,33]. Pure samples were initially vacuum-dried at 25 °C for a minimum of 1 day before starting the test, which means that the starting point of the measurement corresponds to the lowest hydration state of the hydrate studied. The mass of the test samples ranged between 50 and 100 mg.

The salt pair–humidity buffer method described in [14] was used for certain samples in order to study transition RH between two adjacent hydration states as well as the thermodynamic properties associated with these changes. In addition to the study of monosulfoaluminate reported earlier, the hydroxy-AFm was examined using this method.

A physisorption analyser ASAP^{TM} 2020 (Micromeritics) (adsorptive gas N_2) was used to measure the surface area and the complete isotherm (adsorption/desorption) of initially degassed (high vacuum — 50 °C) samples.

While XRD and TGA were used to determine the molar volume of the different hydration states under specific drying conditions (temperature and RH), they cannot identify the exact value of RH at which an absorption/desorption process takes place. Complementary information obtained by sorption balance, sorption calorimetry and the salt pair–humidity buffer method can provide this data. Moreover, sorption calorimetry gives values of enthalpies associated to changes of hydration states. For more details about the methodology please refer to reference [14].

Table 1
Equilibrium RH of selected saturated salt solution [29].

Salt solution	RH (%)		
	5 °C	25 °C	50 °C
Na(OH)	10.5[a]	8.2	5
KCH_3CO_2	26[a]	22.5	19[a]
$MgCl_2$	33.6	32.8	30.5
$Mg(NO_3)_2$	58.9	52.9	45.4
NaCl	75.7	75.3	74.4
KCl	87.7	84.3	81.2
K_2SO_4	98.5	97.3	95.8

[a] Measured.

3. Thermodynamics equations

Changes of hydration states considered in this study follow the reference reaction (1):

$$A \cdot xH_2O(s) + (y-x)H_2O(g) \leftrightarrow A \cdot yH_2O(s) \quad (1)$$

where s and g are solid and gas, respectively, A is a hydrate containing x or y water molecules, where $x \geq 0$ and $y > x$. The Gibbs free energy of reaction (1) is given by:

$$\Delta G_r^o = -RT \ln K = -RT \ln \frac{a(A \cdot yH_2O)}{a(A \cdot xH_2O)\, a(H_2O)^{y-x}}.$$

By assuming that the activity of all solids equals 1.0,

$$\Delta G_r^o = -RT \ln \left[a(H_2O)^{x-y}\right] = (y-x)RT \ln [f(H_2O)] = (y-x)RT \ln \frac{f^*(H_2O)RH}{100} \quad (2)$$

where ΔG_r° is the standard Gibbs free energy of the reaction (1), T is the absolute temperature, K is the equilibrium constant, R is the gas constant (8.31451 J/K mol), $a(H_2O)$ is the activity of H_2O vapour [or in

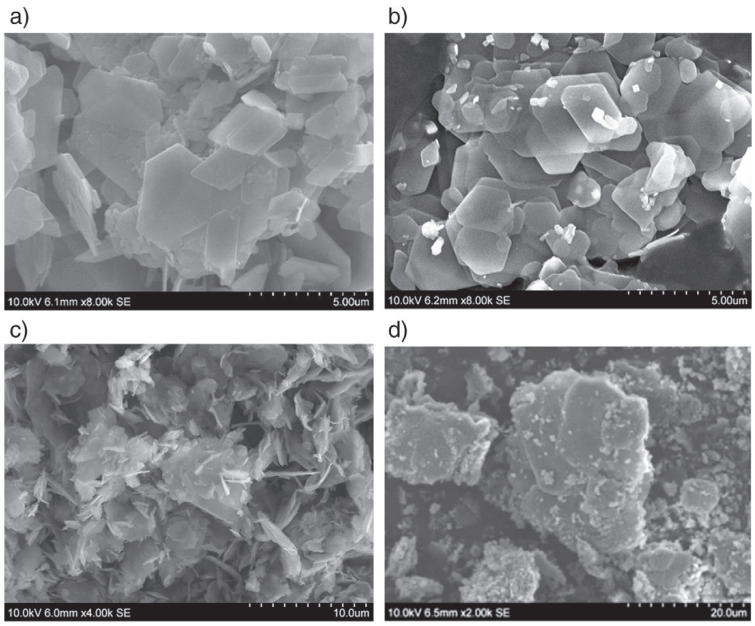

Fig. 2. SEM pictures of a) monocarboaluminate, b) hemicarboaluminate, c) strätlingite and d) hydroxy-AFm. Some hydrogarnet impurities are observed on top of the hemicarboaluminate crystals.

vapour state], $f(H_2O)$ is the equilibrium fugacity, $f^*(H_2O)$ is the fugacity of pure H_2O at T and RH is the equilibrium relative humidity [34–37]. The standard enthalpy of reaction ΔH_r° can be calculated with the van't Hoff equation:

$$\frac{\partial(\ln K)}{\partial(1/T)} = -\frac{\Delta H_r^o}{R}. \quad (3)$$

The standard entropy of reaction ΔS_r° can be calculated from the following equation:

$$\Delta G_r^o = \Delta H_r^o - T\Delta S_r^o. \quad (4)$$

The enthalpy of reaction ΔH_r° can also be determined from sorption calorimetry with the following relations:

$$\Delta H_{sorp} = \Delta H_{cond} + \Delta H_{mix} \quad (5)$$

$$\Delta H_r^o = \Delta H_{sorp} \cdot n \quad (6)$$

where ΔH_{sorp} is the enthalpy of sorption (enthalpy value per g or mol of H_2O absorbed), ΔH_{cond} is the enthalpy of condensation of water at 25 °C (−2440 J/g H_2O or −44 kJ/mol H_2O), ΔH_{mix} is the enthalpy of mixing (output of the sorption calorimetry test), and n is the number of absorbed water molecules during a change of hydration state (equal to y−x from reaction (1))[3].

[3] Notice that this paper investigates stoichiometric hydrates formed by the absorption of water molecules in the hydrated crystal structure. There can, however, also be adsorption (on surfaces) and capillary condensation (in pores), but as the specific surfaces and surface/volume-ratios of our samples are comparatively low, we believe that such effects are small except in the high RH region in some cases.

4. Results and discussion

The results obtained for the different hydration states and their thermodynamic properties are presented for each of the studied phases. Simplified sorption isotherms and a summary of the derived thermodynamic properties of the different hydration states are shown at the end of this section.

4.1. Monocarboaluminate

Fig. 2a shows the typical hexagonal morphology of monocarboaluminate. The surface area corresponds to 5.1 m^2/g (as measured with ASAP™ 2020). XRD patterns of some samples aged at different conditions are shown in Fig. 3. Lattice parameters were refined using the crystal structure published by Francois et al. [21] (ICSD# 59327) and the values are presented in Fig. 4. The refined parameters do not present any significant change in the range 5%–100% RH at any of the studied temperatures (5 °C, 25 °C and 50 °C). The hydration state at these conditions corresponds to Mc11 as confirmed by TGA. Some hydrogarnet impurities were observed at 50 °C. In order to study the lowest hydration state, a sample consisting of pure Mc11 was vacuum dried for 15 h at 25 °C. The sample dehydrates but still some Mc11 is observed as shown in Fig. 3, probably due to incomplete dehydration or partial rehydration during XRD sample preparation and/or measurement. The TGA measurement of the vacuum dried sample shows a water content of around 9.3 H_2O mol. Since the sample was not completely dehydrated it was assumed that this lower hydration state corresponds to Mc9. An in situ measurement using a humidity chamber shows that under nitrogen flow and 80 °C (during 70 min) Mc11 completely dehydrates into Mc9. Attempts to index this lower hydration state were unsuccessful due to the presence of impurities (small amounts of C_3AH_6 and CH)

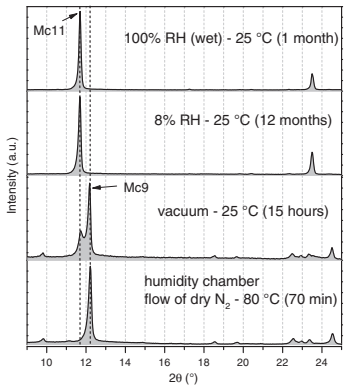

Fig. 3. XRD patterns of some Mc samples dried at different conditions. Every sample dried at 5 °C, 25 °C and 50 °C down to 5% RH (inside glass bottles with salt solutions) were composed of Mc11, for this reason not every pattern is shown. Under vacuum Mc12 starts to dehydrate into Mc9, which is rapidly formed at high temperatures and low RH as shown in the humidity chamber test. The small peak at around 9.8° may correspond to Mc9.

and low quality of the XRD patterns. Thus, it was assumed that Mc9 keeps the same space group as Mc11. Further research is needed to correctly index this lower hydration state.

The sorption balance results are shown in Fig. 5. The graph was normalized assuming a water content of 11 H_2O (Mc11) at 20% RH (as measured by TGA). The absorption/desorption behaviour was completely reversible. During testing the minimum total water content achieved was approximately 10.45 H_2O i.e. the sample consisted probably of a mix of Mc11 and Mc9, because it did not reach equilibrium after 12 h under pure N_2 flow, even though the initial sample mass was only 5.6 mg. The desorption kinetics can thus be considered as rather slow.

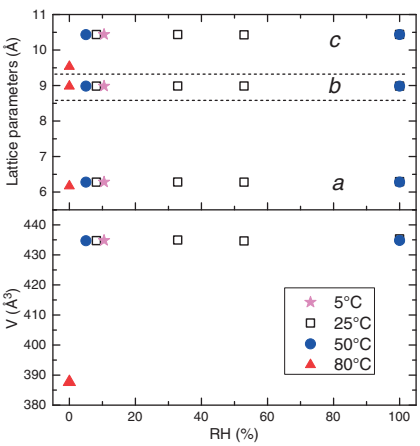

Fig. 4. Refined lattice parameters of Mc dried at 5, 25 and 50 °C and different RHs during 12–24 months. Sample at 80 °C was dried in the humidity chamber under N_2 flow during 70 min before the measurement.

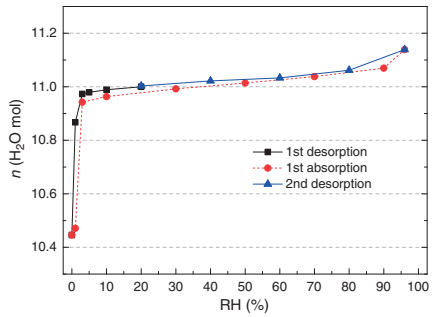

Fig. 5. Water content of monocarboaluminate as function of RH at 25 °C measured by sorption balance. Water contents larger than 11 H_2O probably correspond to water adsorbed on the surface of the crystals or capillary condensation between the crystals. The lower water content corresponds to 10.45 H_2O due to incomplete dehydration during the test.

The sorption calorimetry results of initially vacuum dried monocarboaluminate (Fig. 6) shows a single absorption step as previously identified by sorption balance measurements. The initial sample corresponds to Mc9.3, probably due to incomplete dehydration during vacuum drying or partial rehydration before the start of the test. But since the mixing enthalpy (ΔH_{mix}) is constant for the whole process (−29.4 kJ/mol H_2O) it can be assumed that the rehydration process follows the reaction:

$$Mc9(s) + 2H_2O(g) \rightarrow Mc11(s). \quad (7)$$

The related sorption enthalpy ΔH_{sorp} can be calculated according to Eq. (5) and the total enthalpy of reaction ($\Delta H_r°$) with Eq. (6). In order to calculate the standard Gibbs free energy of reaction ($\Delta G_r°$) it was assumed that the absorption process takes place at 1% RH at 25 °C as observed by sorption balance and sorption calorimetry. Then $\Delta G_r°$ for reaction (7) can be calculated according to Eq. (2) and the standard entropy of reaction $\Delta S_r°$ with Eq. (4). A summary of the thermodynamic properties determined is given in Tables 2 and 3, and a simplified sorption isotherm at 25 °C is shown in Fig. 24 at the end of this section. For

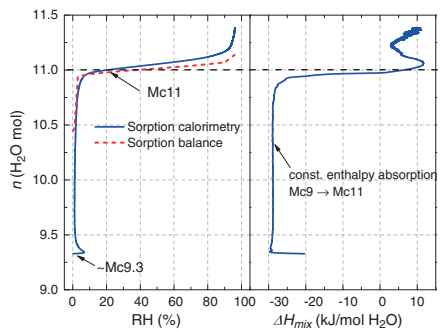

Fig. 6. Sorption calorimetry results showing the calculated sorption isotherm (left) and mixing enthalpy (right) of dry monocarboaluminate at 25 °C (for comparison the isotherm measured by sorption balance is superimposed in the left graph). Graph was normalized assuming a water content of 11 H_2O at 20% RH.

Table 2
Derived thermodynamic data for the changes of hydration states of AFm phases at 25 °C and 1 bar.

Reaction	RH of change of hyd. state (%)	$\Delta G_r°$ (kJ/mol)	$\Delta H_{mix}°$ (kJ/mol)[a]	$\Delta H_r°$ (kJ/mol)	$\Delta S_r°$ (J/mol K)
		Monocarboaluminate			
$Mc9(s) + 2H_2O(g) \rightarrow Mc11(s)$	1.0	−39.8	−58.6	−146.6	−358.2
		Hemicarboaluminate			
$Hc10.5(s) + 1.5H_2O(g) \rightarrow Hc12(s)$	7.0	−22.6	−27.2	−93.2	−236.5
$Hc9(s) + 1.5H_2O(g) \rightarrow Hc10.5(s)$	1.0	−29.9	−33.2	−99.2	−232.4
		Strätlingite			
$Str7(s) + H_2O(g) \rightarrow Str8(s)$	20.0[b]	−12.5	−6.9	−50.9	−128.7
$Str5.5(s) + 1.5H_2O(g) \rightarrow Str7(s)$	2.0	−25.8	−33.8	−99.8	- 351.7
		Hydroxy-AFm			
$Oh13(s) + 6H_2O(g) \rightarrow Oh19(s)$	92.5	−52.2	−37.1	−301.1	−835.0
$Oh11(s) + 2H_2O(g) \rightarrow Oh13(s)$	13.5	−26.9	−35.4[c]	−123.4[c]	−323.7
			−30.6[d]	−118.6[d]	−307.6
			−33.0[e]	−121.0[e]	−315.6
		Monosulfoaluminate[f]			
$Ms12(s) + 2H_2O(g) \rightarrow Ms14(s)$	97.0	−17.2	9.7	−78.3	−205.2
$Ms10.5(s) + 1.5H_2O(g) \rightarrow Ms12(s)$	28.5	−17.4	−17.2	−83.2	−220.6
$Ms12(s) \rightarrow Ms10.5(s) + 1.5H_2O(g)$[g]	12.0	20.5	17.2	83.2	210.2
$Ms9(s) + 1.5H_2O(g) \rightarrow Ms10.5(s)$	2.0	−27.3	−36.8	−102.8	−253.3

[a] Corresponds to the enthalpy of mixing, excluding the enthalpy associated with the condensation of water.
[b] Although the change of hydration state Str8 ↔ Str7 does not take place stepwise, for the calculations it was assumed that it occurs at 20% RH in order to use Str8 and Str7 as end-members of an ideal solid solution Str8–Str7.
[c] From sorption calorimetry.
[d] From the hydrate pair–humidity buffer method.
[e] Average value.
[f] Taken from [14].
[g] Calculated with the desorption branch of the isotherm.

more details about the calculation of the thermodynamic properties of de/rehydration using sorption calorimetry we refer to reference [14].

According to our results monocarboaluminate only dehydrates when exposed to very low RH (<1%) and/or high temperatures. The high stability of Mc is most likely due to the formation of strong hydrogen bonds between the carbonate groups and interlayer water, which seems to contribute to the strong cohesion between layer and interlayer [21].

Table 3
Standard molar thermodynamic properties of the studied cement hydrates at 25 °C and 1 bar.

Phase	$\Delta G_f°$ (kJ/mol)	$\Delta H_f°$ (kJ/mol)	$S°$ (J/mol K)	$C_p°$ (J/mol K)[a]	Density (kg/m³)[b]	$V°$ (cm³/mol)[b]	Ref.
			Monosulfoaluminate				
Ms16: $C_4A\hat{S}H_{16}$	−8726.8	−9930.5	975.0	1114.8[c]	1981.7	350.5	t.s.
Ms14: $C_4A\hat{S}H_{14}$	−8252.9	−9321.8	960.9	1028.5[c]	1985.9	331.6	t.s.
Ms12: $C_4A\hat{S}H_{12}$	−7778.4	−8758.6	791.6	948.4	2007.7	310.1	t.s.
Ms10.5: $C_4A\hat{S}H_{10.5}$[d]	−7417.9	−8311.9	731.2	888.3	2114.9	281.6	t.s.
Ms10.5: $C_4A\hat{S}H_{10.5}$[e]	−7414.9	−8311.9	720.9	888.3	2114.9	281.6	t.s.
Ms9: $C_4A\hat{S}H_9$	−7047.6	−7845.5	703.6	828.2	2070.2	274.6	t.s.
			Monocarboaluminate				
Mc11: $C_4A\hat{C}H_{11}$	−7337.5	−8250.0	656.9	881.4	2170.0	262.0	[39]
Mc9: $C_4A\hat{C}H_9$	−6840.3	−7618.6	640.6	801.2	2279.6	233.6	t.s.
			Hemicarboaluminate				
Hc12: $C_4A\hat{C}_{0.5}H_{12}$	−7336.0	−8270.0	712.6	905.8	1984.0	284.5	[39]
Hc10.5: $C_4A\hat{C}_{0.5}H_{10.5}$	−6970.3	−7813.3	668.3	845.7	2057.1	261.3	t.s.
Hc9: $C_4A\hat{C}_{0.5}H_9$	−6597.4	−7349.7	622.5	785.6	2047.4	249.3	t.s.
			Strätlingite				
Str8: C_2ASH_8	−5705.1	−6360.0	546.2	602.7	1935.8	216.1	[39]
Str7: C_2ASH_7[f]	−5464.0	−6066.8	487.6	562.6	1857.6	215.5	t.s.
Str5.5: $C_2ASH_{5.5}$	−5095.2	−5603.4	454.8	502.5	1754.2	212.8	t.s.
			Hydroxy-AFm				
OH-AFm19: C_4AH_{19}	−8749.9	−10,017.9	1120.0	1382.4	1816.3	368.7	[40]
OH-AFm13: C_4AH_{13}	−7325.7	−8262.4	831.5	1142.0	2041.8	274.5	t.s.
OH-AFm11: C_4AH_{11}	−6841.4	−7656.6	772.6	1061.8	2038.2	257.3	t.s.

t.s. this study.
[a] $C_p°$ was calculated assuming $\Delta C_p = 0$ for the changes of hydration states shown in Table 2.
[b] Calculated from the unit cell parameters following the procedure shown in [14].
[c] The heat capacities of Ms14 and Ms16 were calculated based on the reference reactions $C_4A\hat{S}H_{14} \leftrightarrow C_4A\hat{S}H_{12} + C\hat{S}H_2$–$C\hat{S}$ and $C_4A\hat{S}H_{16} \leftrightarrow C_4A\hat{S}H_{12} + 2C\hat{S}H_2$–$2C\hat{S}$ following the procedure used by Matschei [20].
[d] Calculated with the absorption branch of the isotherm shown in [14].
[e] Calculated with the desorption branch of the isotherm shown in [14].
[f] Str7 must be used together with Str8 in an ideal solid solution.

4.2. Hemicarboaluminate

Fig. 2b shows the hexagonal crystal morphology of synthetic hemicarboaluminate; some cubic hydrogarnet (C_3AH_6) impurities can be observed. The surface area measured with ASAP™ 2020 corresponds to 2.7 m^2/g.

XRD diffractograms on samples dried at 5, 25 and 50 °C and different RHs during 6 to 30 months and under vacuum for several hours are shown in Fig. 7. Hydrogarnet was always observed in the samples aged at 25 and 50 °C, in large amounts in the latter, varying from 25 to 45 wt.% (measured by Rietveld analysis). Some portlandite (CH) impurities were also observed at 25 °C, but in very small amounts <1 wt.%. In the samples conditioned at 50 °C portlandite content was significant, varying from 2 to 10 wt.%. Also some calcite was observed in some of the samples (up to 4%), most likely due to carbonation.

The lattice parameters were refined using the crystal structure published by Runcevski et al. [25]. The results are presented in Fig. 8. Some samples show a shoulder-type peak together with the (0 0 1) reflections, probably due to disorder in the stacking of the layers, transition between higher to lower hydration states or partial carbonation. For simplicity these reflections were omitted during refinement.

The stable hydration state at high RHs (>95% RH) at all temperatures is Hc12, as confirmed by TGA and in agreement with data reported by Fisher and Kuzel [17], although at 100% RH (wet state) and 50 °C up to 10% of hydrogarnet was present in the sample (measured by Rietveld analysis). Hc12 was the stable hydration state at 5 °C at all RHs studied, although some dehydration was observed at 5% RH. A second (0 0 6) reflection at 2θ ~ 11.4° (d ~ 7.75 Å) starts to appear at 25 and 50 °C with decreasing RH, which may correspond to a lower hydration state of Hc or to a solid solution between Hc and Mc. TGA of a sample aged at 25 °C and 23% RH during 30 months, which contains mostly this secondary phase, confirms a higher CO_2 and lower water content, which agrees with values reported by Runcevski et al. [25] for a phase called carbonated hemicarboaluminate (cHc or $C_4A\hat{C}_{0.8}H_{10.2}$). Since it could not be proved that this phase corresponds to a lower hydration state of hemicarboaluminate, it was assumed that the lower hydration state present at 25 °C and 50 °C is cHc10.2. It seems that the formation of carbonated hemicarboaluminate is promoted with increasing temperature and decreasing RH in the presence of small amounts of CO_2. At 25 °C the formation of cHc (from Hc) may be due to the presence of small CO_2 contamination, whereas at 50 °C the CO_2 may come from the decomposition of Hc into C_3AH_6, CH and $\hat{C}$.

The lowest hydration states of hemicarboaluminate were studied using a sample initially aged at 98% RH and 5 °C, composed of almost pure Hc12 as measured by XRD, and then vacuum dried for 12 and 36 h at 25 °C. As observed in Fig. 7d, two different hydration states are present in the sample with main reflections at 2θ ~ 11.65° and 12.21° (d ~ 7.59 Å and 7.24 Å, respectively). The lattice parameters of these two lower hydration states were refined assuming that the space group is the same as that reported by Runcevski et al. [25]. After 36 h there are still 2 hydration states, probably due to incomplete dehydration or to partial rehydration during testing. The water content of the 36 hour vacuum dried sample was 9.5 H_2O, but since the sample was not completely dehydrated it was assumed that this lower hydration state corresponds to 9 H_2O, or Hc9. The other hydration state was assigned as Hc10.5, whose water content was deduced by sorption calorimetry as shown below. No presence of hydrogarnet or portlandite was observed in the samples and the CO_2 weight loss (measured by

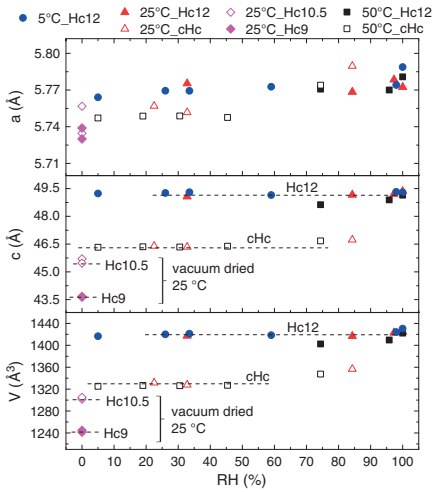

Fig. 8. Refined lattice parameters of Hc dried at 5, 25 and 50 °C. Under vacuum at 25 °C two lower hydration states Hc10.5 and Hc9 were identified by sorption calorimetry and TGA.

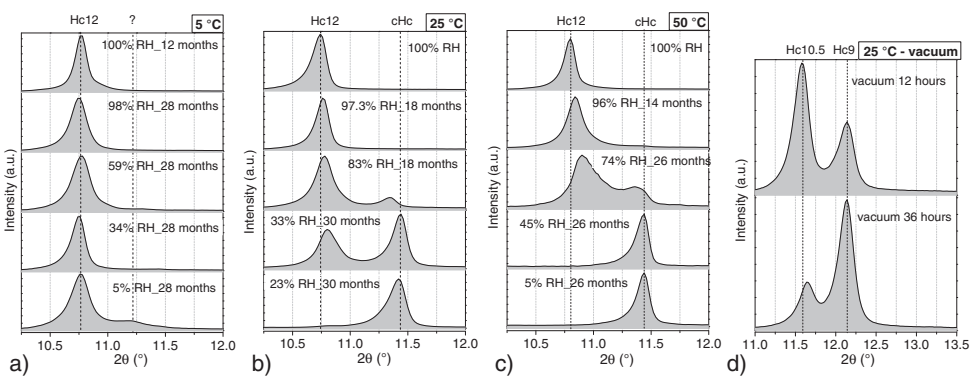

Fig. 7. XRD patterns of hemicarboaluminate dried at a) 5 °C, b) 25 °C and c) 50 °C at different RHs inside hermetic glass bottles, and d) vacuum dried at 25 °C during 12 h and 36 h.

TGA) corresponds to Hc rather than to cHc, which indicates that the sample did not carbonate during vacuum drying.

In order to study the stability of cHc10.2, a sample initially dried at 50 °C and 5% RH, composed of cHc, hydrogarnet and portlandite, was exposed to high RH at 5 °C and 25 °C and tested by XRD after 30 days (Fig. 9). The sample did rehydrate and the refined lattice parameters are close but do not completely fit with Hc12. Whether this rehydration product corresponds to Hc12 or to a higher hydration state of cHc is not clear. The sample rehydrated at 5 °C and 88% RH contained lower quantities of hydrogarnet. Further studies are required to better understand the stability and formation of cHc.

A sorption balance experiment was carried out on a sample composed of Hc12 as confirmed by XRD and TGA. The resulting sorption isotherm is shown in Fig. 10. In order to normalize the water content it was assumed (rather arbitrarily) that at 80% RH the sample is composed of pure Hc12 with negligible adsorbed water or capillary condensation. The isotherm presents two stepwise de/re-hydration processes, the first one from 0 to 2% RH and the second one from 4 to 10% RH approximately. From 12 to 90% RH the sample undergoes a steady absorption/desorption of water, probably due to slow kinetics of de/rehydration. The minimum water content was not reached during the test (sample was still losing water during the first desorption under pure N_2 flow), so the values should be seen as indications of the absorption/desorption behaviour, rather than as quantitative results.

Sorption calorimetry was carried out on a hemicarboaluminate sample similar to the one used in the sorption balance test, but vacuum dried overnight. The calculated sorption isotherm and the mixing enthalpy associated with the absorption of water are presented in Fig. 11. For comparison the isotherm measured by the sorption balance is also shown in Fig. 11. The graph was also normalized assuming Hc12 as the stable hydration state at 80% RH. The rehydration behaviour is very similar to that observed with the sorption balance except that complete dehydration during the sorption balance test was not achieved. According to the mixing enthalpy plot, none of the absorption processes is at constant enthalpy. It seems that the transition between different hydration states of hemicarboaluminate is a complex process which involves metastable hydrates with slightly different water content, which

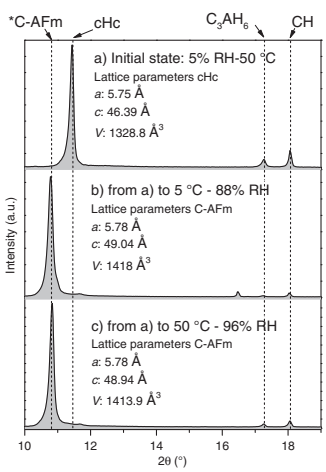

Fig. 9. XRD patterns of a sample initially containing cHc, hydrogarnet (C_3AH_6) and portlandite (CH), and subsequently exposed to high RH at 5 and 50 °C. Shift of the main reflection towards lower 2θ indicates higher water content. *C-AFm refers to a carbonated AFm phase of unknown composition.

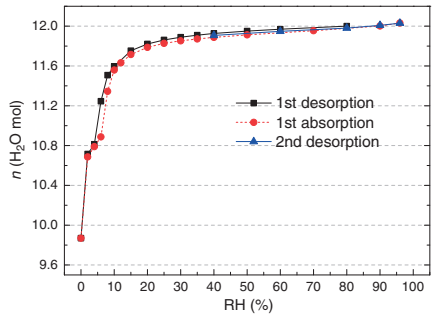

Fig. 10. Sorption isotherm of hemicarboaluminate at 25 °C measured by sorption balance method.

is confirmed by the scatter in lattice parameters as shown in Fig. 8. Since the mixing enthalpy values are not constant, they were calculated from the integral of the curve ΔH_{mix} vs. n in the water content regions of interest (as Fig. 11 right, with axes swapped). The standard Gibbs free energy of reaction $\Delta G_r°$ was calculated according to Eq. (2) assuming a change of hydration state taking place at 1% and 7% RH for the transitions Hc9 ↔ Hc10.5 and Hc10.5 ↔ Hc12, respectively. A summary of thermodynamic properties and a simplified sorption isotherm and volume of hemicarboaluminate are given in the next section.

As observed in the experimental results hemicarboaluminate presents a complex absorption/desorption behaviour as evidenced by the shoulder-like peak together with the (0 0 1) plane reflections in the XRD patterns, the dehydration and decomposition into cHc with increasing temperature and decreasing RH, and the non-constant enthalpy absorption behaviour. Also the large amount of C_3AH_6 at high temperatures is an indication of the low stability of Hc at high temperatures.

Whether the occurrence of cHc from Hc12 is time dependent, even in the absence of significant CO_2 impurities, remains unknown. For this reason sorption balance and sorption calorimetry experiments were crucial in order to enable a fast determination of the different hydration states of Hc, because tests were carried out relatively fast (3–5 days), avoiding the formation of cHc. It is surprising that cHc has

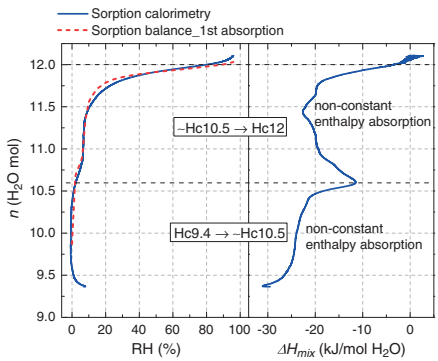

Fig. 11. Calculated sorption isotherm (left) and mixing enthalpy (right) of initially dry hemicarboaluminate at 25 °C from sorption calorimetry testing (for comparison the isotherm measured by sorption balance is superpose in the left graph). Notice the two stepwise water uptakes and the variability of the mixing enthalpy during absorption.

never been reported in hydrated cement pastes, even when both Hc and Mc are present in the sample. This suggests that it only forms in the presence of gaseous CO_2, which would tend to give calcite in a paste situation.

4.3. Strätlingite

Fig. 2c shows the typical hexagonal platelets morphology of synthetic strätlingite, comparable to the one presented by Matschei [20]. The surface area corresponds to 17 m^2/g (as measured with ASAP™ 2020) X-ray diffractograms of strätlingite dried at different conditions are very similar. The main difference can be seen in shifting (0 0 1) reflections. As shown in Fig. 12 at 25 °C from 100% RH down to 8% RH a steady and small decrease of the (0 0 1) basal space is observed, followed by a more abrupt shift at 0% RH (vacuum dried). Samples at 5, 25 and 50 °C were conditioned for a minimum of 12 months. Although not shown here, the complete XRD patterns of the samples indicate good crystallinity, as opposed to other reported studies on synthetic strätlingite [20]. Some calcite (Cc) and monocarboaluminate (Mc) impurities are observed in the samples, although Mc was not always detected and when present it was in amounts lower than 2 wt.% according to Rietveld analysis. It has been reported that C–S–H might be present as an impurity when synthesizing strätlingite [20]. We have disregarded its presence in our samples because the N_2 sorption isotherm measurement carried out on one sample (not shown here) presented a sorption/desorption behaviour similar to that observed on other studied AFm phases, with no significant hysteresis, in contrast to what is observed for C–S–H, either synthetic or occurring in Portland cement pastes.

The refined lattice parameters and volume of the lattice are summarised in Fig. 13. It can be seen that the lattice parameters *a* and *c* decrease with decreasing humidity, and thus the volume of the lattice shrinks slightly during drying.

A sorption balance measurement was done on a sample which was previously equilibrated at 33% RH for 1 year. The sorption isotherm (Fig. 14) was normalized assuming a water content of 7.5 H_2O at 30% RH and a purity of 95%, as previously measured by TGA. There was no hysteresis observed in the desorption/absorption cycles. This seems a characteristic of most of the AFm phases and confirms the lack of a porous phase (C–S–H) within the sample. A stepwise uptake/loss of water is observed between 0% and 5% RH and there is a steady absorption of water in the range 10%–85% RH, which agrees with the volume changes calculated by XRD. The minimum mass at 0% RH was not achieved during 10 h under pure N_2 flow. Over 85% RH most of the weight increase is probably caused by capillary condensation.

Sorption isotherm and mixing enthalpy plots calculated from sorption calorimetry are shown in Fig. 15. For the analysis it was assumed that the sample contained 5 wt.% calcite and that the water content at 30% RH corresponds to Str7.5 (as measured by TGA). Two hydration processes can be differentiated, similar to what is observed by the sorption balance method and XRD.

1) The first absorption process takes place from 0 to about 5% RH, with water content increasing from 5.8 to 7 H_2O. Since TGA measurements in vacuum dried samples give *n* values close to 5.6 H_2O, it was considered that the lowest hydration state corresponds to Str5.5. Then the first absorption process follows the reaction:

$$\mathrm{Str5.5(s)} + 1.5\mathrm{H_2O(g)} \rightarrow \mathrm{Str7(s)}. \quad (8)$$

Thermodynamic properties were calculated with Eqs. (2)–(6). To calculate ΔG_r° it was assumed that reaction (8) takes place at 3% RH. A mixing enthalpy of −22.5 kJ/mol H_2O (Fig. 15) was used to determine ΔH_r°. A summary of the derived thermodynamic properties is given in Table 2.

2) During the second rehydration stage the mixing enthalpy varies as function of the RH, from −18 kJ/mol H_2O at ~5% RH to 0 kJ/mol H_2O at ~80% RH. Above 80% RH, ΔH_{mix} values close to zero confirm the adsorption of water on the surface of the sample rather than absorption inside the crystals.

A summary graph (Fig. 16) was plotted using results obtained with the different techniques. Above 80% RH no further increase in volume is observed, confirming that the large amounts of water measured by sorption balance measurements, sorption calorimetry and TGA are from capillary condensation.

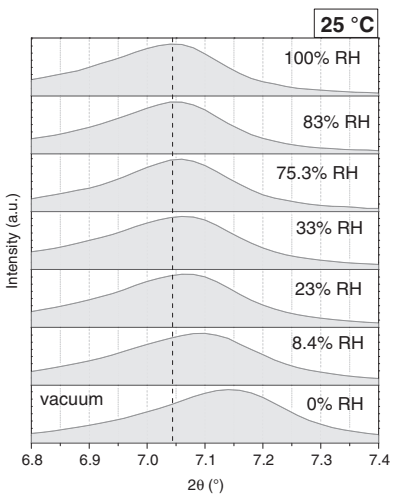

Fig. 12. XRD patterns of strätlingite dried at 25 °C and different RHs, showing the shift of the (0 0 1) reflection towards higher 2θ values (lower d-spacing). A similar trend was observed on samples aged at 5 °C and 50 °C.

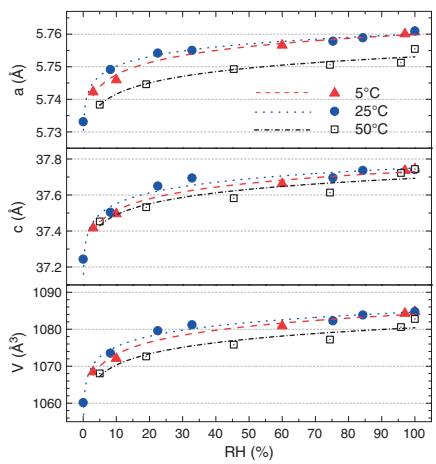

Fig. 13. Refined lattice parameters at 5 °C, 25 °C and 50 °C (sample at 0% RH was vacuum dried).

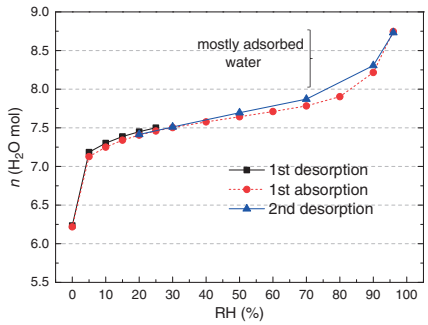

Fig. 14. Sorption isotherm of strätlingite at 25 °C measured by sorption balance.

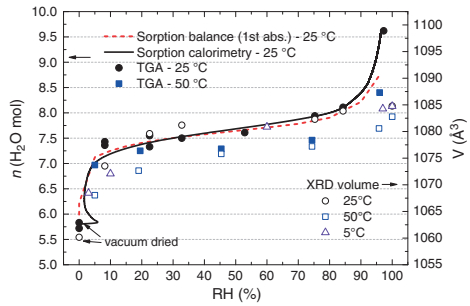

Fig. 16. Summary graph showing water content and volume of the lattice of strätlingite as a function of RH at different temperatures. TGA tests were carried out in samples aged during 12 to 30 months. Proportionality between water content and volume is observed for strätlingite, but not for other AFm phases.

A summary of the absorption/desorption behaviour and the derived thermodynamic properties are shown in the next section. According to our results the lowest and highest hydration states of strätlingite correspond to Str5.5 and Str8, respectively. The chemical composition reported by Rinaldi et al. [28] corresponds to Str7.25, probably due to the lower occupancy (0.25) of a water molecule in the centre of the 6-membered rings of the double tetrahedral layers in the interlayer. If one considers full occupancy of this water molecule the water content of strätlingite would correspond to Str8, which is the hydration state we measured at high RH. From 5 to 80% RH there is a rather constant variation of water content, which approximately corresponds to a change of hydration state from Str7 to Str8. We conclude that this change corresponds to an increase in the occupancy of the interlayer water molecules located in between the 6-membered rings of the double tetrahedral layers, which varies from 0 to 1, at 5 and 85% RH, respectively. The stepwise absorption/desorption taking place from 0 to 5% RH (Str5.5 ↔ Str7) is most likely due to the removal or uptake of interlayer water molecules directly bound to the two Ca atoms which are part of the main octahedral layer. This means that close to 0% RH only 0.5 out of 2 H_2O bound to the Ca atoms are still present, which gives a slight shrinkage of the crystal. According to XRD results, volume changes on strätlingite from 0 to 100% RH at 25 °C were insignificant (~2.3%), although water content varies considerably, from 5.5 to 8 H_2O mol as already mentioned. This means that strätlingite may act as a reservoir, losing or absorbing water during drying or rewetting, while keeping its volume almost unchanged. The reason for the nearly constant volume is the large double tetrahedral (Si/Al = 1) interlayer, keeping the volume relatively constant while allowing the incorporation of 3 H_2O mol, 2 bonded to the Ca atoms of the interlayer and 1 in the centre of the 6-membered rings of the double tetrahedral layers in the interlayer.

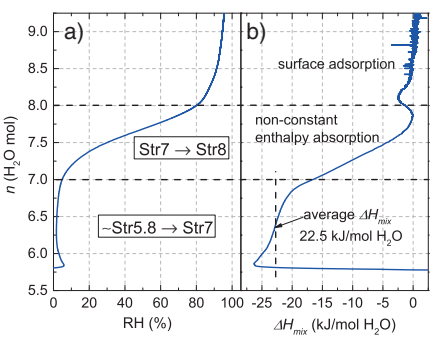

Fig. 15. a) Calculated sorption isotherm and b) measured mixing enthalpy of initially dry strätlingite at 25 °C by sorption calorimetry. The graph was normalized assuming Str7.5 at 30% RH.

4.4. Hydroxy-AFm

The morphology of synthetic hydroxy-AFm can be observed in Fig. 2d. The particle sizes are rather heterogeneous and seem to be formed by stacking of thin crystals. XRD tests were done on samples dried at 5 and 25 °C and different RHs (Fig. 17). Samples aged at 5 °C were tested after 24 months using the humidity chamber. Samples conditioned at 25 °C were investigated after 6 months of drying. Due to the metastability of OH-AFm with increasing temperatures the samples aged at 50 °C completely decomposed into hydrogarnet and portlandite and thus they are not included in the analysis.

As shown in Fig. 17a and b at 5 and 25 °C three different hydration states were observed in the range from 5% to 100% RH: OH-AFm19, OH-AFm13 and OH-AFm11. The water content of the two latter was confirmed by TGA. The water content of the higher hydration state could not be determined because the sample contained significant amounts of adsorbed water on the surface of the crystals. For this reason its water content was considered to be 19 H_2O (or OH-AFm19), which is the commonly reported hydration state at high RH [2,9,17]. A lower hydration state occurring at very low RH (close to 0), OH-AFm7, has been reported by Roberts [13], with a basal space (c') of ca. 5.5 Å. In order to determine the existence of this lower hydration state, a sample consisting of mainly OH-AFm13 was vacuum dried for 48 h. The XRD pattern shows weak reflections (see Fig. 17b) and two different basal spaces can be at around 7.23 Å and 6.61 Å, together with a broad hump at approximately 5.35 Å. It seems that the sample undergoes a decomposition process during vacuum drying rather than dehydrating to a new hydration state. Whether this dehydration product is analogous to OH-AFm or not remains unknown. Further research is needed to evaluate the dehydration and/or decomposition of OH-AFm subjected to severe drying.

The refined lattice parameters are presented in Fig. 17c. It was assumed that all the hydration states belong to the same crystal system and space group, R-3c, as reported by Aruja [38] for the α1 polymorph of OH-AFm19.

A sorption balance measurement was carried out on a hydroxy-AFm sample initially conditioned for one year at 26% RH and 5 °C, corresponding to OH-AFm13 (as confirmed by XRD and TGA) is shown in Fig. 18 shows the measured sorption isotherm. The water content was

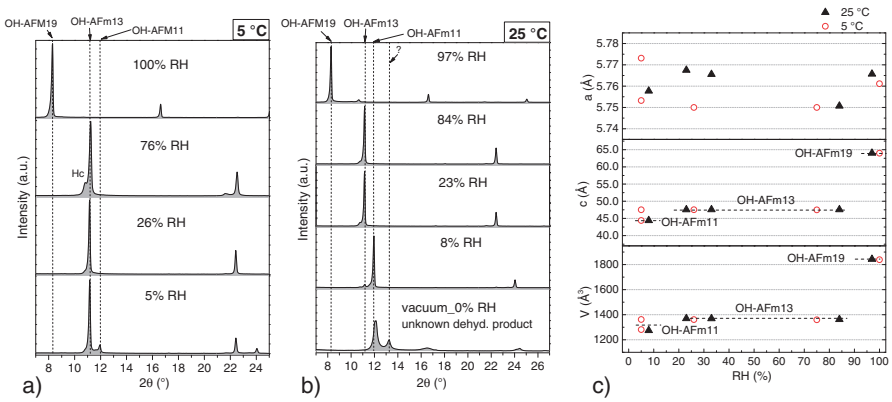

Fig. 17. XRD patterns of OH-AFm dried at a) 5 °C and b) 25 °C. c) Refined lattice parameters *a* and *c* and volume *V* of samples dried at 5 and 25 °C.

normalized assuming OH-AFm13 at 30% RH (as measured by TGA). A step de/re-hydration process is observed between 10 and 15% RH, corresponding to the change of hydration state OH-AFm13 ↔ OH-AFm11. A further de/re-hydration step is observed below 5% RH (under pure N_2 flow) but after 24 h not much water loss was observed. The transition OH-AFm13 ↔ OH-AFm19 was not observed probably due to slow kinetics of rehydration.

Sorption calorimetry was done on a vacuum dried OH-AFm sample. The calculated sorption isotherm and the mixing enthalpy associated with the absorption of water are shown in Fig. 19. For comparison, the sorption isotherm measured by the sorption balance is also plotted. Two different rehydration processes are observed. The first absorption step takes place from 0 to 10% RH, showing two distinctive mixing enthalpy values. Since decomposition rather that change of hydration state was observed at very low RH, this rehydration step is shown but not further analysed. The second rehydration process, from 11.5 to 13 H_2O was considered to be representative of the reaction:

$$OH\text{–}AFm11(s) + 2H_2O(g) \rightarrow OH\text{–}AFm13(s). \quad (9)$$

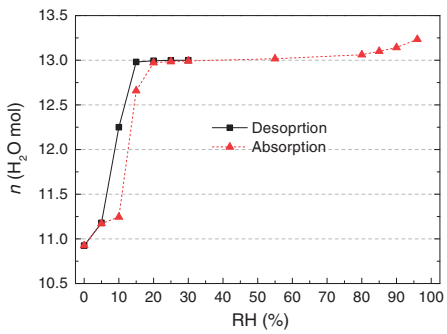

Fig. 18. Sorption isotherm measured on OH-AFm by sorption balance at 25 °C. The graph was normalized assuming $n = 13$ H_2O at 30% RH as measured by TGA.

There is a small absorption of water at around 45% RH probably due to delayed rehydration of some of the decomposition products formed during the initial vacuum drying (see Fig. 17b). The enthalpy of mixing of reaction (9) was calculated from the integral of the curve ΔH_{mix} vs. *n* from 11.5 H_2O to 13 H_2O. A summary of the thermodynamic properties calculated with Eqs. (2)–(6) is given in Table 2.

There seems to be a further uptake of water taking place above 95% RH, most likely due to the hydrate transition:

$$OH\text{–}AFm13(s) + 6H_2O(g) \rightarrow OH\text{–}AFm19(s). \quad (10)$$

During this rehydration step the enthalpy of mixing varies from 0 to 7 kJ/mol H_2O. A bulk absorption process usually has negative values. However, there is a large uncertainty of the enthalpy of mixing measured at water activities over 0.95 (or 95% RH) as mentioned in [14]. In any case the results indicate that the enthalpy of mixing value of this absorption process is small (close to zero).

The hydrate pair–humidity buffer method was used to investigate the critical RH for a temperature dependent hydration state transition.

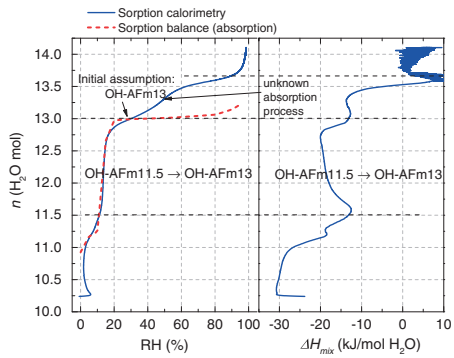

Fig. 19. Calculated sorption isotherm (left) and mixing enthalpy (right) of initially dry OH-AFm at 25 °C by sorption calorimetry. Water content was normalized assuming $n = 13$ H_2O at 30% RH. During vacuum drying the sample partially decomposed, for this reason different absorption processes (varying enthalpy) are observed.

The standard thermodynamic properties ΔG_r°, ΔH_r° and ΔS_r° were calculated from the results shown in Fig. 20 using Eqs. (2), (3) and (4) and are listed in Table 2. There is good agreement between the values measured by sorption calorimetry and those calculated using the hydrate pair–humidity buffer method for the hydrate transition OH-AFm13 ↔ OH-AFm11. Although the change of hydration state OH-AFm19 ↔ OH-AFm13 was not well determined by sorption balance measurements and sorption calorimetry, the data shown in Fig. 20 was used to calculate the thermodynamic properties.

To summarise, hydroxy-AFm shows well defined sequences of hydration states as function of temperature. Nevertheless, when exposed to very low RH (vacuum drying) OH-AFm11 seems to undergo decomposition into a less structured hydrate rather than a change of hydration state. This was concluded due to the large decrease in peak intensity and occurrence of a hump at lower basal space. At 50 °C OH-AFm completely decomposes into hydrogarnet and portlandite, and even at 25 °C large amounts of these impurities were observed when dried for long periods. At low temperatures OH-AFm was the main hydrate, together with minor Hc impurities due to carbonation. Although OH-AFm presents the larger crystal volume shrinkage when drying from OH-AFm19 to OH-AFm 13 at 92.5% RH and 25 °C (approximately 25.5 vol.%), its formation in hydrated cement is very unlikely due to its metastability with respect to hydrogarnet at normal curing conditions and the presence of sulfate and carbonate in Portland cements which stabilize other AFm phases [18].

4.5. Monosulfoaluminate

Different hydration states of monosulfoaluminate (Ms14, Ms12, Ms10.5 and Ms9) were previously reported by Baquerizo et al. [14]. The existence of a water-rich hydration state, Ms16, was noted but not fully characterized and is therefore further investigated in this study.

In [14] we noted that Ms16 is apparently preferably formed at lower temperatures. Therefore a Ms16 sample stored at 5 °C was used for the initial stability (Fig. 21). The sample was initially conditioned in situ at 97% RH in the XRD humidity chamber for 1 h and subsequently investigated at lower RHs down to 2.5%. Some Ms12 was still present in the initial sample resulting from incomplete rehydration during the sample equilibration. When the RH is decreased to 85%, the Ms12 reflection at 2θ ~ 9.83° starts to increase in intensity, and at 80% RH this increase is observed for Ms12 and Ms14 reflections (see inset in Fig. 21). With further decrease of RH, Ms16 completely disappears at 60% RH and Ms14 and Ms12 intensities continue increasing. The results indicate that Ms14 is a transition hydrate between Ms16 and Ms12 and that it is potentially metastable at low temperatures. At 50% RH a hydration state

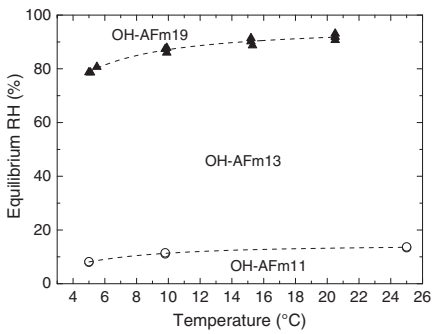

Fig. 20. OH-AFm19-OH-AFm13 and OH-AFm13–OH-AFm11 equilibria at 1 bar measured with the hydrate pair–humidity buffer method.

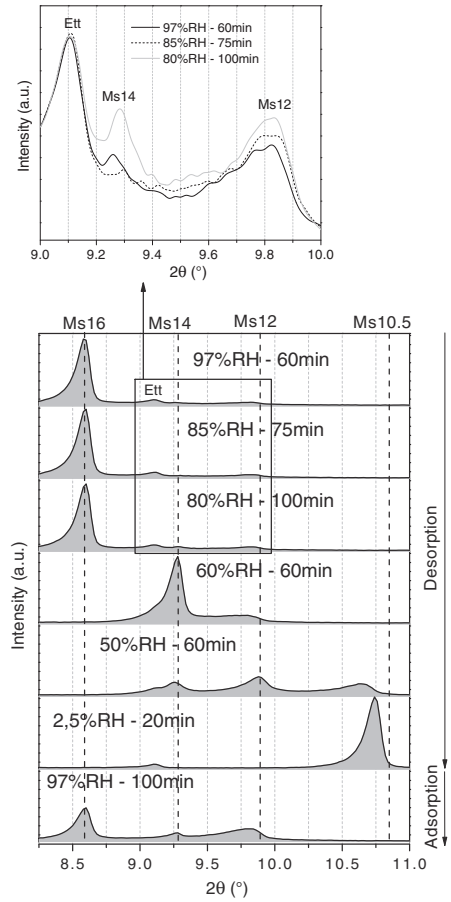

Fig. 21. XRD patterns of monosulfoaluminate tested in situ using a humidity chamber at 5 °C. The inset shows the parallel increase of Ms14 and Ms12 when dehydrating Ms16. Intensities axes are equal.

with reflections close to Ms10.5 (a_o 5.74 Å and c_o 24.7 Å) is observed and its (0 0 1) reflection increases in intensity down to 2.5% RH. This hydration state was not observed in the tests carried out at 25 °C and 50 °C reported in [14]. No further investigation was done in this study on the stability of this hydration state. When the sample was dried at 2.5% RH and is re-exposed to 97% RH, the crystals start to rehydrate back into Ms16. However small amounts of Ms12 and Ms14 remain.

In order to determine the impact of higher temperatures on the stability of Ms16, a short in situ XRD experiment was done in the humidity chamber. Initially the temperature was stepwise increased from 5 °C to 18 °C at a constant RH of 92% (see Fig. 22). As mentioned before, small amounts of Ms12 were present at the beginning of the experiment. From 5 °C to 12 °C Ms16 seems to be a persistent hydration state; this is concluded from similar intensities of the basal reflections in this temperature range. A further temperature increase to 18 °C (at constant RH of 92%) leads to a rapid dehydration of Ms16 first to Ms14 and then to

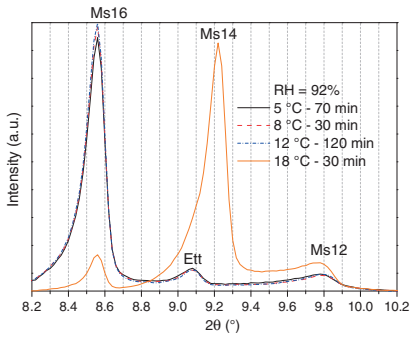

Fig. 22. XRD patterns of monosulfoaluminate tested in situ using a humidity chamber at 92% RH from 5 °C to 18 °C.

Ms12, indicating again a potential metastability of Ms14 at low temperatures.

The approximate stability of Ms16 is shown in Fig. 23. Thermodynamic properties of Ms16 (shown in Table 3) were empirically determined to fit experimental results, assuming that this hydration state will dehydrate at 85% and 92% RH, at 5 °C and 14 °C, respectively.

4.6. Summary of results

In the current study the impact of relative humidity and temperature on the formation of different hydration states of the most important AFm phases was investigated. To summarise the findings simplified sorption isotherms and volume change plots of the lattice of monocarboaluminate, hemicarboaluminate, hydroxy-AFm, strätlingite and monosulfoaluminate at 25 °C are presented in Fig. 24.

Based on the results it was possible to derive a thermodynamic dataset which enables a significantly improved prediction of the mineralogical constitution of hydrated cement paste at unsaturated conditions i.e. RH < 100%. Thermodynamic properties of the changes of hydration states of the aforementioned phases are summarised in Table 2. Standard molar thermodynamic properties of all the different hydration states, including density values are presented in Table 3.

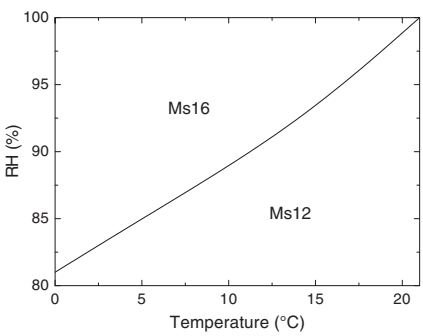

Fig. 23. Approximate stability regions of Ms16 and Ms12 < 20 °C. Ms14 does not appear in the graph because it was assumed that it is metastable at low temperatures.

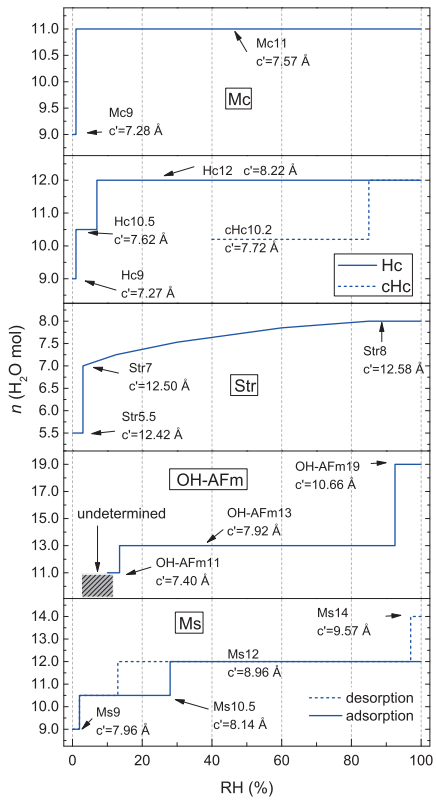

Fig. 24. Summary graph showing the different hydration states of strätlingite (Str), monocarboaluminate (Mc), hemicarboaluminate (Hc), carbonated hemicarboaluminate (cHc) and hydroxy-AFm (OH-AFm) as function of RH at 25 °C. The sorption isotherm corresponding to cHc is an approximation based on experimental results. The isotherms only consider water that is part of the crystalline samples (structural + interlayer), excluding adsorbed or capillary condensed water, which is negligible on AFm phases due to their low surface area (compared to C–S–H). The interlayer distance c′ is the average value of several measurements.

5. Discussion and implications on volume stability of cement paste

All the cement hydrates studied in this work existed in different hydration states depending on the external conditions (temperature and RH). From Fig. 25 the sensitivity of some phases and the high volume stability of others with respect to drying are evident. The most stable hydrate studied was monocarboaluminate, since very low RH (close to zero) and/or high temperatures are required to dehydrate the phase. In the absence of CO_2, hemicarboaluminate is also stable, but it tends to decompose at high temperatures and with prolonged times of drying into cHc, hydrogarnet and portlandite. Its stability might be linked to the crystal structure and the bonding of the anion in the interlayer but, since no structural data on atomic positions was obtained in this study, this hypothesis could not be confirmed. Strätlingite shows very good volume stability, although its water content varies considerably. This means that strätlingite may act as a reservoir, losing or absorbing water during drying or rewetting, while keeping its volume almost

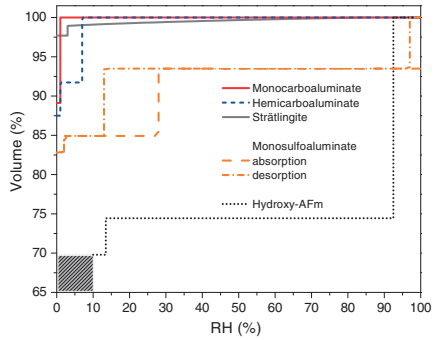

Fig. 25. Volume changes of the AFm phases studied as function of RH at 25 °C. 100% volume corresponds to the higher hydration state of each phase.

unchanged due to the large double tetrahedral (Si/Al = 1) interlayer. Even though hydroxy-AFm was the hydrate with the larger crystal volume shrinkage when drying, its formation is improbable due to its metastability with respect to hydrogarnet and the presence of other ions in solution which stabilize other AFm phases. A higher hydration state of monosulfoaluminate was observed at low temperatures and its thermodynamic properties determined. Higher hydration states at lower temperatures were not detected in any of the other AFm phases studied.

From a practical perspective it is known that concrete expands slightly with a gain in moisture and contracts with a loss in moisture [41], mainly due to absorption/desorption of water from the main cement hydrate present in Portland based binders, C–S–H. Although the impact of AFm phases is rather small in Portland cements, their influence in volume stability might be significant in cementitious systems containing SCM with high alumina content, such as metakaolin, calcined clay, and some types of slag and fly ash, where large amounts of AFm phases can be formed. In this work it was shown that some AFm phases present very good volume stability, which means that cementitious systems containing large amounts of monocarboaluminate and strätlingite, for instance, should be almost insensitive to changes of environmental conditions (temperature and RH), resulting in a potentially improved resistance to drying shrinkage or swelling. Although the volume stability of such systems should be better, their strength might not be as good as typical Portland cement binders because of the absence of C–S–H, which is the responsible of the strength development. This is something that requires further research.

An important fact is that every studied AFm phase loses water when exposed to very low RH (close to 0%) and increasing temperature, conditions that can easily be achieved during drying methods such as vacuum drying, P-drying, oven drying, etc. Also different methods to stop hydration of cementitious systems, including solvent exchange with acetone and isopropanol, may impact the water content of some AFm phases due to a decrease in the water activity of the sample. This is something that has to be taken into account when preparing a sample prior characterization, especially by XRD and TGA.

The current paper presents, for the first time, a complete picture of the stability of the most important AFm phases present in cement and concrete when exposed to varying external conditions, including critical conditions of de/rehydration and thermodynamic properties related to changes of hydration states. This data will enable the modelling of the volume stability of cementitious systems exposed to different external conditions and opens the possibility to engineer cement mixes less sensitive to changing exposure conditions, which can positively impact the performance and durability of cement based materials.

Acknowledgements

The research leading to these results has received funding from the European Union Seventh Framework Programme (FP7/2007–2013) under grant agreement 264448. We would like to thank Holcim Technology Ltd. for actively promoting cement research, especially the Innovation Function and the Analytical Lab of the Cement Manufacturing Function.

References

[1] B.Z. Dilnesa, E. Wieland, B. Lothenbach, R. Dähn, K.L. Scrivener, Fe-containing phases in hydrated cements, Cem. Concr. Res. 58 (2014) 45–55.
[2] H.F.W. Taylor, Cement Chemistry, second ed. Thomas Telford, London, 1997.
[3] H.F.W. Taylor, Crystal structures of some double hydroxide minerals, Mineral. Mag. 39 (1973) 377–389.
[4] A. Mesbah, M. Francois, C. Cau-dit-Coumes, F. Frizon, Y. Filinchuk, F. Leroux, J. Ravaux, G. Renaudin, Crystal structure of Kuzel's salt $3CaO\cdot Al_2O_3\cdot 1/2CaSO_4\cdot 1/2CaCl_2\cdot 11H_2O$ determined by synchrotron powder diffraction, Cem. Concr. Res. 41 (2011) 504–509.
[5] H.J. Kuzel, Initial hydration reactions and mechanisms of delayed ettringite formation in Portland cements, Cem. Concr. Compos. 18 (1996) 195–203.
[6] R. Allmann, Refinement of the hybrid layer structure $[Ca_2Al(OH)_6]+\cdot[1/2SO_4\cdot 3H_2O]-$, Neues Jb. Miner. Monat. 136–144 (1977).
[7] H.E. Schwiete, U. Ludwig, Crystal Structures and Properties of Cement Hydration Products (Hydrated Calcium Aluminates and Ferrites), 5th ISCC, Vol 2, 1968, pp. 37–67.
[8] H. Pöllmann, Characterization of different water contents of ettringite and kuzelite, Proceeding of the XII Int. Congress on the Chemistry of Cement, Montreal, Canada, 2007.
[9] W. Dosch, H. Keller, H. Strassen, 5th ISCC, Vol 2, 1968, pp. 72–77.
[10] D. Damidot, F.P. Glasser, Thermodynamic investigation of the $CaO–Al_2O_3–CaSO_4–H_2O$ at 50 °C and 85 °C, Cem. Concr. Res. 22 (1992) 1179–1191.
[11] I. Kapralik, F. Hanic, Phase relations in the subsystem $C_4A_3S–CSH_2–CH–H_2O$ of the system $CaO–Al_2O_3–CS–H_2O$ referred to hydration of sulphoaluminate cement, Cem. Concr. Res. 19 (1989) 89–102.
[12] H. Pöllmann, Die Kristallchemie der Neubildungen bei Einwirkung von Schadstoffen auf hydraulische Bindemittel(PhD Dissertation) University of Erlangen–Nuernberg, 1984.
[13] M.H. Roberts, Calcium aluminate hydrates and related basic salt solid solutions, 5th ISCC, Vol 2, 1968, pp. 104–117.
[14] L.G. Baquerizo, T. Matschei, K.L. Scrivener, M. Saedipour, A. Thorell, L. Wadsö, Methods to determine hydration states of minerals and cement hydrates, Cem. Concr. Res. 65 (2014) 85–95.
[15] S.J. Ahmed, H.F.W. Taylor, crystal structures of the lamellar calcium aluminate hydrates, Nature 215 (1967) 622–623.
[16] F.G. Buttler, D. Glasser, H.F.W. Taylor, Studies on $4CaO\cdot Al_2O_3\cdot 13H_2O$ and the related natural mineral hydrocalumite, J. Am. Ceram. Soc. 42 (1959) 121–126.
[17] R. Fischer, H.J. Kuzel, Reinvestigation of the system C4A·nH2O–C4A·CO2·nH2O, Cem. Concr. Res. 12 (1982) 517–526.
[18] T. Matschei, B. Lothenbach, F.P. Glasser, The AFm phase in Portland cement, Cem. Concr. Res. 37 (2007) 118–130.
[19] D. Damidot, S. Stronach, A. Kindness, M. Atkins, F.P. Glasser, Thermodynamic investigation of the $CaO–Al_2O_3–CaCO_3–H_2O$ closed system at 25 °C and the influence of Na_2O, Cem. Concr. Res. 24 (1994) 563–572.
[20] T. Matschei, Thermodynamics of Cement Hydration(PhD Dissertation) University of Aberdeen, 2007.
[21] M. Francois, G. Renaudin, O. Evrard, A cementitious compound with composition $3CaO\cdot Al_2O_3\cdot CaCO_3\cdot 11H_2O$, Acta Crystallogr. C54 (1998) 1214–1217.
[22] G. Renaudin, M. Francois, O. Evrard, Order and disorder in the lamellar hydrated tetracalcium monocarboaluminate compound, Cem. Concr. Res. 29 (1999) 63–69.
[23] J. Moon, J.E. Oh, M,. Balonis, F.P. Glasser, S.M. Clark, P. Monteiro, High pressure study of low compressibility tetracalcium aluminum carbonate hydrates $3CaO\cdot Al_2O_3\cdot CaCO_3\cdot 11H_2O$, Cem. Concr. Res. 42 (2012) 105–110.
[24] J. Moon, J.E. Oh, M, Balonis, F.P. Glasser, S.M. Clark, Pressure induced reactions amongst calcium aluminate hydrate phases, Cem. Concr. Res. 41 (2011) 571–578.
[25] T. Runcevski, R.E. Dinnebier, O.V. Magdysyuk, H. Pöllmann, Crystal structures of calcium hemicarboaluminate and carbonated calcium hemicarboaluminate from synchrotron powder diffraction data, Acta Crystallogr. B68 (2012) 493–500.
[26] H.G. Midgley, P. Bhaskara Rao, Formation of stratlingite, $2CaO\cdot SiO_2\cdot Al2O_3\cdot 8H_2O$, in relation to the hydration of high alumina cement, Cem. Concr. Res. 8 (1978) 169–172.
[27] J. Ding, Y. Fu, J.J. Beaudoin, Stratlingite formation in high alumina cement — zeolite systems, Adv. Cem. Res. 7 (1995) 171–178.
[28] R. Rinaldi, M. Sacerdoti, E. Passaglia, Strätlingite: crystal structure, chemistry, and a reexamination of its polytype vertumnite, Eur. J. Mineral. 2 (1990) 841–849.
[29] L. Greenspan, Humidity fixed points of binary saturated aqueous solutions, J. Res. Natl. Bur. Stand. 81 (1977) 89–96.
[30] A. Le Bail, H. Duroy, J.L. Fourquet, Ab-initio structure determination of $LiSbWO_6$ by X-ray powder diffraction, Mater. Res. Bull. 23 (1988) 447–452.
[31] L. Wadsö, A. Anderberg, I. Åslund, O. Söderman, An improved method to validate the relative humidity generation in sorption balances, Eur. J. Pharm. Biopharm. 72 (1) (2009) 99–104.

[32] L. Wadsö, N. Markova, A double twin isothermal microcalorimeter, Thermochim. Acta 360 (2000) 101–107.
[33] L. Wadsö, N. Markova, A method to simultaneously determine sorption isotherms and sorption enthalpies with a double twin microcalorimeter, Rev. Sci. Instrum. 73 (2002) 2743–2754.
[34] I.M. Chou, R.R. Seal II, B.S. Hemingway, Determination of melanterite–rozenite and chalcanthite–bonattite equilibria by humidity measurements at 0.1 MPa, Am. Mineral. 87 (2002) 108–114.
[35] I.M. Chou, R.R. Seal II, Determination of epsomite–hexahydrite equilibria by the humidity-buffer technique at 0.1 MPa with implications for phase equilibria in the system $MgSO_4$–H_2O, Astrobiology 3 (2003) 619–630.
[36] I.M. Chou, R.R. Seal II, Determination of goslarite–bianchite equilibria by the humidity-buffer technique at 0.1 MPa, Chem. Geol. 215 (2005) 517–523.
[37] I.M. Chou, R.R. Seal II, Acquisition and evaluation of thermodynamic data for morenosite–retgersite equilibria at 0.1 MPa, Am. Mineral. 88 (2003) 1943–1948.
[38] E. Aruja, The unit cell and space group of $4CaO·A1_2O_3·19H_2O$ polymorphs, Acta Crystallogr. 14 (1961) 1213–1216.
[39] T. Matschei, B. Lothenbach, F. Glasser, Thermodynamic properties of Portland cement hydrates in the system $CaO–Al_2O_3–SiO_2–CaSO_4–CaCO_3–H_2O$, Cem. Concr. Res. 37 (2007) 1379–1410.
[40] B. Lothenbach, L. Pelletier-Chaignat, F. Winnefeld, Stability in the system $CaO–Al_2O_3–H_2O$, Cem. Concr. Res. 42 (2012) 1621–1634.
[41] Design and Control of Concrete Mixtures, 15th ed. Portland Cement Association, 2011.